UNIVERSITÀ DEGLI STUDI DI TRIESTE

XXVIII CICLO DEL DOTTORATO DI RICERCA IN SCIENZE E TECNOLOGIE CHIMICHE E FARMACEUTICHE
CHEMICAL AND PHARMACEUTICAL SCIENCES AND TECHNOLOGIES

COVALENT FUNCTIONALIZATION OF NANODIAMONDS FOR BIOAPPLICATIONS

Settore scientifico-disciplinare: CHIM/08

DOTTORANDA
VALENTINA ARMUZZA

COORDINATORE
PROF. MAURO STENER

SUPERVISORE DI TESI
PROF. TATIANA DA ROS

ANNO ACCADEMICO 2014 / 2015

“Nothing in life is to be feared,

it is only to be understood.”

Marie Curie

Riassunto

Tra i vari nanomateriali di carbonio i nanodiamanti (NDs) stanno emergendo come nuova alternativa per numerose applicazioni che vanno dall'ambito biologico a quello dei materiali. Diversi studi hanno infatti dimostrato il loro possibile uso per il trasporto di biomolecole in sistemi cellulari agendo, in alcuni casi, contemporaneamente da sonda fluorescente.
Strutturalmente, i nanodiamanti sono caratterizzati da un nucleo di diamante sp^3, circondato da uno strato di carbonio composto da atomi di carbonio ibridizzati sp^2 e sp^3. La superficie è costituita da gruppi funzionali di diversa natura come acidi carbossilici, esteri, ammidi, idrossili, epossidi, che possono essere sfruttati per legare covalentemente diverse molecole o catene solubilizzanti. È necessario infatti ricordare la forte propensione dei nanodiamanti ad aggregare in soluzione, cosa che ne può limitare le applicazioni in ambito biologico.

Nell'ambito di questa tesi di dottorato ci si è occupati dello studio e funzionalizzazione di diversi tipi di nanodiamanti. Sono stati caratterizzati tramite microscopia a trasmissione elettronica (TEM), analisi termogravimetrica (TGA), spettroscopia fotoelettronica a raggi X (XPS), diffrazione a raggi X su polvere (pXRD), spettroscopia Raman e IR, spettroscopia di assorbimento UV-visibile.
La superficie dei nanodiamanti è stata ossidata per trattamento con una miscela solfonitrica così da aumentare il numero di gruppi carbossilici e, allo stesso tempo, così da rendere la superficie più omogenea. Le reazioni di ammidazione sono state effettuate sia sui NDs iniziali che quelli ossidati, facendo uno studio di ottimizzazione delle condizioni sperimentali, in cui si sono variati le metodologie di attivazione degli acidi carbossilici e i tempi di reazione.
Un'altra possibile variazione della struttura superficiale dei NDs può essere ottenuta mediante un processo detto di *annealing*, grazie al quale vengono rimossi i diversi gruppo funzionali e si ha uno strato esterno costituito principalmente da atomi di carbonio con ibridizzazione sp^2.
I campioni ottenuti da diversi processi di *annealing* sono stati utilizzati per studiare le reazioni che convenzionalmente vengono impiegate per la derivatizzazione di fullereni e nanotubi di carbonio.
A tal proposito è stato condotto uno studio approfondito sulle reazioni di arilazione, cicloaddizione 1,3-dipolare di ilidi azometiniche e nitrene su nano diamanti che hanno precedentemente subito il trattamento di annealing, considerando anche in questo caso variazioni di singoli parametri e, inoltre, la possibilità di usare l'irraggiamento tramite microonde.

Si è inoltre valutata la citotossicità di NDs ossidati e ammidati recanti una funzione amminica terminale o un gruppo fluorescente (la fluoresceina). Per questi studi si sono utilizzate cellule PBMC (Periferal Blood Mononuclear Cells) ed è emerso che i derivati così preparati presentano bassi livelli di citotossicità. Sulla base di questi risultati si è infine deciso di utilizzare i nanodiamanti ossidati come possibili vettori di farmaci e a tale scopo sono stati funzionalizzati con peptidi di tipo *tumor-homing*. La presenza di questi ultimi può avere un ruolo chiave nel trasporto di farmaci chemioterapici da parte di vettori a base di nanodiamanti e, contemporaneamente, potrebbe aumentare la dispersibilità del nanomateriale in solventi acquosi. I peptidi sono stati sintetizzati su fase solida (SPPS), purificati e caratterizzati tramite cromatografia liquida ad alta prestazione in fase inversa (RP-HPLC) e spettroscopia di massa ad alta risoluzione (HR-MALDI) e infine coniugati ai NDs. Anche questi composti saranno oggetto di studi biologici.

Abstract

In the last years, nanoscale diamonds are emerging as important materials for a variety of high performance technologies, thanks to their characteristics as the presence of a stable inert core and an alterable surface chemistry, the small primary particle size (from 4-5 nm to about 20 nm) and, in some cases, the fluorescence. Nanodiamonds (NDs) have been demonstrated to be promising tools for the delivery of biomolecules into cellular systems and to act as fluorescent label at the same time. However, diamond particles possess a strong propensity to aggregate in liquid formulation media, restricting their applicability in biomedical sciences.

Nanodiamonds are characterized by a sp^3 diamond core, surrounded gradually by a distorted-strained diamond layer and by an envelope of non-crystalline carbon that is a mixture of sp^2 and sp^3 hybridized atoms. The surface of pristine nanodiamond particles contains a complex array of functional groups as carboxylic acids, esters, ethers, lactones, amines, etc. so several chemical modifications could be introduced.

Pristine detonation nanodiamonds were fully characterized by transmission electron microscopy (TEM), thermogravimetric analysis (TGA), X-ray photoelectron spectroscopy (XPS), powder X-ray diffraction (pXRD), Raman, infrared (IR) and UV-visible spectroscopies.

The surface of nanodiamonds was oxidized using a mixture of sulfuric and nitric acids in order to make the surface more homogeneous and to increase the number of carboxylic groups.

The amidation on pristine and oxidized NDs was studied using both thionyl chloride and *O*-(Benzotriazol-1-yl)-*N,N,N′,N′*-tetramethyluronium tetrafluoroborate (TBTU) as coupling reagents.

The amine used was the *tert*-butyl (2-(2-(2-aminoethoxy)ethoxy)ethyl)carbamate, so after the Boc- deprotection a further grafting of the NDs was performed with fluorescent dyes or electrochemical active moieties. On the NDs surface it was also possible to obtain a sp^2 hybridized atoms' layer by means of annealing processes, so addition reactions on double bonds, typically used for the functionalization of carbon nanotubes, were applied. The arylation with functionalized aryl diazonium salts, the 1,3-dipolar cycloaddition and the nitrene reactions were applied on annealed NDs studying both classical conditions and microwave irradiation.

Moreover, oxidized NDs were functionalized with tumor homing and cell-penetrating peptides. The presence of this kind of peptides on the nanodiamond surface could be useful for the drug delivery and at the same time it can improve the dispersion stability.

Tumor homing sequences and cell-penetrating peptides (CPPs) were synthesized using the solid phase peptide synthesis (SPPS) approach and they were fully characterized by reverse-phase high pressure liquid chromatography (RP-HPLC) and high resolution mass spectroscopy.

List of Abbrevations

ND	Nanodiamond
DND	Detonation ultrananocrystalline diamonds
TNT	2-methyl-1,3,5-trinitrobenzene
XRD	1,3,5-trinitroperhydro-1,3,5-triazine
UNCD	Ultrananocrystalline diamonds
NCD	Nanocrystalline diamonds
HPHT	High-Pressure-High-Temperature
CVD	Chemical Vapor Deposition
RS	Raman Scattering
IR	Infrared Spectroscopy
TGA	Thermogravimetric Analysis
Powder XRD	Powder X-Ray Diffraction
XPS	X-Ray Photoelectron Spectroscopy
TEM	Tranmission Electron Microscopy
SPPS	Solid Phase Peptide Synthesis
RP-HPLC	Reverse Phase- High Pressure Liquid Chromatography
MALDI	Matrix-Assisted Laser Desorption/Ionization
DCC	*N*,*N*'-Dicyclohexylcarbodiimide
DMF	Dimethylformamide
EDT	1,2-Ethanedithiol
EDTA	Ethylenediaminetetraacetic acid
Fmoc	Fluorenylmethyloxycarbonyl
HATU	*O*-(7-Azabenzotriazol-1-yl)-*N*,*N*,*N*',*N*'-tetramethyluronium hexafluorophosphate
HBTU	*O*-(Benzotriazol-1-yl)-N,N,N',N'-tetramethyluroniumhexafluorophosphate

DIPEA or DIEA	*N*,*N*-Diisopropylethylamine
NHS	*N*-Hydroxysuccinimide
NMP	*N*-Methyl-2-Pyrrolidone
FITC	Fluorescein isothiocyanate
TBTU	*N,N,N′,N′*-Tetramethyl-*O*-(benzotriazol-1-yl)uronium tetrafluoroborate
MW	Microwave
PBMC	Peripheral Blood Mononuclear Cell
MTT	3-(4,5-dimethylthiazol-2-yl)-2,5-diphenyltetrazolium bromide
ZPL	Zero-Phonon Line
AA	Amino Acid

Table of content

1. Chapter 1- Introduction 1

1.1 Origin 1

1.2 Synthesis and purification 1

1.2.1 Detonation nanodiamonds 1
1.2.2 Synthesis of diamond from graphite in presence of metal catalysts 3
1.2.3 Synthesis by Chemical Vapor Deposition 3

1.3 Characteristics 4

1.3.1 Types of nanodiamonds 4
1.3.2 Structure 5

1.4 Surface functionalization 6

1.5 Characterization methods 7

1.5.1 Raman Spectroscopy 7
1.5.2 Infrared Spectroscopy 8
1.5.3 Fluorescence 9
1.5.4 X-Ray Photoelectron Spectroscopy 10
1.5.5 **(**High Resolution) Transmission Electron Microscopy 11

1.6 Applications 11
1.6.1 Electrochemistry 11
1.6.2 Bioanalytical applications 12
1.6.3 *In vitro* biological studies 12
1.6.4 *In vivo* biological studies 15

1.7 Bibliography 17

2. Chapter 2- Aim of the project 19

3. Chapter 3- Results and Discussion 20

3.1 Characterization of pristine nanodiamonds 20
3.1.1 Detonation ultrananocrystalline diamonds 20
3.1.2 Commercial detonation ultrananocrystalline diamonds 22
3.1.3 Nanocrystalline diamonds 24

3.2 Oxidation 26
3.2.1 Oxidation using sulfonitric mixture 26
3.2.2 Oxidation using selective oxidation in air 28

3.3 Amidation 31

3.3.1 Amidation on ultrananocrystalline diamonds 31

3.4 Annealing 35
3.4.1 Study of annealing on commercial detonation nanodiamond 36

3.5 Cycloaddition reactions 38
3.5.1 Study of 1,3-dipolar cycloaddition of azomethine ylides 38

3.6 Arilation 42

3.7 Nitrene reaction 48

3.8 Functionalization of nanodiamonds with tumor-homing peptide 51
3.8.1 Synthesis of ND-c(RGDfK) and ND-AcPHSCNK-C(O)NH_2 conjugates 53
3.8.2 Synthesis of peptide conjugates by maleimide function 56

3.9 Study of biocompatibility of pristine and functionalized ultrananocrystalline diamonds 60

3.10 Bibliography 65

4. Experimental Part 67

4.1 Materials 67

4.2 Instrumentation 67
4.2.1 Thermogravimetric analysis 67
4.2.2 UV-visible spectra 67
4.2.3 IR spectra 67
4.2.4 Raman spectra 67
4.2.5 X-Ray Photoelectron Spectroscopy (XPS) 67
4.2.6 Transmission electron microscopy (TEM) 67
4.2.7 X-Ray Diffraction analysis (XRD) 68
4.2.8 Solid phase peptide synthesis (SPPS) 68
4.2.9 MALDI-TOF mass spectrometry 68
4.2.10 Reverse Phase-High Pressure Liquid Chromatography (RV-HPLC) 68
4.2.11 Thin layer chromatography 68
4.2.12 Flash column chromatography 68
4.2.13 Fluorescence spectroscopy 68
4.2.14 ^{1}H-Nuclear Magnetic Resonance (^{1}H-NMR) 69

4.3 Methods 69
4.3.1 Thermogravimetric analysis 69
4.3.2 Kaiser test 69
4.3.3 Raman spectroscopy 70
4.3.4 Transmission electron microscopy 70
4.3.5 X-ray photoelectron spectroscopy 71
4.3.6 X-ray powder diffraction 71
4.3.7 Solid-phase peptide synthesis 71

4.4 Experimental procedures 73
4.4.1 Amino acids synthesis 73
4.4.1.1 Synthesis of compound 1 74
4.4.1.2 Synthesis of compound 2 74
4.4.1.3 Synthesis of compound 3 75
4.4.1.4 Synthesis of compound 4 75
4.4.1.5 Synthesis of compound 5 75
4.4.1.6 Synthesis of compound 6 75
4.4.1.7 Synthesis of compound 7 76
4.4.2 Synthesis of azide derivative 76
4.4.2.1 Synthesis of compound 8 76
4.4.2.2 Synthesis of compound 9 77
4.4.2.3 Synthesis of compound 10 77

4.4.3 Synthesis of peptides 77
4.4.3.1 Synthesis of c(RGDfK) 77
4.4.3.2 Synthesis of NH_2-NGRSLC-C(O)NH_2 79
4.4.3.3 Synthesis of NH_2-FRVGVADVC-C(O)NH_2 80
4.4.3.4 Synthesis of N-acetylPHSCNK-C(O)NH_2 82
4.4.3.5 Synthesis of NH_2-CGFLGK(Rho)-C(O)NH_2 83

4.4.4 NDs functionalization 86
4.4.4.1 Oxidation using sulphuric and nitric acids 86
4.4.4.2 Synthesis of DND2-1 and DND2-3 86
4.4.4.3 Synthesis of DND2-2 and DND2-4 87
4.4.4.4 Synthesis of DND2-5 87
4.4.4.5 Synthesis of ANND3 88
4.4.4.6 Synthesis of ANND4 88
4.4.4.7 Synthesis of DND4-2, DND5-2, DND6-2 and DND7-2 88
4.4.4.8 Synthesis of DND4-5, DND5-5, DND6-5, DND7-5, DND4-6, DND5-6, DND6-6 and DND7-6 89
4.4.4.9 Synthesis of DND4-5A 90
4.4.4.10 Synthesis of DND4-5B 90
4.4.4.11 Synthesis of DND4-5C 90
4.4.4.12 Synthesis of DND5-7 90
4.4.4.13 Synthesis of DND4-9, DND5-8, DND6-7, DND7-7, ANND3-1, ANND4-1, DND4-10, DND5-9, DND6-8, DND7-8, ANND3-2, ANND4-2 91
4.4.4.14 Synthesis of DND4-9 and DND4-12 91
4.4.4.15 Synthesis of DND4-10 and DND4-13 91

4.4.4.16 Synthesis of DND4-11 and DND4-14 92
4.4.4.17 Synthesis of DND4-15 92
4.4.4.18 Synthesis of DND4-16 92
4.4.4.19 Synthesis of DND4-19 and DND4-21 92
4.4.4.20 Synthesis of DND4-20 and DND4-22 93
4.4.4.21 Synthesis of DND6-9, DND7-9, DND6-10, DND7-10 93
4.4.4.22 Synthesis of DND6-11, DND7-11, DND6-12, DND7-12, ANND3-3, ANND3-4, ANND4-3, ANND4-4 93
4.4.4.23 Synthesis of DND6-13, DND6-14, DND7-13, DND7-14 93

4.4.4.24 Synthesis of ANND1-1 93
4.4.4.25 Synthesis of ANND1-2 94
4.4.4.26 Synthesis of ANND1-3, ANND1-4 95
4.4.4.27 Synthesis of ANND1-5 95
4.4.4.28 Synthesis of ANND1-6 96
4.4.4.29 Synthesis of ANND1-7 96
4.4.4.30 Synthesis of ANND1-8 97

4.4.5 Bibliography 98

5. Conclusions 99

1. Introduction

1.1 Origin

In 1963 a Ukrainian physicist named Vladimir Danilenko found that the soot from the explosion of military explosive called Composition B (a mixture of 2-methyl-1,3,5-trinitrobenzene – TNT - and of 1,3,5-trinitroperhydro-1,3,5-triazine – RDX – still used in military) contained nanodiamond (ND) in high concentration.[1]
Nanodiamonds remain essentially unknown to the rest of the world until the end of the 1980s. Since about 1990, crude detonation nanodiamond is being produced on industrial scale mainly in Russia and China, using the overproduced stocks of Composition B as row material.
Only in 1987 there was the discovery of NDs in meteorites, announced by Lewis *et al*.[2] After a strong acid treatment of various minerals composing a meteorite, a greyish powder was obtained and diamond peaks in the X-ray diffraction patterns were observed. Moreover it was possible to date these nanodiamonds before the formation of the solar system for the presence of krypton and xenon anomalous isotopes of extra-solar origin.[3]

Nowadays, nanoscale diamonds are emerging as important materials for a variety of high performance technologies, thanks to their characteristics as the presence of a sp^3 diamond core and an alterable surface chemistry, the small primary particle size (from 4-5 nm to about 100 nm) and, in some cases, the fluorescence.

Nanodiamonds are characterized by a sp^3 diamond core, surrounded gradually by a distorted-strained diamond layer and by an envelope of non-crystalline carbon that is a mixture of sp^2 and sp^3 hybridized atoms. The surface of pristine nanodiamond particles contains a complex array of functional groups as carboxylic acids, esters, ethers, lactones, amines, etc. so several chemical modifications could be introduced in order to have a controlled surface chemistry.[4]

1.2 Synthesis and purification

The term “nanodiamond” is usually applied to several subjects: ND powders and suspensions obtained by detonation, nanocrystals obtained by fragmentation of large crystals grown at high temperatures and pressures from graphite, crystalline grains of nanocrystalline chemical vapour deposition (CVD) diamond films, ND crystals discovered in meteorites.

1.2.1 Detonation nanodiamonds

As already mentioned, nanodiamonds prepared by detonation (DND) were originally produced in the Soviet Union.[3] As starting material a mixture TNT and RDX is generally used, in a mass ratio ranging from 40:60 to 70:30, respectively. A shock wave produced by the detonator compresses and heats the composition mixture, leading to its explosion.[5] A large

amount of energy is released, reaching temperature and pressure values (T = 3000-4000 °C, P = 20-30 GPa) which correspond to the synthesis of the diamond particles.
As temperature and pressure decrease, carbon atoms condense into nanoclusters, coalescing into larger liquid droplets and crystallizing and when the pressure goes below the diamond-graphite equilibrium line in the carbon phase diagram, the growth of the diamond is then replaced by the formation of graphite (Figure 1.1).[4]

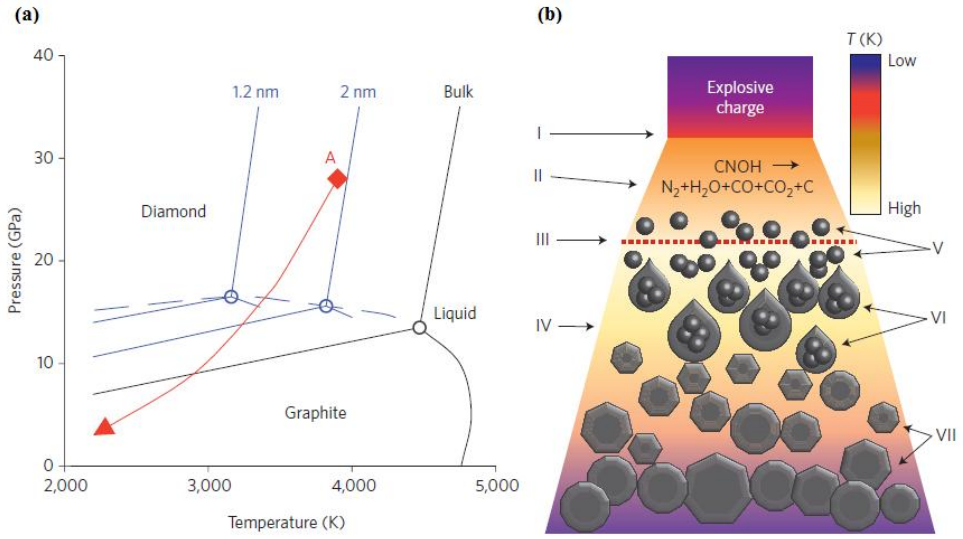

Fig. 1.1: (**a**) Phase diagram showing that during detonation temperature and pressure rise immediately reaching the Jouguet point (point A), as the temperature and pressure decrease following the isentrope (red line) and carbon atoms condense into nanoclusters. When the pressure goes under the diamond-graphite equilibrium line, the diamond formation is replaced by the graphite one. (**b**) Detonation wave propagation scheme showing the front of the shock wave (I), the area of chemical reactions (II), the Chapman-Jouguet plane corresponding to the (A) point in the previous graph (III), expanding detonation products (IV), presence of carbon nanoclusters and coagulation into liquid nanodroplets (V, VI), crystallization and growth of nanodiamonds (VII).[4]

The detonation takes place in a close steel chamber filled with an inert gas (dry synthesis) or water (wet synthesis) or ice (ice synthesis), in order to cool the system after the explosion and to avoid secondary reactions of the products.[6]
The average primary particle size of nanodiamonds generated by this technique is 4-5 nm, well suited for biomedical applications, which require high standard on nanodiamond purity so a post-synthesis process can be needed.
The detonation soot obtained from the chamber generally contains, in addition to the diamond phase, both graphite-like structures and incombustible impurities (metals and their oxides).
The powder can be subjected to thermal oxidation with nitric acid under pressure to separate the diamond phase from metals, which are dissolved, and non-diamond carbon, that is simultaneously oxidized. Other methods are based on the use of liquid oxidizers such as sulfuric acid, mixture of sulfuric and nitric acids or hydrochloric acid.[7]
Alternatively, DND can be purified from non-diamond carbon in an environmentally friendly manner, using a gas phase treatment with ozone at high temperatures.[8]

1.2.2 Synthesis of diamond from graphite in presence of metal catalysts

The first synthesis of diamond from graphite was successfully performed in 1955, by General Electric.[9] Depending on the metal catalyst used, the required pressure and temperature can vary in the range P = 5.0-7.0 GPa, T = 1300-1800 °C.[10] An increase of the synthesis time results in a growth of diamond crystals, while higher pressure and temperature during synthesis affect the graphite-diamond transformation. Actually, the so-called high-pressure-high-temperature (HPHT) synthesis is a well-known process, used to obtain submillimeter-sized crystals. These can then be used as starting material to produce diamond nanocrystals of less than 100 nm in size by mechanical milling.

The diamond crystals created by the HPHT technique are commonly used for polishing, cutting and grinding.

1.2.3 Synthesis by Chemical Vapor Deposition

In the late 1960s and 1970s, Dejaguin *et al.*[11] and Angus *et al.*[12] introduced the concept of activating mixture containing hydrogen and a hydrocarbon gas for low-pressure chemical vapour deposition (CVD) of diamond coatings. The CVD technique can be used to produce nanocrystalline diamond thin films with characteristics and properties, which depend on the nucleation and growth conditions.[13] In general with this process the diamond growth is very low, due to the high activation energy needed for the decomposition of methane on the surface of the diamond (230-243 kJ/mol). To enhance the process, carbon-containing compounds are dissociated by thermal, plasma or combustion treatments, having the so-called filament-assisted thermal CVD, plasma-enhanced CVD, combustion-flame-assisted CVD respectively (Figure 1.2).

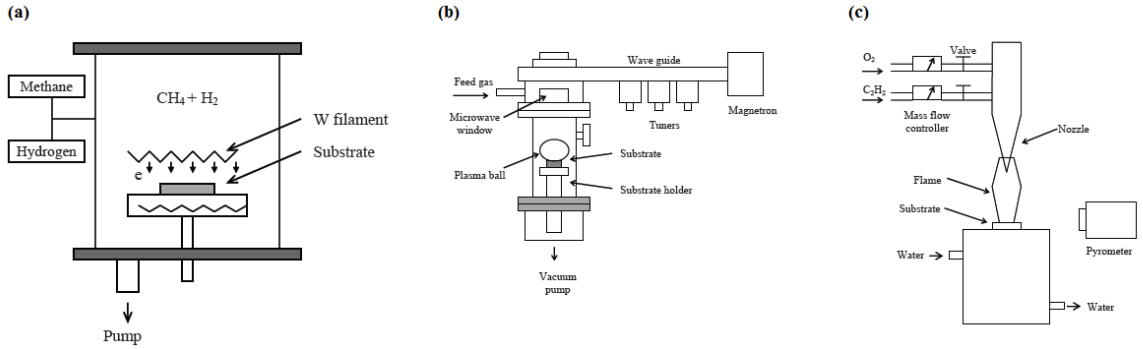

Fig. 1.2: Schematic diagrams of (**a**) filament-assisted (**b**) microwave-plasma combustion (**c**) combustion-flame-assisted apparatus.[13]

For all the CVD methods, the presence of atomic hydrogen for the process is required, because diamond is more stable towards atomic hydrogen than graphite. The first process is then the carbon deposition primarily in the form of graphite with a small amount of diamonds, the second is the selective etching of graphite by atomic hydrogen. The films are usually grown on non-diamond substrates (i.e. silicon wafers or silicon wafers coated with other materials, like metals or silicon dioxide) but treatments with diamond sources are necessary to start the nucleation process. Generally, the diamond growth takes place at substrate

temperature between 500 and 1200 °C, in order to avoid the graphite or diamond-like deposits.
The products obtained from CVD films are classified as ultra-nanocrystalline-diamond (UNCD) or nanocrystalline-diamond (NCD).[14] UNCD films are generally grown in argon-reach and hydrogen-poor atmosphere and they are characterized by crystalline grains of 2-5 nm size, containing significant sp^2-hybridzed carbon atoms. NCD films are formed using a hydrogen-rich environment and they have grain sizes up to 100-200 nm with moderate amounts of sp^2-carbon atoms.
Chemical and physical properties of NCD and UNCD determine possibility to use these materials in medical applications.[15]

1.3 Characteristics

1.3.1 Types of nanodiamonds

According to the primary particle size, nanodiamonds can be classified into nanocrystalline diamond particulate (10-100 nm), ultrananocrystalline diamond particulate (0-10 nm), diamondoids (1-2 nm) (Figure 1.3).[16]

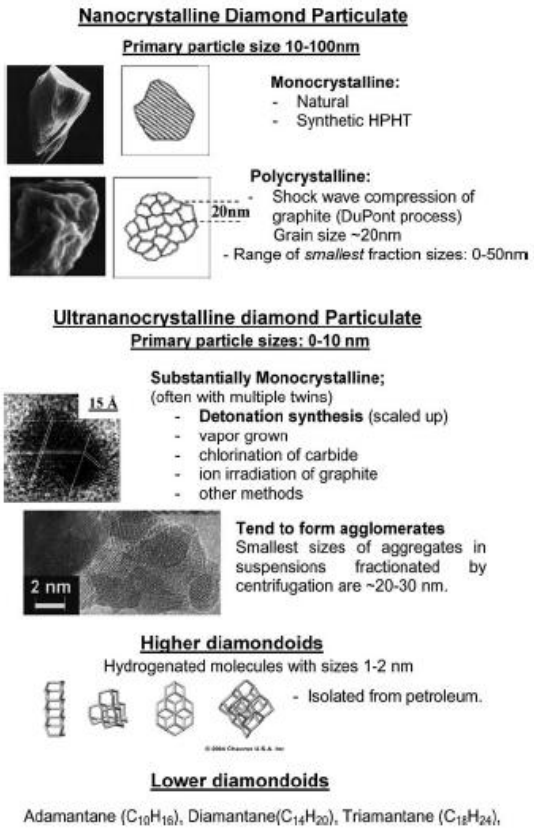

Fig. 1.3: Classification of nanodiamond particles based on their primary particle size: nanocrystalline particle, ultrananocrystalline particle, diamondoids.[16]

Nanocrystalline diamonds, containing up to 95-98% sp^3-bonded carbon, represent a very interesting material since they have been recently used as material to fabricate UV transparent electrodes on SiC,[17] or two dimensions photonic crystals.[18] The ultrananocrystalline diamond

particles are frequently used for bioapplication, such as protein adsorption, carriers of genetic materials, drug delivery. Diamondoids can be isolated from crude oil, natural gas and other hydrocarbon-rich materials but they can also be synthetized in the laboratory. Thanks to their high stability under extreme conditions, they can be used as internal standards for liquefaction studies of coal.[19]

1.3.2 Structure

Nanodiamond is generally described as a crystalline diamond core, surrounded by a shell composed by sp^2/sp^3 carbon and, depending on the synthesis and post-synthesis treatment, several kinds of groups could be present on the nanoparticles surface. The size of the diamond core is estimated to be about 3 nm, with the transient region made up of few layers (0.8-1.2 nm) for a particle 3.5-4.5 nm in size.[20]

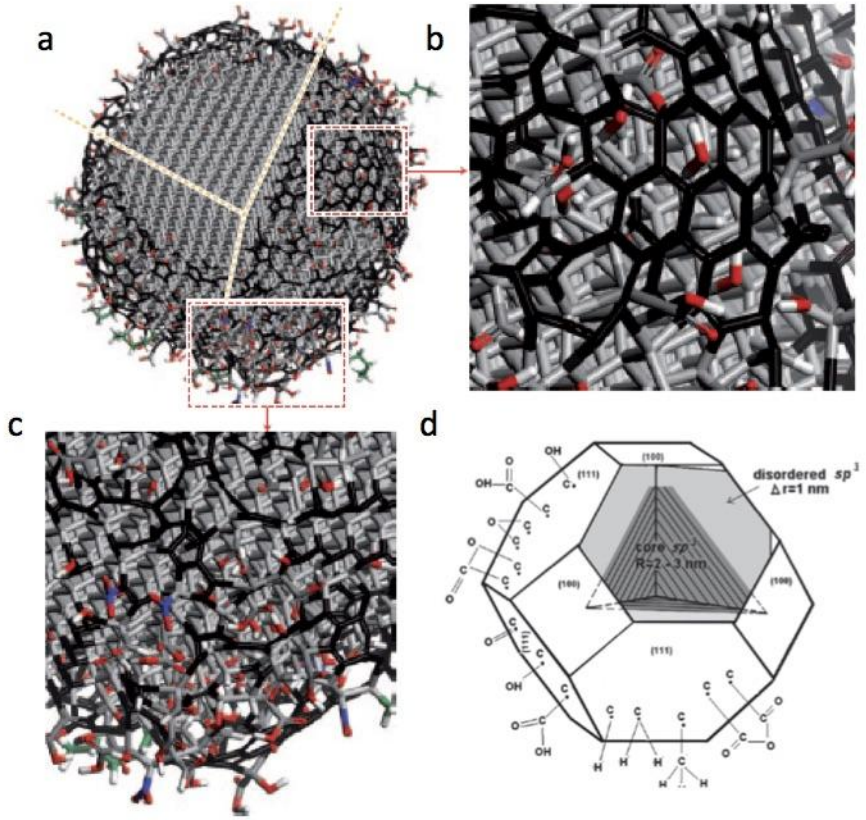

Fig. 1.4: (**a**) Schematic model showing the structure of a single ~5 nm nanodiamond after oxidative purification. The diamond core is covered by a layer of functional groups but the surface can present, after an annealing treatment, sp^2 carbon (black). A section of the particle has been cut along the dashed line and removed to show the inner sp^3-core. (**b**), (**c**) The majority of the surface atoms are terminated with oxygen-containing (blue) groups. Some hydrocarbon chains (green) and hydrogen (white) terminations are also present.[4] (**d**) Truncated octahedron model of DND structure with (100) and (111) surfaces. Various groups are shown on (111) faces as hydroxyl, carboxyl, epoxy, ester, anhydride, methyl, methylene groups.[19]

Theoretical studies on nanodiamonds have predicted both spherical and polyhedral structures. The first microimages of DND particles were performed on aggregated powders and the spherical shape observed in these images was due to the overlap of images of a large number of particles. It was possible to obtain the structure of single DND particles after solving aggregation problems by milling and annealing, followed by ultrasonic treatments and centrifugations.[21] High-resolution transmission electron microscope (HRTEM) images

provided then evidence of polyhedral (octahedral, truncated octahedral, cuboctahedral – Figure 1.5) shape of nanodiamonds.
Theoretical calculations have shown that the truncated octahedral structure is the best model to describe detonation nanodiamond particle, characterized by (111) faces by 76% and (100) faces by 24%.

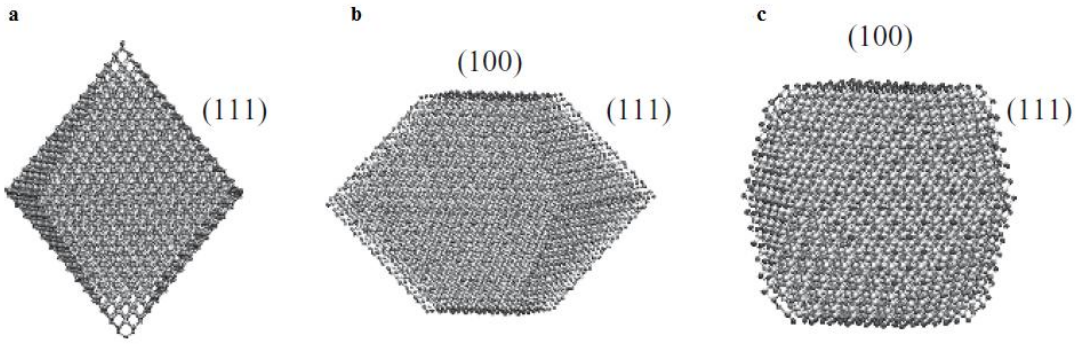

Fig. 1.5: Schematic (**a**) octahedral, (**b**) truncated octahedral and (**c**) cuboctahedral models of detonation nanodiamond morphologies.[21]

Nanodiamonds have a high surface area with respect to other nanoparticles, in fact particles of 0.5 μm in size have calculated area equal to 3 to 22 m^2/g, while for smaller particles it can be 250-450 m^2/g.

1.4 Surface functionalization

In comparison with carbon nanotubes and other graphitic carbon nanoparticles, the surface of nanodiamonds contains a complex array of groups, including carboxylic acids, esters, ethers, lactones, amines, etc. (Figure 1.6).
Reactions with hydrogen, chlorine, and fluorine have been explored in order to obtain a homogeneous surface and an enhanced reactivity, that allows to introduce other groups as in the case of chlorinated NDs, further modified with hydroxyls or amines.[22,23,24] Moreover, reactions of NDs with alkyl lithium, ethylenediamine and glycine ethyl ester hydrochloride generated alkyl-, amino- and glycine- functionalized NDs.[25]
After air purification or acid treatments, the nanodiamonds surface is covered by carboxylic groups. After being activate, they can be involved in esterification to give nanodiamonds terminated by long alkyl chain or biomolecules.[26,27,28]
Starting from nanodiamonds with carboxylic groups, hydrogenated nanodiamonds can be obtained by treatment in hydrogen microwave CVD plasma at temperatures above 700 °C. The wet chemistry is also used to obtain hydrogen-terminated nanodiamonds in milder conditions.
The annealing process generates nanodiamonds with sp^2 surfaces, on which reactions generally used on carbon nanotubes and fullerene can be applied. It is important to choose carefully temperature and pressure conditions in order to avoid modifications of the diamond

core. In fact, it was seen that high temperatures (>1000 °C) and long time of reaction can give origin to the so-called carbon-onion where the diamond core is replaced by graphitic shells.[29]
Annealed nanodiamond have been functionalized by means of Diels-Alder reactions and diazonium chemistry.[30] The last reaction was also used on hydrogenated nanodiamonds, in order to produce C-C bonds between the attached moiety and the diamond core, and with hydroxylated nanodiamonds to form C-O-C bonds.[31]
Most of the data obtained from functionalized nanodiamonds are qualitative so one challenge is to develop techniques for quantitative analysis of the groups present on the ND surface.

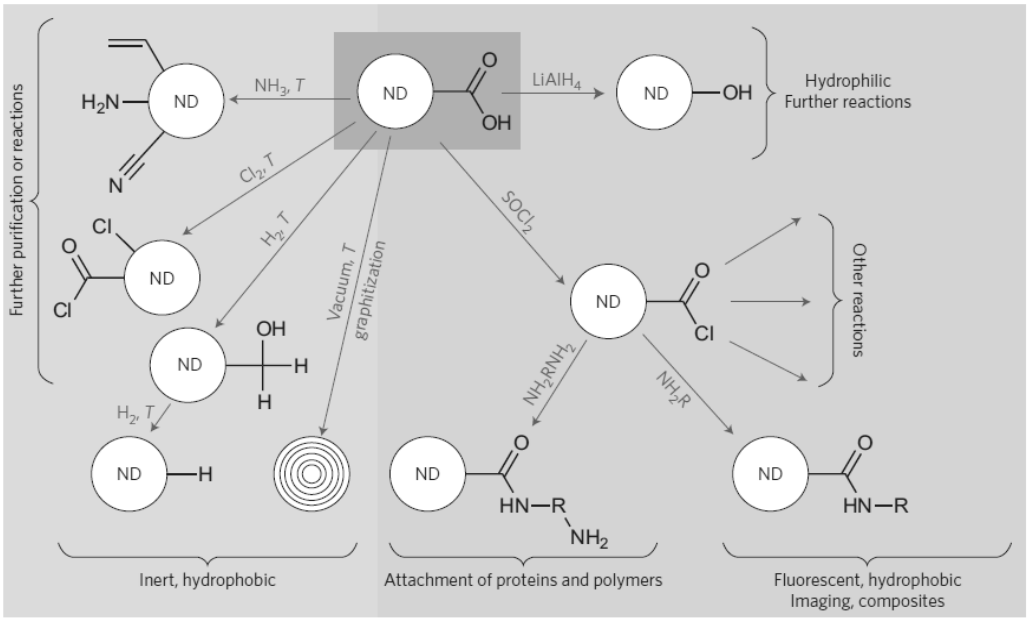

Fig. 1.6: Schematic representation of modifications of nanodiamonds surface. The –COOH groups can be modified by high-temperature gas treatments (left) or ambient-temperature wet chemistry techniques (right).[4]

1.5 Characterization methods

1.5.1 Raman Spectroscopy

Raman scattering (RS) spectroscopy has broad application in diagnostic of carbon-based materials, in fact the method is non-destructive, it requires a small amount of material and each allotropic form of carbon is identifiable by its Raman spectrum.
Raman spectra of nanodiamonds can depend on purity, sp^3/sp^2 ratio, crystal size and surface chemistry. For nanodiamonds of few nanometers size, the peak at 1328 cm^{-1}, due to the RS-active diamond lattice vibrations, is broad and down-shifted with respect to bulk diamond (Figure 1.7). Only recently the peak at about 1140 cm^{-1} was assigned to *trans*-polyacetylene vibrations[32] and the shoulder at ~1250 cm^{-1} is attributed to smaller nanodiamond particles or, in larger nanodiamond particles, to smaller domains separated by defects.[33]
The broad band at 1500-1800 cm^{-1} depends on several contributions: the graphitic carbon band at 1590 cm^{-1}, an O-H bending peak at 1640 cm^{-1} and a shoulder at 1740-1760 cm^{-1} due to the C=O stretching coming from surface functional groups.[34]

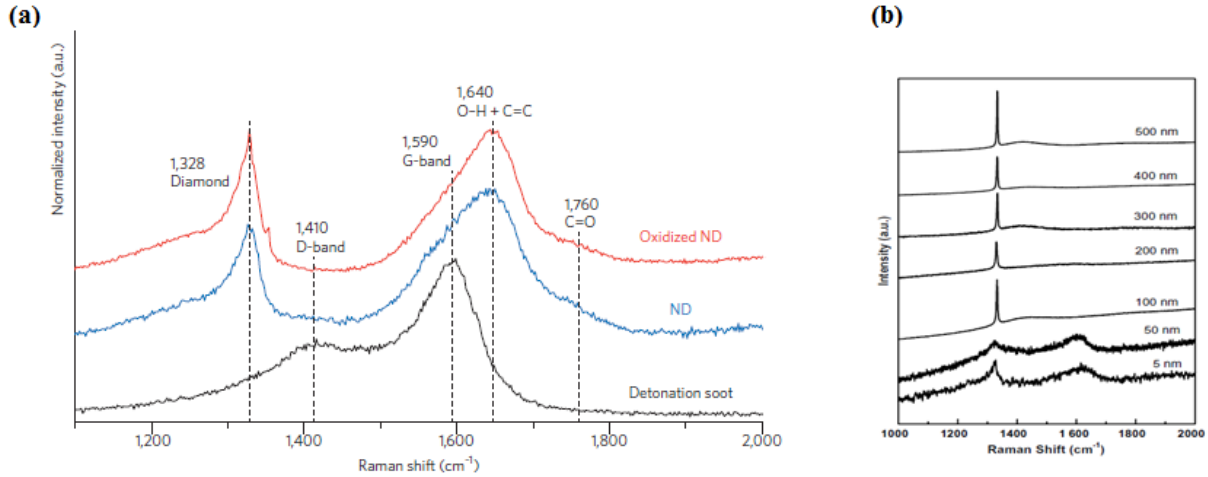

Fig. 1.7: (**a**) Raman spectra of detonation soot (black line), purified (blue line) and oxidized 5 nm nanodiamonds (red line). Diamonds cores in detonation soot seem to be totally covered by graphitic shells so the Raman spectrum is dominated by the G-band of graphitic carbon at 1590 cm^{-1}. Purified and oxidized nanodiamonds have the diamond peak at 1328 cm^{-1}. The broad band at 1500-1800 cm^{-1} is due to surface functional groups and adsorbed molecules with a contribution of sp^2 carbons. Raman spectra were recorded at 325 nm.[4] (**b**) Raman spectra of different sizes nanodiamonds recorded at 532 nm. The diamond peak becomes more pronounced by increasing the size of the nanoparticle.[35]

For nanodiamonds of hundreds nanometers size, Raman spectra have similar behaviour, with an intense diamond peak at 1332 cm^{-1} and traces of graphitic/amorphous carbon at 1400 cm^{-1}. In this case the structure is usually explained as diamond polycrystal with graphitic form on the surface.

1.5.2 Infrared Spectroscopy

Infrared (IR) spectroscopy provides information about the nature of functional groups and adsorbed molecules on the surface of nanodiamonds. Most characteristic features after oxidation treatment include the O-H stretching (3200-3600 cm^{-1}) and bending (1630-1640 cm^{-1}), due to both alcoholic groups covalently attached to the surface and adsorbed species, C=O stretching (1700-1800 cm^{-1}) that can be part of a ketone, aldehyde, ester, carboxylic acid or lactone and C-H stretching for the presence of CH_2 and CH_3 groups. Moreover, nitrogen defects can give two broad bands in the region 1100-2500 cm^{-1}. Most of the nanodiamonds have a broad absorption at 1000-1500 cm^{-1} (the so-called "fingerprint region") that is an overlapping of C-O-C stretching vibrations, epoxy C-O stretching, C-C stretching, and amide C-N stretching.

Tu *et al.* studied the size dependent C=O stretching (between 1680 and 1820 cm^{-1}) for particle diameter sizes from 5 to 500 nm.[36] The peak was detected at 1820 cm^{-1} for NDs of 500 nm and, decreasing the particle size, it was down-shifted to 1750 cm^{-1} (Figure 1.8). The authors explained this behaviour as result of hydrogen bond formation between the –COOH groups in the carboxylated nanodiamond surfaces.

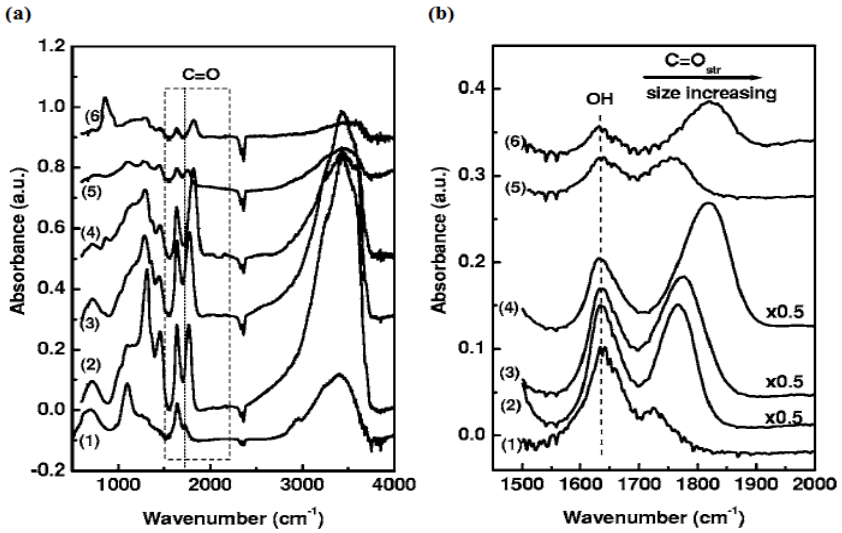

Fig. 1.8: (**a**) The surface C=O spectra of different size nanodiamonds (1) 5 nm, (2) 100 nm, (3) 200 nm, (4) 300 nm, (5) 400 nm, (6) 500 nm. (**b**) Enlarged spectra of the C=O stretching.[36]

1.5.3 Fluorescence

Fluorescence properties of diamond were studied for the first time in the 1950s. Based on the presence or absence of nitrogen impurities in the crystal lattice structure, natural diamonds are classified as type I or type II, respectively. The arrangement of nitrogen impurities is used to sub-classify type I diamonds into type Ia and type Ib. In the first case diamonds comprise an aggregated form of nitrogen, while type Ib contains atomically dispersed single nitrogen impurities. Diamonds synthetized by HPHT method are known to contain a high amount of nitrogen as impurity. Irradiation damage of type Ib diamond crystals creates intrinsic defects such as vacancies that, after thermal annealing, move towards nitrogen centers and become trapped within to form N-V color defect centers. After 2 hours of annealing at 800 °C, irradiated synthetic type Ib NDs mainly generated two types of N-V defect centers: neutral nitrogen vacancy, $(N\text{-}V)^0$, and negatively charged nitrogen vacancy, $(N\text{-}V)^-$.[37] The last defect center absorbs light photons at ~ 560 nm and fluoresces at ~ 700 nm with a quantum efficiency close to 1. The extreme photostability provides a great advantage to NDs so they emerged as an excellent candidate for long-term cellular imaging over commonly used fluorophores (Figure 1.9).[38]

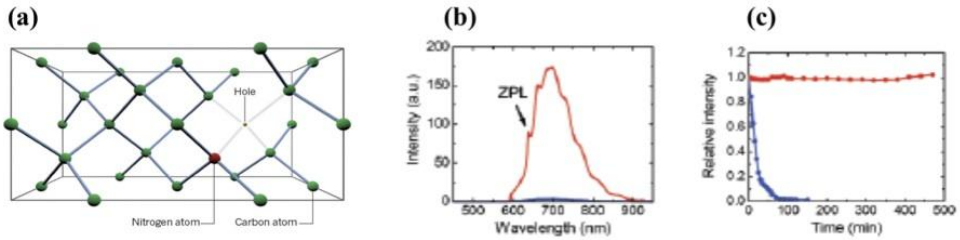

Fig. 1.9: (**a**) Structure of the nitrogen-vacancy defect $(N\text{-}V)^-$ in diamond. (**b**) Fluorescence spectra of annealed NDs with (red) or without (blue) proton beam irradiation. The excitation was made at 510-560 nm and the emission was collected at λ>590 nm. (**c**) Photostability test on fluorescent NDs (red) and polystyrene nanospheres (blue) excited under same conditions.[39]

A high efficient photoluminescence originates from the silicon-vacancy (Si-V) complex, with zero-phonon line (ZPL) at 738 nm, reported in ultrananocrystalline particles. These defects are structurally similar to the N-V centers, with a silicon atom close to a vacancy. The SiV defect offers several advantages over the N-V defects. For instance, the Si-V transition occurs at 738 nm, a wavelength far from the typical broadband photoluminescence of nanodiamond spread between 450 nm and 650 nm (Figure 1.10).[40]

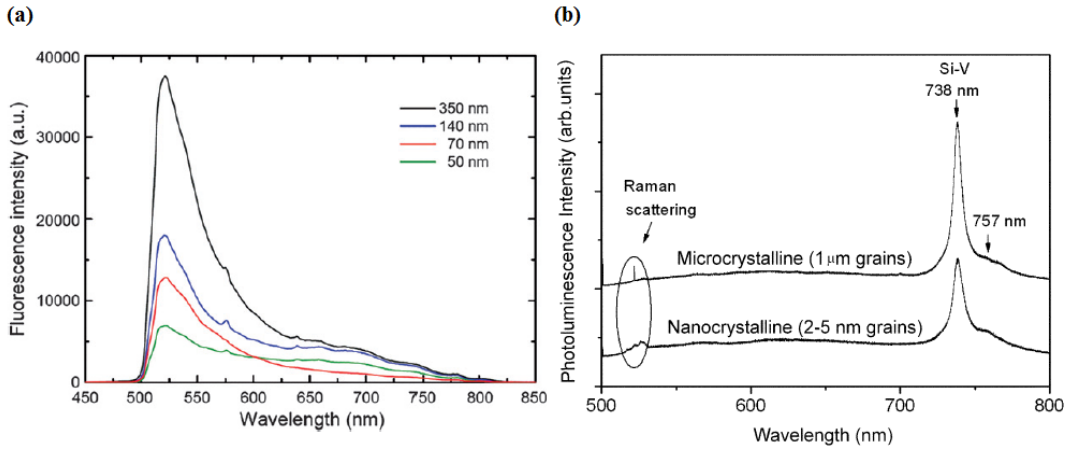

Fig. 1.10: (**a**) Size-dependent fluorescence spectra of green fluorescent NDs, prepared by 40keV He^+ irradiation. Excitation at 473 nm and emission collection at > 500 nm. (**b**) Photoluminescence spectra of ultrananocrystalline diamond (2-5 nm grain size, 1 μm film thickness) and microcrystalline diamond (1 mm grain size, 3 μm film thickness). Excitation at 488 nm.[40]

1.5.4 X-Ray Photoelectron Spectroscopy (XRD)

X-ray photoelectron diffraction (XRD) is widely used to investigate the structures of various materials. This technique can give information about purity, size and structure of the nanodiamonds. The typical XRD pattern of nanodiamonds is characterized by the presence of the peak at 2θ = 44° that correspond to the (111) surface of the diamond core, and of the peak at 2θ = 75° related to the diamond (220).

Shenderova *et al.* have shown how the starting material influences the XRD pattern of nanodiamonds, in fact, if the precursor is graphite, rather strong peaks from graphite and from other similar phases are present. This can be evinced by a broad band at 2θ = 26.9° and a number of superimposed peaks (Figure 1.11).[41]

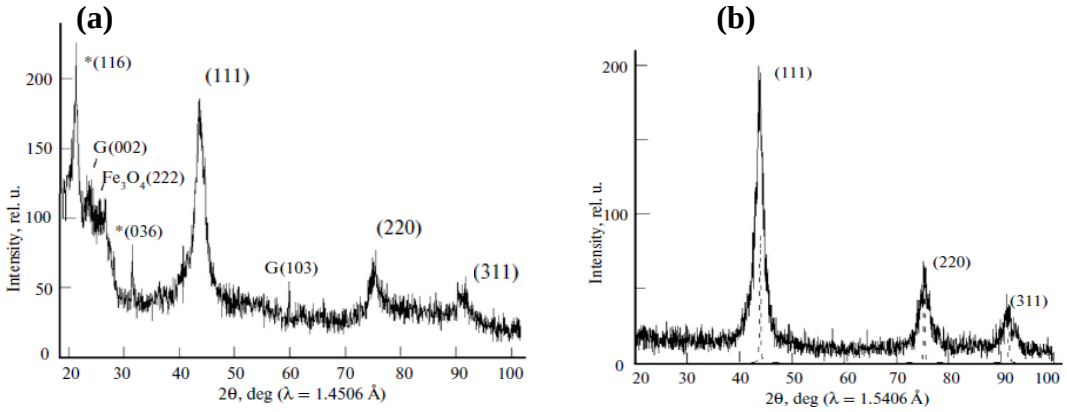

Fig. 1.11: (**a**) XRD pattern of detonation nanodiamond containing soot. It is possible to observe reflections of impurity phases of graphite (G), Fe_3O_4. (**b**) XRD pattern of purified detonation nanodiamond, typical (111), (220) and (311) peaks are detected.[42]

1.5.5 (High Resolution) Transmission Electron Microscopy

Transmission electron microscopy (TEM) is a useful technique to analyse dimensions, shapes and purity of diamond nanoparticles. Nanocrystalline diamonds are characterized by an irregular shape and, depending on the synthesis and purifications, populations of different nanometers size can be recovered. The shape of ultrananocrystalline particles is almost spherical, with an average size equal to 5 nm. By high resolution transmission electron microscopy (HRTEM) the diamond core is easily recognized by the presence of straight lines that correspond to the (111) surfaces (Figure 1.12). The fringe spacing calculated is equal to 0.206 nm. The HRTEM could be helpful to recognise inside nanoparticles the presence of structural defects.[43]

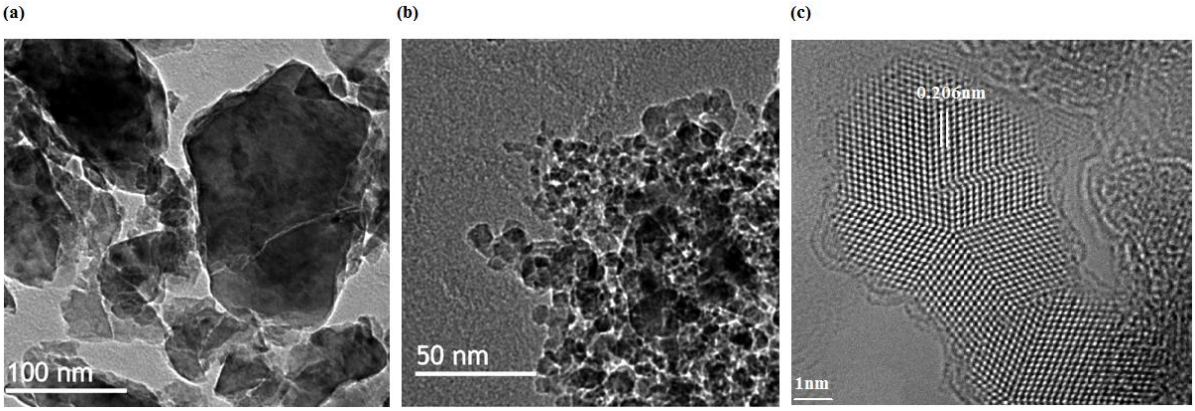

Fig. 1.12: TEM images of (**a**) nanocrystalline particles (**b**) ultrananocystalline particles (**c**) HRTEM image of ultrananocrystalline particles. Straight lines correspond to the (111) surfaces of the diamond core with fringe spacing equal to 0.206 nm.[43,44]

1.6 Applications

1.6.1 Electrochemistry

Microcrystalline and nanocrystalline doped diamond films are well-known electrode materials. In fact, the diamond is generally considered as an insulator, with a band gap of 5.47 eV, and the boron is the most widely used dopant to produce conducting diamond electrodes. Diamond electrodes are characterized by a very high overpotential for both oxygen and hydrogen evolution, giving in this way the widest potential window known for aqueous solutions (3.5 V). Furthermore, these electrodes have a very low capacitance (high signal-to-noise ratio) and no surface oxide formation and reduction reactions are observed, typical of metal and metal oxide electrode materials. Considering these unique properties, doped diamond electrodes can be used for inorganic and organic electrosynthesis, electroanalytical applications and bioelectrochemical applications as biosensors.

Detonation nanodiamonds have an electrically insulating core but the surface atoms (about 15 %) can play a role in the charge transfer in electrode-immobilized DND. It was seen that the oxidation of DND powder by heat treatment in air gave an increase in the redox activity while surface-hydrogenated DNDs presented a decreased one.

Differential impulse voltammetry of the electrode-DND layers without redox species has shown oxidation and reduction peaks that can be attributed only to direct electron transfer reactions of the NDs. Holt *et al.* suggested a mechanism explaining the DND electroactivity.[45] DND surfaces contain unsaturated carbon bonds (C=C) and carbonyl groups (C=O), and the electron transfer takes place between these particles and redox species in solution or the electrode (Figure 1.13). A reversible reduction of these nanoparticles can occur through the electron transfer into unoccupied surface states, available as a consequence of unsaturated bonding on the surface layer of DND, at defined potentials so DNDs are source and sink of electrons for the redox reactions in solution.

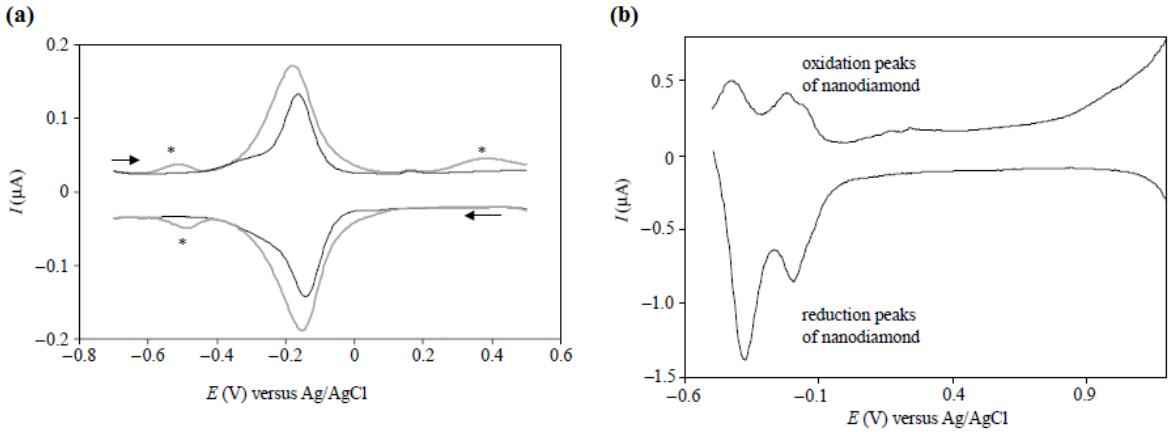

Fig. 1.13: (**a**) Differential pulse voltammogram of graphite electrode (black line) and graphite electrode with drop-coated layer of 5 nm ND (grey line) in 1 mM hexaammineruthenium (III) ($Ru(NH_3)_6^{3+}$) with 0.1 M KCl. The signed peaks are detected only in presence of the ND layer. (**b**) Differential pulse voltammogram of glassy carbon electrode, with a layer of ND-mineral oil paste distributed on the surface, in 0.1 M KCl. Peaks show the reduction and the oxidation of ND layer.[45]

1.6.2 Bioanalytical applications

The highly developed surface and the presence of different kinds of groups that can be modified make nanodiamonds good candidates for several bionalytical applications. In fact, they can be used as sorbents in different kinds of chromatography such as liquid adsorption (normal and high pressure), gas, ion exchange and affinity.[46] Literature contains also information on the use of nanodiamonds as stationary phase in gas chromatography and high-performance liquid chromatography (HPLC).[47]

Moreover, considering their high affinity for proteins and peptides, nanodiamonds can be employed in solid-phase extractions. For example, 100 nm size DNDs were used to isolate proteins as myoglobin, cytochrome c, bovine serum albumin from diluted solutions.[48] In particular, it was demonstrated that the binding capacity of DND for the sorption of lysozyme was ten times greater than silica gel powder with the same dimension (100 nm). This was assigned to the larger surface area of porous nanodiamond aggregates with respect to silica gel so each protein can occupy 10 nm^2 in the first case, and 2 nm^2 on the silica substrate.[49]

1.6.3 *In vitro* biological studies

Several studies suggested that nanodiamonds can be internalized into cells and interact with organelles and, depending on their structural properties and on the possibility to modify their surface, they can be used as cellular biomarkers.

As mentioned, nanodiamonds with nitrogen vacancy centers are fluorescent in the red and the green regions and their fluorescence is strong enough to allow intracellular imaging of a single nanoparticle. Moreover the emission in the red region (575-750 nm) permits to study easily these systems since the inherent cellular fluorescence involves the 300-500 nm region. Moreover, these emitters are photostable and no photobleaching is observed for 300 seconds while for common organic dyes it takes place in about 10 seconds.[38,39b,40,50]

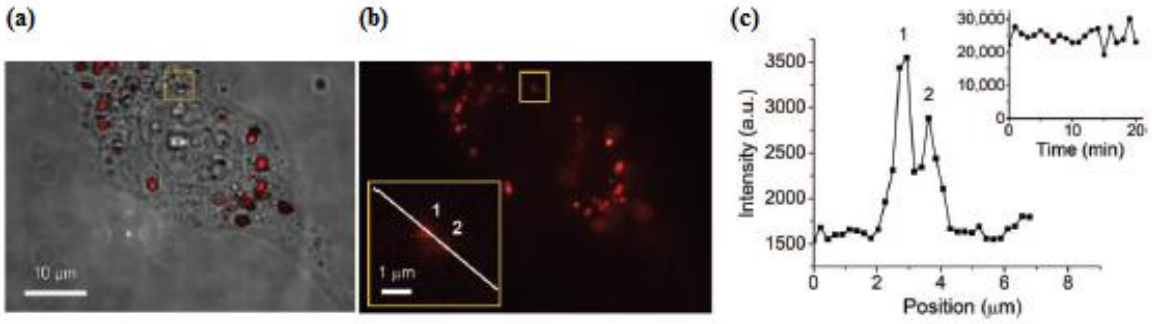

Fig. 1.14: (**a**) Bright-field and epifluorescence images of HeLa cell after uptake of 35 nm NDs. Most of NDs are localized in the cytoplasm. (**b**) Epifluorescence image of the HeLa cell. In the inset the distance between two NDs is about 1 μm. (**c**) Intensity profile obtained following the line traced in B inset. Integrated fluorescence intensity as function of time. No photobleaching was detected after continuous excitation of particles for 20 minutes.[51]

Carboxyl-modified nanodiamonds were covalently functionalized with poly-L-lysine, followed by non-covalent adsorption of DNA. It was observed that these systems were able to penetrate HeLa cells and their localization in the cytoplasm was detected by their fluorescence, which was not quenched (Figure 1.14).[51] Moreover, using appropriate targeting molecules, it was possible to selectively address ND-conjugates to intracellular structures such as mitochondria.[52]

It was observed that the presence of graphitic shells on 5 nm NDs can quench the luminescence, while an oxidative treatment can restore it.[53] Fluorescent particles can also be produced by linking or adsorbing organic dyes onto the carbon core. For example, thionine, a fluorescent dye, was covalently attached to oxidized DNDs via a silyl linker and the system was able to penetrate through cellular membranes and to reach nuclei without causing damages to the cells.[54]

Another way to visualize NDs in living structures is the confocal Raman spectroscopy, since the diamond peak at 1332 cm^{-1} is quite intense and narrow (especially for diamonds with dimensions of 50 nm and above) and it is not affected by the surface functional groups or the bounded biomolecules. Moreover, Raman investigation is a non-invasive method, can be used in ambient conditions and it does not require physical or chemical treatment of the nanodiamonds. By mapping the Raman signal, it was possible to demonstrate that DND-lysozyme complex was able to penetrate *E. coli* bacteria, unlike uncoated nanodiamonds.[55]

The interaction of carboxylated nanodiamonds (average diameters 5-100 nm) with A549 human lung epithelial cells, their undamaging penetration and their accumulation was detected using both Raman and fluorescence signals (Figure 1.15).[56]

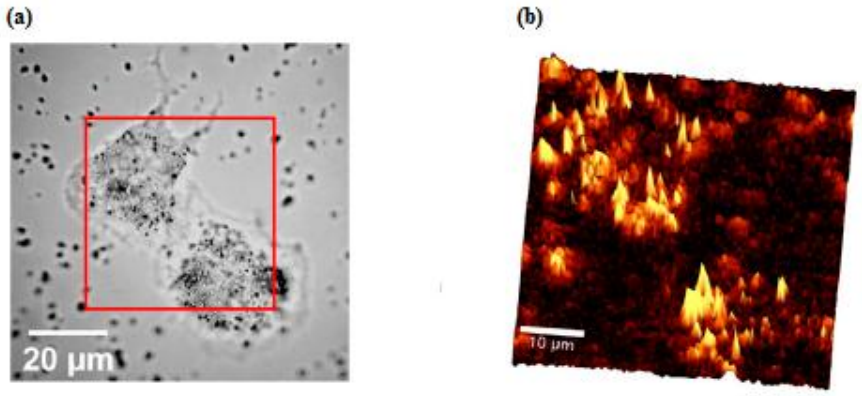

Fig. 1.15: (**a**) Optical microscope images of two A549 cells. (**b**) Confocal Raman mapping locked on the diamond signals reveals the positions of carboxylated-ND aggregates in A549 cells.[56]

Because of their high refraction index, nanodiamonds are good scattering optical labels, in fact it was observed that a diamond nanoparticle of 55 nm can appear 300 times brighter than a cellular organelle of the same size.[57] Due to this property, nanodiamonds can be visualized by differential interference contrast microscopy, useful for large (more than 40 nm) particles (Figure 1.16).[58]

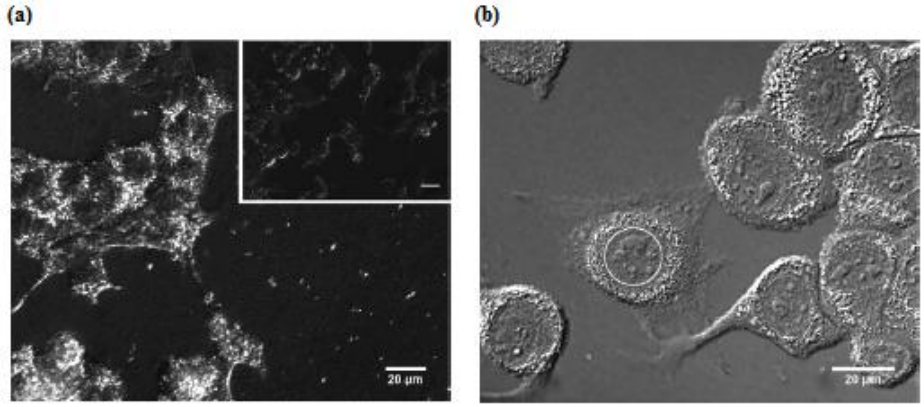

Fig. 1.16: Contrast enhanced images of NDs deposited into cells (**a**) Hoffman modulation contrast of live 293T cells. NDs contrast strongly with the cell background, shown in the inset. (**b**) Differential interference contrast image of fixed 3T3 cells, NDs are visible as bright rims around the impermeable nuclei (a nucleus is labelled with a circle).[58]

By using Raman and fluorescence techniques it was observed that the mechanism responsible for nanodiamonds internalizations depends on the nature on the cell lines involved and on the nature of the surface and size of the nanodiamonds themselves. NDs were internalized in cells generally via the endocytosis, and a not receptor-mediated mechanism was found, for example, for the internalization of carboxylated nanodiamonds by human embryo kidney cells 293T, normal human fibroblast HFL-1, human epithelial lung cells A549. Moreover Faklaris *at al*. demonstrated that nanodiamonds of 46 nm in size are internalized into HeLa cells mostly by clathrin-mediated endocytosis after 2 hours of incubation.[59] As for other nanoparticles, the surface of nanodiamond can be functionalized with various biological ligands in order to increase their ability to penetrate cells or to prefer a specific pathway to be internalized.

After the penetration, a perinuclear localization of nanodiamonds was observed but Fenton-treated nanodiamonds were found in the nucleus of HeLa cells.[54,59a]
The biocompatibility of nanodiamonds (size 2-10 nm) was first demonstrated in neuroblastoma, keranocyte, macrophage and PC-12 cells.[60] Concentrations up to 100 μg/ml were not cytotoxic over 24 hours of incubation and nanodiamonds showed higher biocompatibility with respect to single- and multiwalled carbon nanotubes and carbon black in neuroblastoma and alveolar macrophage cells.
Similarly, Liu *at al.* have shown that the toxicity of carboxylated carbon nanotubes on human lung A549 epithelial cells and HFL-1 normal fibroblast was significantly higher than for carboxylated nanodiamonds (size 5 and 100 nm).[59d] Although the effect of nanodiamonds size has not been shown to play a key role in biocompatibility, 5 nm diameter NDs have more than the 15% of carbon atoms on their surface so they show different properties than larger as 100 nm NDs.[36]
Considering their biocompatibility and low toxicity, nanodiamonds can be used to delivery drugs into cells. Moreover, it was found in several studies that a compound (covalently or not) immobilized on nanodiamonds retains almost completely its native activity. For example, selective antibodies attached to fluorescent nanodiamonds were still able to target actinic filaments.[52] It was also observed that a growth hormone molecule, covalently conjugated to 100 nm diameter carboxylated nanodiamonds, was specifically recognised to growth hormone receptors of A549 cells.[61]

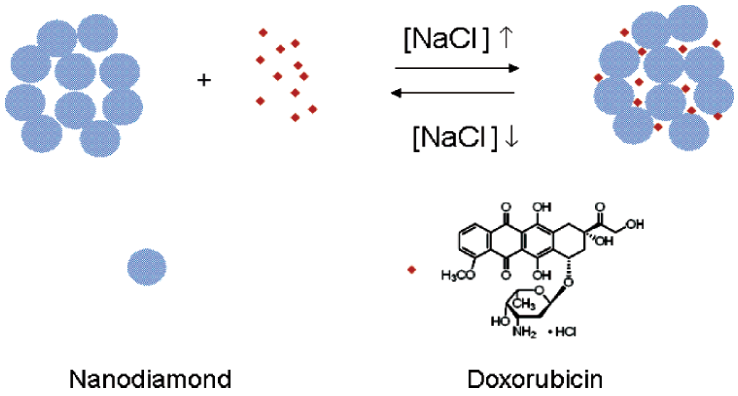

Fig. 1.17: Controlled NaCl-mediated loading and release of doxorubicin hydrochloride. The addition of the salt induces the functionalization of the drug onto the nanodiamond aggregate surface, the removal of the salt induces the drug release.[62]

In 2007 Ho and coworkers reported the suitability of nanodiamonds to act as delivery agent of doxorubicin hydrochloride (DOX). The study was performed considering that the presence of carboxylic and hydroxyl groups on the surface of the nanoparticles allows the interaction with the amine groups of DOX via ionic forces. Moreover, it was possible to observe that this process was reversible and mediated by properly varying the concentration of Cl^- ions (Figure 1.17).[62]

1.6.4 *In vivo* studies

Nanodiamonds can be used not only in drug delivery, but also for coating medical implants and imaging detection so a key requirement is the study of possible biological consequences

of NDs presence into organisms. Moreover, considering that detonation nanodiamonds are produced as powder with low density, and they tend to spread in the air during the production procedures, several studies related to their toxicity on the respiratory system were performed. Intratracheal instillation of NDs (diameter of 4 and 50 nm) was studied in mice and a low pulmonary toxicity was found according to the hystopathological and ultrastructural investigations. Moreover, no peroxidation of the lungs was observed. Based on the HRTEM images of alveoli and bronchia at different time points, NDs engulfed by macrophages on the alveolar surface migrate upward, move up with mucus to the trachea by the mucociliary system and then they enter to the pharynx.[63] The toxicity of NDs administered by intratracheal instillation was studied also by Zhu *et al.* and a dose-dependent response was detected in the lung, liver, kidney and blood.[64]

Yuan *et al.* have found that 50 nm NDs intravenously injected in mice predominantly accumulated in liver, lung and spleen, in fact about the 60% of the injected NDs were found in the mouse liver 30 minutes after the administration and the level was maintained over 28 days.[65]

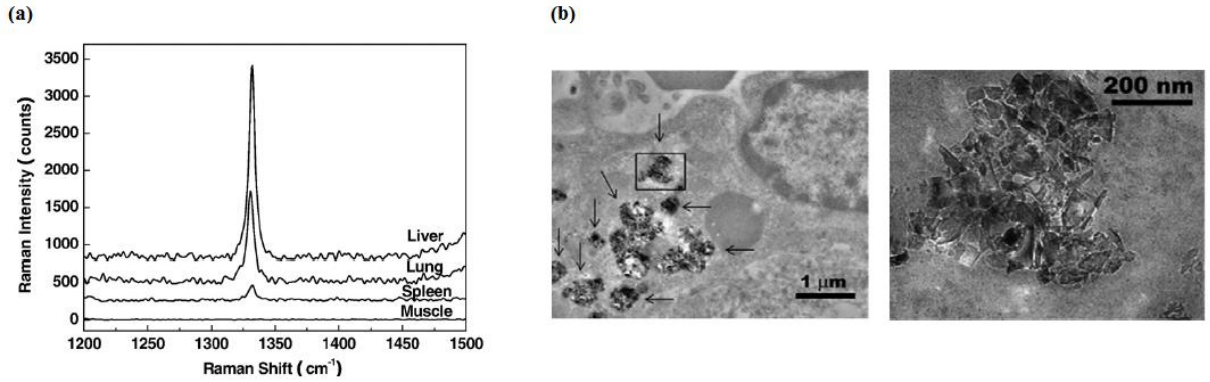

Fig. 1.18: (**a**) Raman spectra (recorded at 532 nm) of digested solutions of mouse tissues 28 days after exposure to NDs. (**b**) TEM images of liver sections from mice exposed to 20 mg/kg body weight and sacrificed at day 28 post exposure. Black arrows show NDs entrapped in phagosomes.[65]

1.7 Bibliography

[1] V. V. Danilenko, *Phys. Sol. Stat.* **2004**, 46, 595
[2] R. S. Lewis, T. Ming, J. E. Wacker, E. Anders, E. Steel, *Nature* **1987**, *326*, 160
[3] O. Shenderova, D. Gruen, *Synthesis, Properties and Applications of Ultrananocrystalline Diamond*, Springer **2005**
[4] V. N. Mochalin, O. Shenderova, D. Ho, Y. Gogotsi, *Nat. Nanotechnol.* **2011**, *7*, 11
[5] R. Kaur, I. Badea, *Int. J. Nanomedicine* **2013**, *8*, 203
[6] A. Y. Vul', O.A. Shenderova, *Detonation Nanodiamonds*, Pan Stanford Publishing 2013
[7] a) V.Y Dolmatov, *Russ. Chem. Rev*. **2001**, *70*, 607; b) A.M. Schrand, S. A. C. Hens, O. A. Shenderova, *Crit. Rev. Solid State Mater. Sci.* **2009**, *34*, 18
[8] Method for removal of impurities of non-diamond carbon and device for its realization, E. V. Pavlov, J. A. Skrjabin, RU Patent 2019502, **1994**
[9] F. P. Bundy, H. T. Hall, H. M. Strong, R. H. Wentorf, *Nature* **1955**, *176*, 51
[10] R. Abbaschian, H. Zhu, C. Clarke, *Diam. Relat. Mater.* **2005**, *14*, 1916
[11] B. V. Derjaguin, D. B. Fedoseev, *Sci. Am.* **1975**, *233*, 102
[12] C. Angus, H. A. Will, W.S. Stanko, *J. Appl. Phys.* **1968**, *39*, 2915
[13] J. J. Gracio, Q. H. Fan, J. C. Madaleno, *J. Phys. D: Appl. Phys.* **2010**, *43*, 37
[14] J. E. Butler, A. V. Sumant, *Chem., Vap. Depos.* **2008**, *14*, 145
[15] a) W. S. Yang, O. Auciello, J. E. Butler, W. Cai, J. A. Carlisle, J. Gerbi, D. M. Gruen, T. Knickerbocker, T. L. Lasseter, J. N. Russel, L. M. Smith, R. J. Hamers, *Nature Mater*. **2002**, *1*, 253; b) W. S. Yang, J. E. Butler, J. N. Russel, R. J. Hamers, *Analyst* **2007**, *132*, 296
[16] A. M. Schrand, S. A. C. Hens, O. A. Shenderova, *Crit. Rev. Solid State Mater. Sci.* **2009**, *34*, 18
[17] M. J. Tadjer, K. D. Hobart, J. D. Caldwell, J. E. Butler, K. X. Liu, J. C. R. Eddy,D. K.Gaskill, K. K. Lew, B. L. Van Mil, R. L. Myers-Ward, M. G. Ancona, F. J. Kub, T. I. Feygelson, *Appl. Phys. Lett.* **2007**, *91*, 163508
[18] W. Baldwin, M. Zalalutdinov, T. Feygelson, J. E. Butler, B. H. Houston, *J. Vac. Sci. Technol. B* **2006**, *24*, 50
[19] H. Schwertfeger, A. A. Fokin, P. R. Schreiner, *Angew. Chemie Int. Ed.* **2008**, *47*, 1022
[20] a) O. O. Mykhaylyk, Y. M. Solonin, D. N. Batchelder, R. Brydson, *J. Appl. Phys.* **2005**, *97*, 074302; b) I. I. Kulakova, *Phys. Solid State* **2004**, *46*, 636
[21] A. Krüger, F. Kataoka, M. Ozawa,T. Fujino, Y. Suzuki, A. E. Aleksenskii, A. Y. Vul', E. Osawa, *Carbon N. Y.* **2005**, *43*, 1722
[22] T. Tsubota, S. Tanii, S. Ida, M. Nagata, Y. Matsumoto, *Diam. Relat. Mater.* **2004**, *13*, 1093
[23] S. Ida, T. Tsubota, S. Tanii, M. Nagata, Y. Matsumoto, *Langmuir* **2003**, *19*, 9693
[24] T. Ando, M. Nishitani-Gamo, R. E. Rawles, K. Yamamoto, M. Kamo, Y. Sato, *Diam. Relat. Mater.* **1996**, *5*, 1136
[25] Y. Liu, Z. Gu, J. L. Margrave, V. N. Khabashesku, *Chem. Mater.* **2004**, *16*, 3924
[26] A. Krueger, J. Stegk, Y. J. Liang, L. Lu, G. Jarre, *Langmuir* **2008**, *24*, 4200
[27] A. Krueger, *Chem. Eur. J.* **2008**, 14, 1382
[28] A. Kruger, Y. J. Liang, G. Jarre, J. Stegk, *J. Mater. Chem.* **2006**, *16*, 2322
[29]) J. Chen, S. Z. Deng, J. Chen, Z. X. Yu, N. S. Xu, *Appl. Phys. Lett.* **1999**, *74*, 3651; b) D. Lang, A. Krueger, *Diam. Relat. Mater.* **2011**, *20*, 101
[30]) G. Jarre, Y. J. Liang, P. Betz, D. Lang, A. Krueger, *Chem. Commun.***2011**, *47*, 544; b) Y. Liang, T. Meinhardt, G. Jarre, G., M. Ozawa, P. Vrdoljak, A. Schöll, F. Reinert, A. Krueger, *J. Colloid Interface Sci.* **2011**, *354*, 23
[31] a) W. S. Yeap, S. M. Chen, K. P. Loh, *Langmuir* **2009**, *25*, 185; b) Y. J. Liang, M. Ozawa, A. Krueger, *ACS Nano* **2009**, *3*, 2288
[32] A. C. Ferrari, J. Robertson, *Philos. Trans. A. Math. Phys. Eng. Sci.* **2004**, *362*, 2477
[33] S. Osswald,V. N. Mochalin, M. Havel, G. Yushin, Y. Gogotsi, *Phys. Rev. B* **2009**, *80*, 075419
[34] V. Mochalin, S. Osswald, Y. Gogotsi, *Chem. Mater*. **2009**, *128*, 273
[35] P. H. Chung, E. Perevedentseva, C. L. Cheng, *Surf. Sci.* **2007**, *601*, 3866
[36] J.-S. Tu, E. Perevedentseva, P.-H. Chung, C.-L. Cheng, *J. Chem. Phys.* **2006**, *125*, 174713
[37] R. Kaur, I. Badea, *Int. J. Nanomedicine* **2013**, *8*, 203
[38] D. Ho, *Nanodiamonds*, Springer **2010**

[39] S. J. Yu, M. W. Kang, H. C. Chang, K. M. Chen, Y.-C. Yu, *J. Am. Chem. Soc.* **2005**, *127*, 17604
[40] A. S. Barnard, *Analyst* **2009**, *134*, 1751
[41] O. A. Shenderova, J. Phys. Chem. C **2011**, *115*, 14014
[42] G. S. Yur'ev, V. Y. Dolmatov, *J. Superhard Mat.* **2010**, *32*, 31
[43] V. A. Popov, A. V. Egorovn S. V. Savilov, V. V. Lunin, A. N. Kirichenko, V. N. Denisov, V. D. Blank, O. M. Vyaselev, T. B. Sagalova, *J. Surf. Investig. X-ray, Synchrotron Neutron Tech.* **2014**, *7*, 1034
[44] T. S. Valey, M. Hirani, G. Harrison, K. B. Holt, *Faraday Discuss.* **2014**, *172*, 349
[45] K. B. Holt, *Phil. Trans. R. Soc. A* **2007**, 365, 2845
[46] a) W. S. Yeap, Y. Y. Tan, K. P. Loh, *Anal. Chem.* **2008**, *80*, 4659; b) W. H. Chen, S. C. Lee, S. Sabu, H. C. Fang, S. C. Chung, C. C. Han, H. C. Chang, *Anal. Chem.* **2006**, *78*, 4228; c) P. N. Nesterenko, O.N. Fedyanina, Y.V. Volgin, P. Jones, *J. Chromatogr. A* **2007**, *1155*, 2
[47] G. Saini, D. S. Jensen, L. A. Wiest, M. A. Vail, A. Dadson, M. L. Lee, V. Shutthanandan, M. R. Linford, *Anal. Chem.* **2010**, *82*, 4448
[48] a) W. H. Chen, S. C. Lee, S. Sabu, H. C. Fang, S. C. Chung, C. C. Han, H. C. Chang, *Anal. Chem.* **2006**, *78*, 4228; b) X. Kong, L. C. L. Huang, S.-C. V. Liau, C.-C.Han, H.-C. Chang, *Anal. Chem.* **2005**, *77*, 4273
[49] V. W.-K. Wu, *Chem. Lett.* **2006**, *35*, 1380
[50] O. Faklaris, D. Garrot, V. Joshi, J.-P. Boudou, T. Sauvage, P. A. Curmi, F. C. F. C. Treussart, *J. Eur. Opt. Soc. Rapid Publ.* **2009**, *4*, 09035
[51] C.-C. Fu, H.-Y. Lee, K. Chen, T.-S. Lim, H.-Y. Wu, P.-K. Lin, P.-K. Wei, P.-H. Tsao, H.-C. Chang, W. Fann, *Proc. Natl. Acad. Sci. U. S. A.* **2007**, *104*, 727
[52] M. Mkandawire, A. Pohl, T. Gubarevich, V. Lapina, D. Appelhans, G. Rödel, W. Pompe, J. Schreiber, J. Opitz, *J. Biophotonics* **2009**, *2*, 596
[53] B. R. Smith, D. Gruber, T. Plakhotnik, *Diam. Relat. Mater.* **2010**, *19*, 314
[54] R. Martín, M. Álvaro, J. R. Herance, H. García, *ACS Nano* **2010**, *4*, 65
[55] E. Perevedentseva, C.-Y. Cheng, P.-H. Chung, J.-S. Tu, Y.-H. Hsieh, C.-L. Cheng, *Nanotechnology* **2007**, *18* (31), 315102
[56] J.-I. Chao, E. Perevedentseva, P.-H. Chung, K.-K. Liu, C.-Y. Cheng, C.-C. Chang, C.-L. Cheng, *Biophys. J.* **2007**, *93*, 2199
[57] Y. Colpin, A. Swan, A. V. Zvyagin, T. Plakhotnik, *Opt. Lett.* **2006**, *31*, 625
[58] B. R. Smith, M. Niebert, T. Plakhotnik, A. V. Zvyagin, *J. Lumin.* **2007**, *127*, 260
[59] a) O. Faklaris, V. Joshi Irinopoulou T, *et al.*, *ACS Nano* **2009**, *3*, 3955; b) O. Faklaris, D. Garrot, V. Joshi, F. Druon, J.-P. Boudou, T. Sauvage, P. Georges, P. A. Curmi, F. Treussart, *Small* **2008**, *4*, 2236; c) S. J. Yu, M. W. Kang, H. C. Chang, K. M. Chen, Y. C. Yu, *J. Am. Chem. Soc.* **2005**, *127*, 17604, d) K.-K. Liu, C.-L. Cheng, C.-C. Chang, J.-I. Chao, *Nanotechnology* **2007**, *18*, 325102
[60] A. M. Schrand, H. Huang, C. Carlson, J. J. Schlager, E. Osawa, S. M. Hussain, L. Dai, *J. Phys. Chem. B* **2007**, *111*, 2
[61] C.-Y. Cheng, E. Perevedentseva, J.-S. Tu, P.-H. Chung, C.-L. Cheng, K.-K. Liu, J.-I. Chao, P.-H. Chen, C.-C. Chang, *Appl. Phys. Lett.* **2007**, *90*, 163903
[62] H. Huang, E. Pierstorff, E. Osawa, D.Ho, *Nano Lett.* **2007**, *7*, 3305
[63] Y. Yuan, X. Wang, G. Jia, J.-H. Liu, T. Wang, Y. Gu, S.-T. Yang, S. Zhen, H. Wang, Y. Liu, *Diam. Relat. Mater.* **2010**, *19*, 291
[64] Y. Zhu, J. Li, W. Li, Y. Zhang, X. Yang, N. Chen, Y. Sun, Y. Zhao, C. Fan, Q. Huang, *Theranostics* **2012**, *2* (3), 302
[65] Y. Yuan, Y. Chen, J.-H. Liu, H. Wang, Y. Liu, *Diam. Relat. Mater.* **2009**, *18*, 95

2. Aim of the project

Among all the carbon nanostructures, nanodiamonds are emerging as promising nanomaterial and this is due to their interesting and peculiar properties as their tunable size (from 4-5 nm to about 100 nm), the presence of a stable inert core and a reactive surface, their fluorescence, their ability to form hydrogels.
However several studies suggested that nanodiamonds possess a strong propensity to aggregation when dispersed in a liquid formulation medium and conventional techniques of disintegration, such as milling, emulsification, low power sonication have been ineffective in breaking down core aggregates.
From this point of view, a proper surface functionalization of nanodiamond particles is required for reducing aggregate sizes and to tailor NDs to all their possible applications such as luminescence imaging probes, drug delivery systems, quantum engineering devices.

In this thesis pristine nanodiamonds will be fully characterized and their surface will be modified in order to introduce various functionalities. For example, they will be oxidized using a mixture of sulfuric and nitric acids in order to render the surface more homogeneous and to increase the number of carboxylic groups and a study of amidation on pristine and oxidized nanodiamonds will be performed. The use of bis-amine will be useful to further graft the NDs surface with fluorescent labels or bioactive molecules.
Reactions such as the arylation with functionalized aryl diazonium salts, the 1,3-dipolar cycloaddition and the nitrene reactions will be applied on annealed NDs, studying both classical conditions and microwave irradiation.
Once studied the possible ways to modify nanodiamonds surface, specific biomolecules will be introduced. For example, the covalent functionalization of NDs with peptides could be an excellent way to develop nanoparticles able to act as vectors suitable for transferring specific materials across cellular membranes. The presence of peptides on the nanodiamond surface could be also useful to improve the dispersion stability that is a key requirement for the development of drug delivery formulations.

3. Results and Discussion

As already reported in the Introduction, there are different kinds of nanodiamond structures. They vary in the primary particle size, composition, surface functionalization and so also their reactivity and properties can be rather different. So we decided to study various nanostructures such as ultrananocrystalline diamonds and nanocrystalline diamonds which underwent to different treatment as annealing or air oxidation.

3.1 Characterization of pristine nanodiamonds

3.1.1 Detonation ultrananocrystalline diamonds (DND)

Detonation ultrananocrystalline diamonds were kindly supplied from prof. Terranova, University of Rome "Tor Vergata".

Some of these nanodiamonds were dispersed in DMF and probe-type sonication cycles were performed for 24 h (**DND1**), for 16 h (**DND2**), for 8 h (**DND3**).

Received nanodiamond powders were previously annealed using a hydrogen-plasma treatment in MW-RF-PECVD at 300 °C for 3 h (**DND4**), cold hydrogen-plasma treatment in MW-RF-PECVD for 3 h (**DND5**), cold hydrogen-plasma treatment in MW-RF-PECVD for 1 h (**DND6**), hydrogen-plasma treatment in MW-RF-PECVD at 300 °C for 1 h (**DND7**).

Nanodiamonds were characterized by TEM analysis, TGA and IR, UV-visible and Raman spectroscopies. From TEM images (Figure 3.1) two populations of nanodiamonds were detected, characterized by a diameter equal to 4-5 nm and 9-10 nm and around some nanoparticles it was observed a clear outer ring.

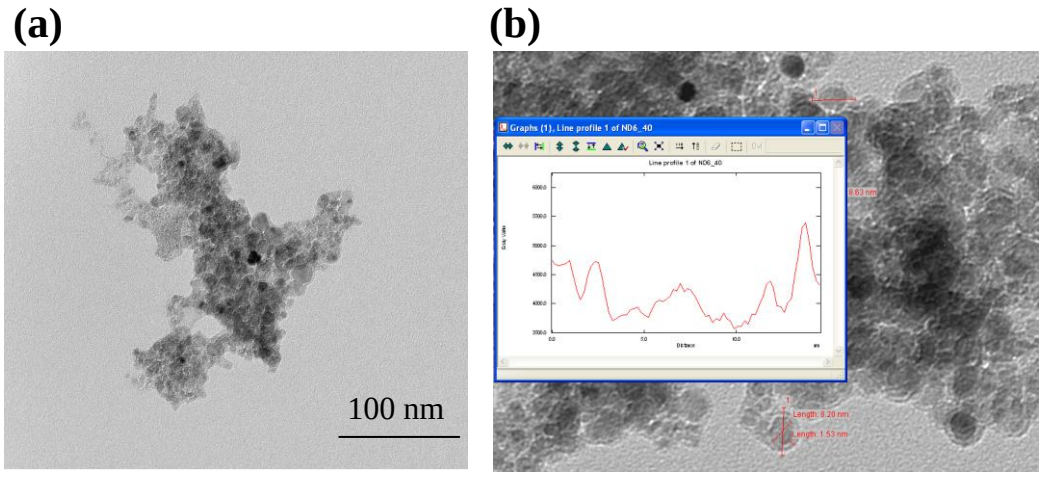

Fig. 3.1: TEM images of **DND6**. (**a**) Typical hundreds nanometers aggregate; (**b**) line profile recorded.

Using the thermogravimetric analysis it was possible to study the thermal stability of the received nanodiamonds. For all the cases a decrease of the weight was detected at ~ 600 °C but for the annealed nanodiamonds (**DND4**, **DND5**, **DND6**, **DND7**) before this temperature an increase of the weight was observed (Figure 3.2).

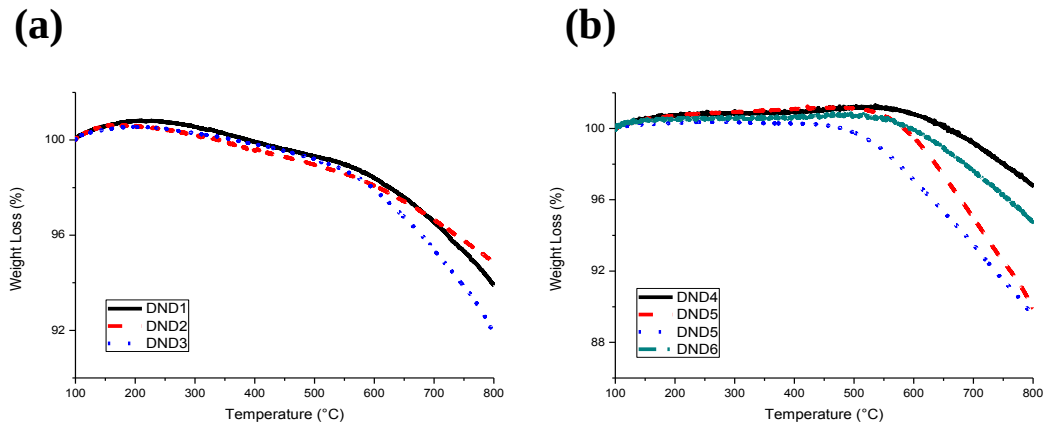

Fig. 3.2: Thermogravigrams (under N_2 atmosphere) of (**a**) not annealed and (**b**) annealed detonation nanodiamonds.

The Raman spectroscopy was performed to study the presence of the diamond peak at 1328 cm^{-1} and the other features typical of ND (Figure 3.3). For all the samples the behaviour of 5-10 nm size nanodiamond was observed[1] but for **DND4**, in which the presence of a pronounced D-band, resembling the carbon onion structure, was observed,[2] in agreement with the annealing process ND4 underwent.

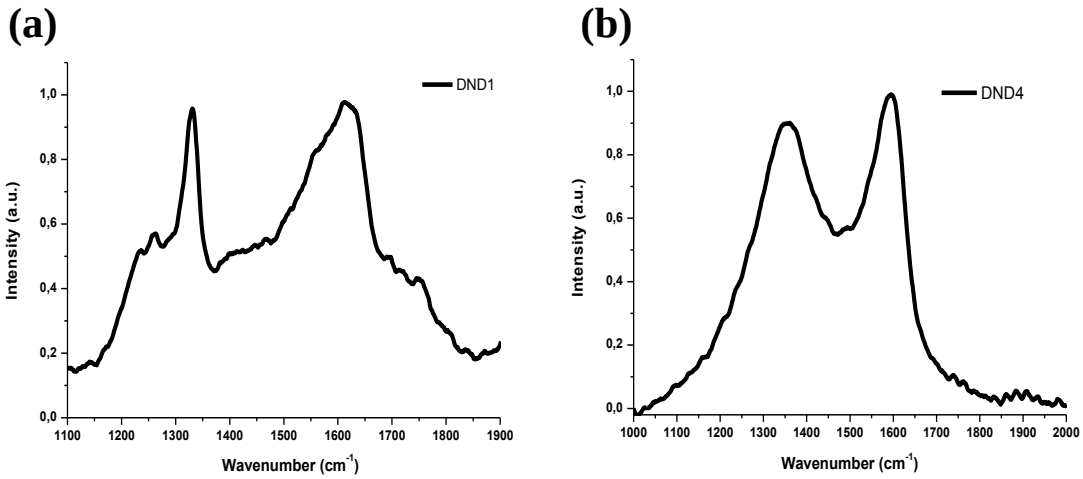

Fig. 3.3: Raman spectra of (**a**) **DND1** and (**b**) **DND4** recorded using a 532 nm laser excitation.

Infrared (IR) spectroscopy (Figure 3.4) provides information about the nature of functional groups and adsorbed molecules on the surface of nanodiamonds. For all analyzed samples, the characteristic features were found, for example the O-H stretching (3200-3600 cm^{-1}) and bending (1630-1640 cm^{-1}), while in the case of **DND7** the C=O stretching (1700-1800 cm^{-1}) was not detected.

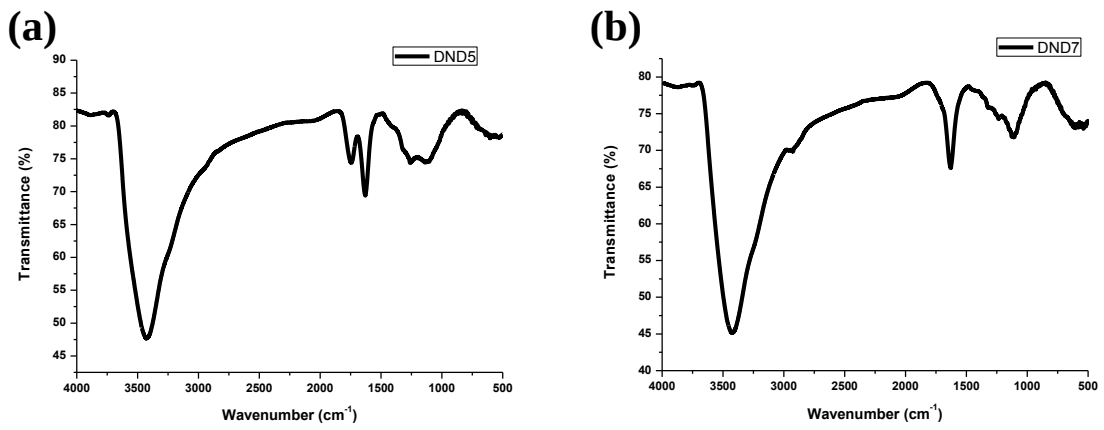

Fig. 3.4: IR spectra, using a KBr pellet, of annealed (**a**) **DND5** and (**b**) **DND7**.

The table 3.1 summarizes the values of binding energy and the surface atomic percentages found by XPS spectroscopy. The components found by fitting were the C1s peak at 286 eV, due to the C-C sp^3 and the other two centered at 287 eV (hydroxyl and ether groups) and 288 eV (carbonyl and carboxyl groups). The presence of oxygen-containing groups on the surface is confirmed by the presence of the O1s peak that, in agreement with the assignment of the components of C, is composed of two components, a majority at 533 eV, which is attributed to oxygen bound to C via single bond, and a minority at 532 eV attributed to O associated with the double bond to carbon. For the annealed **DND4** a lower amount of oxygen was found, as expected.

	C1s	**O1s**	**Surface Atomic Concentration**
DND2	286.0 (63%)	531.7 (13%)	97% C; 3% O
	287.4 (23%)	533.5 (87%)	
	288.6 (14%)		
DND4	286.0 (75%)	531.3 (7%)	98% C; 2% O
	287.3 (15%)	533.3 (93%)	
	288.4 (10%)		

Tab. 3.1: Binding energy and the surface atomic percentages found by XPS spectroscopy.

3.1.2 Commercial detonation ultrananocrystalline diamonds

Commercial detonation ultrananocrystalline diamond (**ANND**), obtained by detonation of high-energy carbon, was produced by *Adamas Nanotechnologies* and received as a grey powder.

The phase is the cubic diamond with an average primary particle size equal to 4 nm (confirmed by TEM, Figure 3.5) and an incombustible impurities content of 1.2-1.6 wt%.

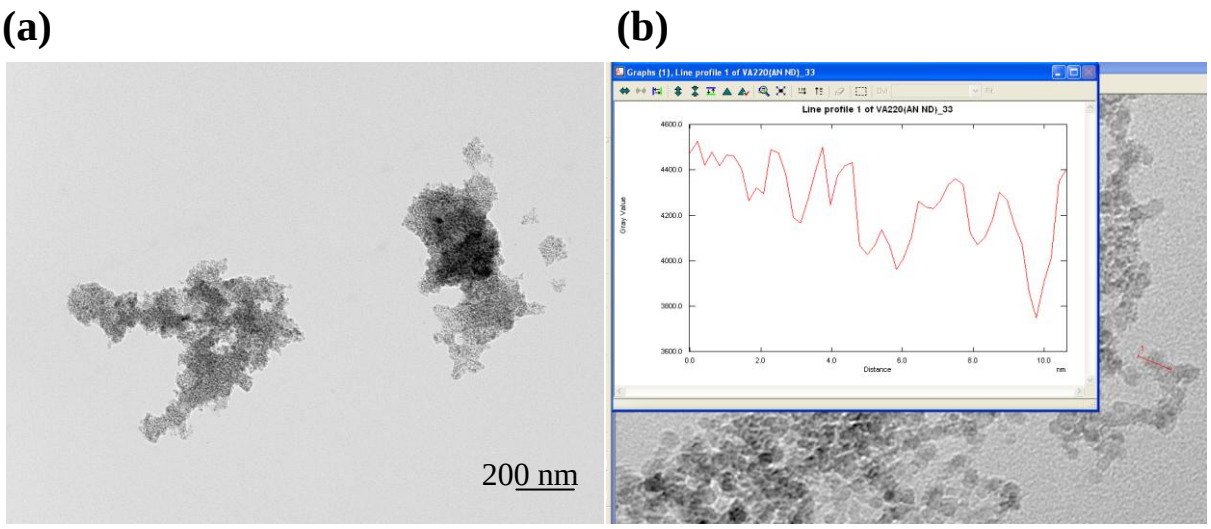

Fig. 3.5: TEM images of **ANND**. (**a**) Typical hundreds nanometers aggregates and (**b**) line profile recorded.

Moreover, the 5-10 nm size was confirmed by Raman spectroscopy, where it was possible to recognize the diamond peak at 1328 cm^{-1} and the so-called G-band at 1600 cm^{-1} (Figure 3.6a). Using the thermogravimetric analysis it was possible to study the thermal stability of the received nanodiamonds and a decrease of the weight was detected at ~600 °C.

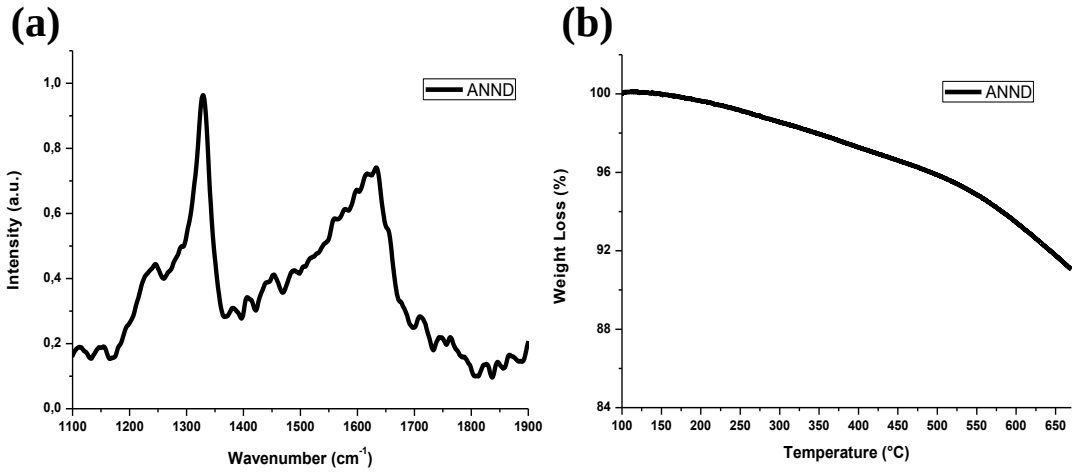

Fig. 3.6: (**a**) Raman spectrum and (**b**).thermogravigram (under N_2 atmosphere) of commercial detonation nanodiamond **ANND**.

The IR spectrum (Figure 3.7) was similar to those obtained for **DND1, DND2** and **DND3** received from Rome, presenting the O-H stretching (3200-3600 cm^{-1}) and bending (1630-1640 cm^{-1}) and the C=O stretching at 1742 cm^{-1}.

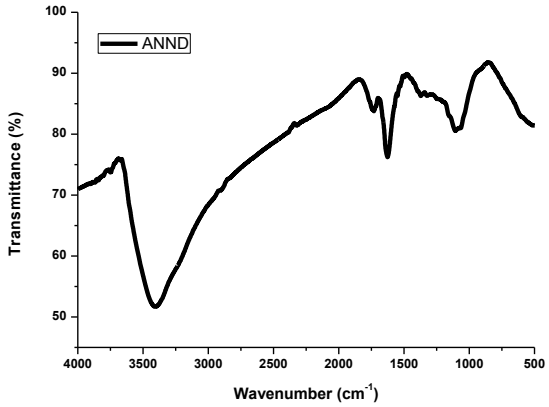

Fig. 3.7: IR spectrum of **ANND** (KBr pellet).

3.1.3 Nanocrystalline diamonds

Nanocrystalline diamonds were kindly supplied by prof. Cicala, CNR (Bari). Both diamond-rich (**dNCD**) and graphite-rich (**gNCD**) diamonds were studied by several techniques.
The TEM images have confirmed the hundreds nm size and the not regular shape (Figure 3.8).

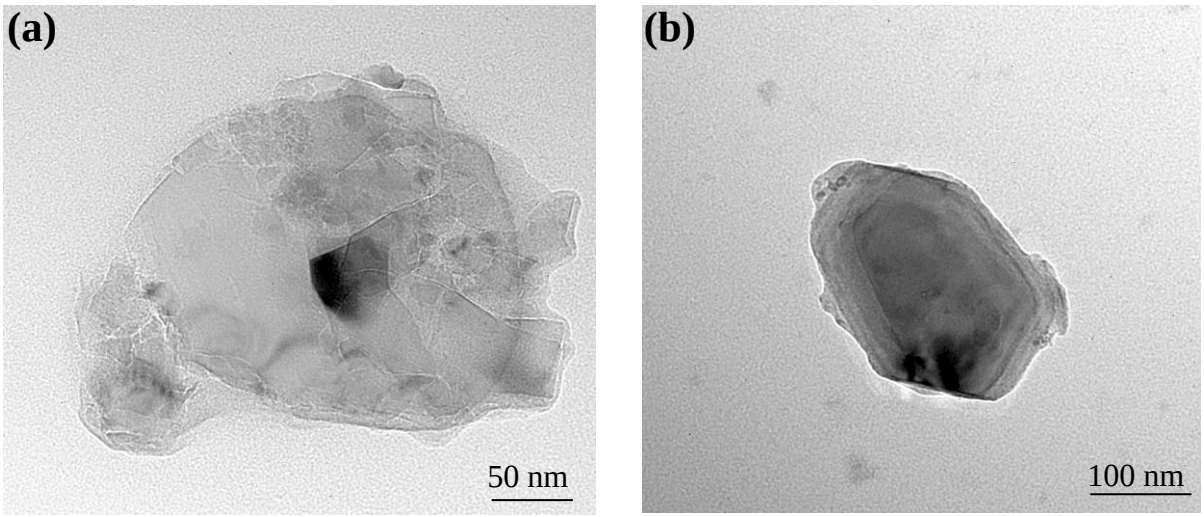

Fig. 3.8: TEM images of diamond-rich (**a**) and graphite-rich (**b**) diamonds.

The Raman spectra (Figure 3.9) are characterized by a very pronounced diamond peak at 1332 cm^{-1}, but the two different kind of NDs present different features: for the diamond-rich nanocrystalline diamond a broad band is present at 1400 cm^{-1} (D-band) and for the graphite-rich one a broad band is at 1600 cm^{-1} (G-band).

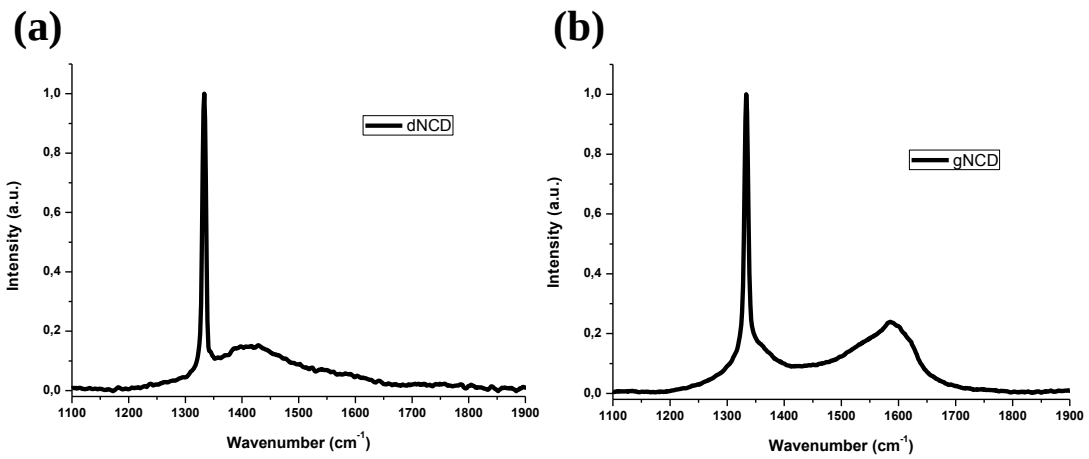

Fig. 3.9: Raman spectra of (**a**) diamond-rich and (**b**) graphite-rich nanocrystalline diamonds, recorded using a 532 nm laser excitation.

Characteristic features of nanocrystalline diamonds include the O-H stretching (3200-3600 cm^{-1}) and bending (1630-1640 cm^{-1}), due to both alcoholic groups covalently attached to the surface and adsorbed species, C=O stretching (1700-1800 cm^{-1}) that can be part of a ketone, aldehyde, ester, carboxylic acid or lactone and C-H stretching for the presence of -CH_2- and -CH_3 groups. The IR spectra of diamond-rich and graphite-rich crystalline diamonds are characterized by a C=O stretching at higher wavenumbers with respect to those of ultrananocrystalline diamonds, in accordance with the study of Tu *et al.*[3]

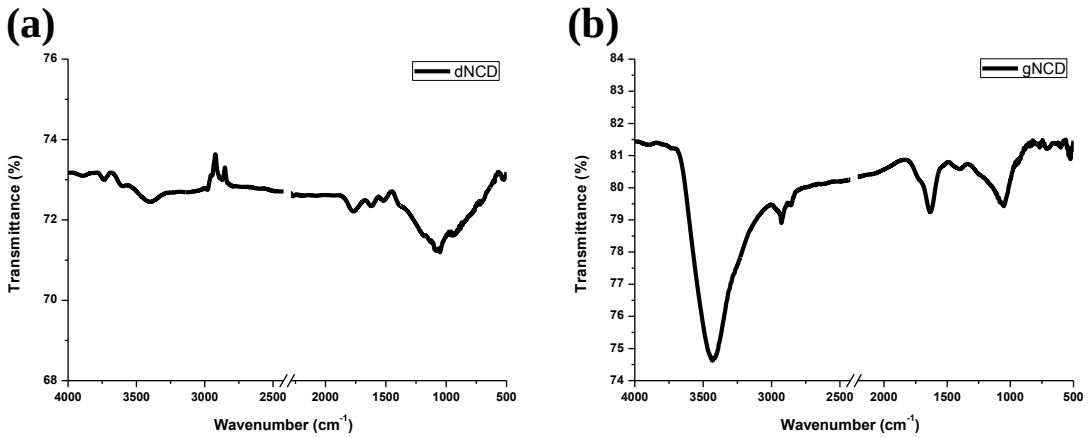

Fig. 3.10: IR spectra of (**a**) diamond-rich and (**b**) graphite-rich nanocrystalline diamonds (KBr pellet).

3.2 Oxidation

Depending on the synthesis and purification treatments, the surface of nanodiamond particles and aggregates is generally covered with a variety of functional groups including carboxylic, lactone, ketone, and hydroxyl groups. The oxidation process is a good way to have a more homogenous surface and, at the same time, carboxylic groups make these nanoparticles an attractive substrate for the production of functionalized nanoparticles.

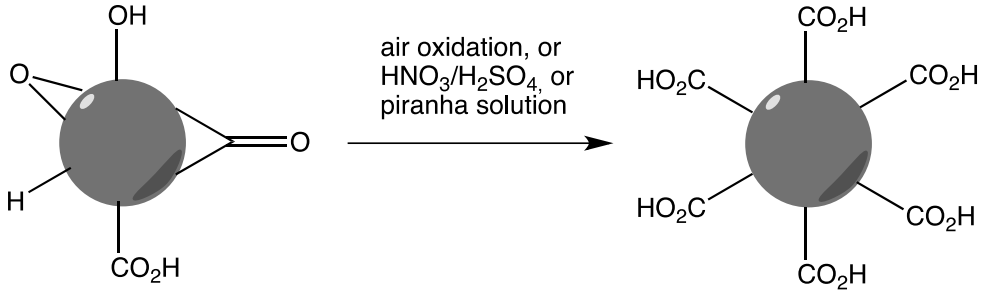

Scheme 3.1: Methods already applied to oxidize the ND surface[4]

In fact, the specific functionalization of NDs with suitable functional groups for further modifications, for example with dyes and/or biologically active moieties, represents an important goal. To get a good degree of functionalization and to achieve a homogeneous layer of carboxylic groups on the nanodiamond surface it is necessary to maximize the oxidation process, inevitably accompanied by material loss and size reduction of the diamond core.[4]
Actually, several ways to oxidize the nanodiamond surface are reported in literature. For example, it is possible to use the "piranha" solution (mixture of sulfuric acid and hydrogen peroxide),[5] concentrated hydrogen peroxide alone[6] or a 3:1 mixture of concentrated sulfuric and nitric acids (Scheme 3.1).[7] Gogotsi *et al.* have proposed a procedure for the air oxidation of detonation nanodiamonds. The chosen temperature of 425 °C was decisive for the selective oxidation of non-diamond carbon, in fact the authors found that that a minimum temperature of 400 °C is required to start the oxidation but above 450 °C all kinds of nanoscale carbon can undergo to oxidation. The obtained products have shown different oxygen-containing groups such as carboxylic and keto groups.[8]
All the described reactions typically require to be carried out over long periods of time, and only in 2013 Mitra *et al.* have reported for the first time the microwave-assisted oxidation of detonation nanodiamonds with shorten reaction time.[9]

3.2.1 Oxidation using sulfonitric mixture

Detonation ultrananocrystalline diamonds **DND2** and **DND3**, and those produced by *Adamas Nanotechnologies*, **ANND**, were oxidized using a 3:1 mixture of concentrated sulfuric and nitric acids at 80 °C, overnight, giving **oDND2**, **oDND3** and **ANND1**, respectively (Scheme 3.2).

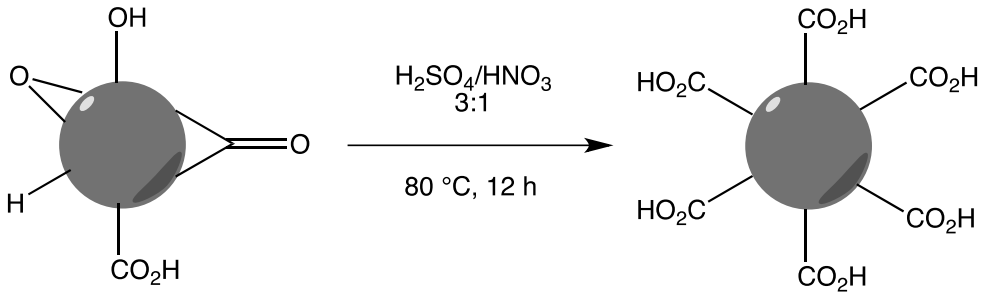

Scheme 3.2: Oxidization of NDs with sulfonitric mixture.

The sample was filtered using a Millipore system and washed with de-ionized water. After the workup the dried samples were analyzed by several techniques.

Infrared spectroscopy could be a good technique to analyze the presence of carboxylic groups, considering that the 1650-1850 cm^{-1} region is usually assigned to the C=O carbonyl stretching modes, depending on the particular type carbonyl-containing compounds. There are not clear differences for the absorption bands at 3435 cm^{-1} and at 1120 cm^{-1}, due to the -OH stretching and deformation vibrations, but a clear peak due to the C=O stretching was obtained after the oxidation at 1742 cm^{-1} (Figure 3.11a).[1]

The Raman spectroscopy was also performed before and after the oxidation and only a small difference was detected, a shoulder at 1740-1760 cm^{-1} that is typically due to the C=O stretch coming from surface functional groups (Figure 2.11b).[10]

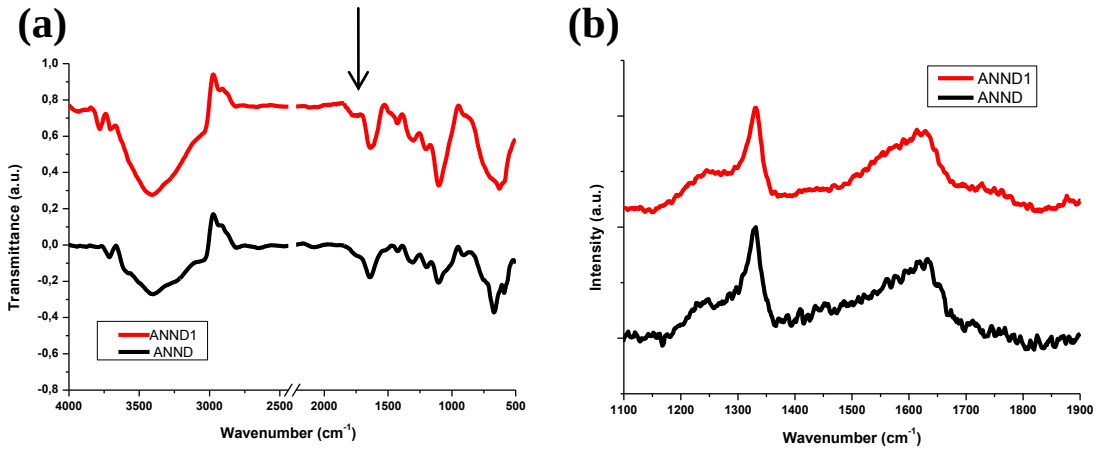

Fig. 3.11: (**a**) IR spectra, using an ATR system, and Raman spectra (**b**) of oxidized (red lines) and pristine (black lines) commercial ultrananocrystalline diamonds. Peak due to the C=O stretching is indicated by an arrow.

The pristine detonation nanodiamonds reacted effectively, leading to a good surface loading as shown in Table 3.2.

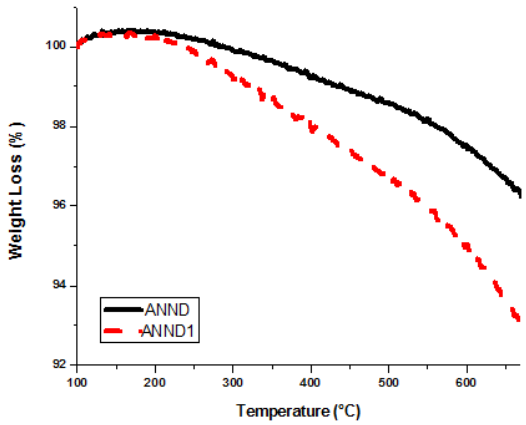

Sample	Surface Loading [µmol/g]
oDND2	544±27
oDND3	539±15
ANND1	310±44

Fig. 3.12: TGA of oxidized (red line) and pristine (black line) **ANND**.
Tab. 3.2: Surface loading values (calculated at 450 °C) obtained for the oxidations on NDs.

The XPS was performed to analyse the presence of oxygen-containing groups and it is possible to notice that, after the acid treatment, the oxygen content increased.

	Atomic Concentration (%)	
	ANND	**ANND1**
C1s	90.9±0.3	89.0±0.5
N1s	0.71±0.06	1.15±0.05
O1s	8.4±0.3	9.9±0.5

Tab. 3.3: Surface atomic percentages found by XPS spectroscopy on commercial ND. An increase of the oxygen percentage after the acid treatment was observed.

3.2.2 Oxidation using selective oxidation in air

An oxidation in air of commercial detonation ultrananocrystalline diamond was performed by the group of prof. Cicala (CNR, Bari) at 425 °C, following the work of Osswald and co-workers, giving the product **ANND2**.[11] The same procedure was performed by the same group on nanocrystalline diamond-rich and graphite-rich diamond but choosing the temperature of 475 °C. The products **dNCD1** and **gNCD1** were characterized by TGA, Raman and IR spectroscopy.
The TGA of oxidized graphite-rich diamond is characterized by a degree of functionalization equal to 33±5 µmol/g (Figure 3.13).

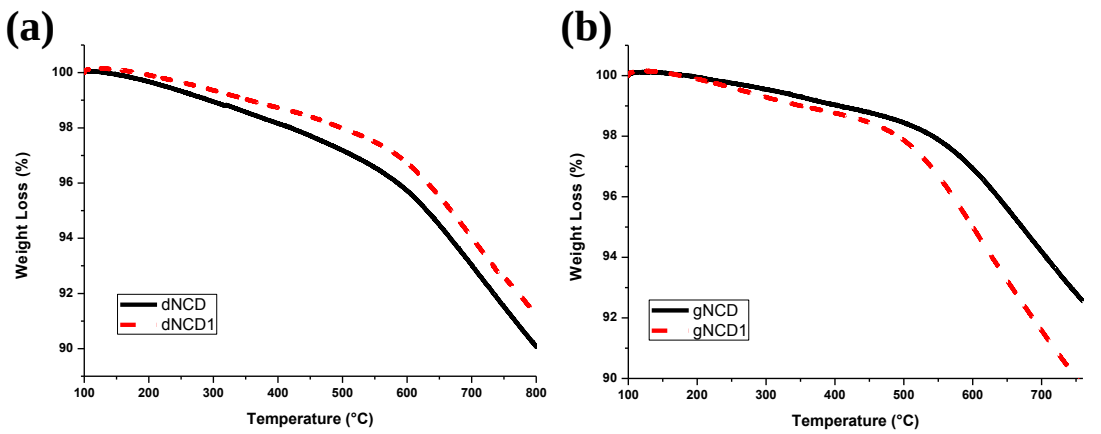

Fig. 3.13: TGA of oxidized (red line) and pristine (black line) (**a**) diamond-rich and (**b**) graphite-rich nanodiamonds.

The Raman spectroscopy on the oxidized ultrananocrystalline diamond was in accordance with the results obtained after the oxidation with strong acids (data not shown). The Raman spectra on oxidized and pristine nanocrystalline diamond-rich diamonds are characterized by the diamond peak and the D-band[1] and no changes in intensity were detected (Figure 3.14). The graphite-rich diamonds after the oxidation have shown a D-band and the disappearance of the G-band found previously.

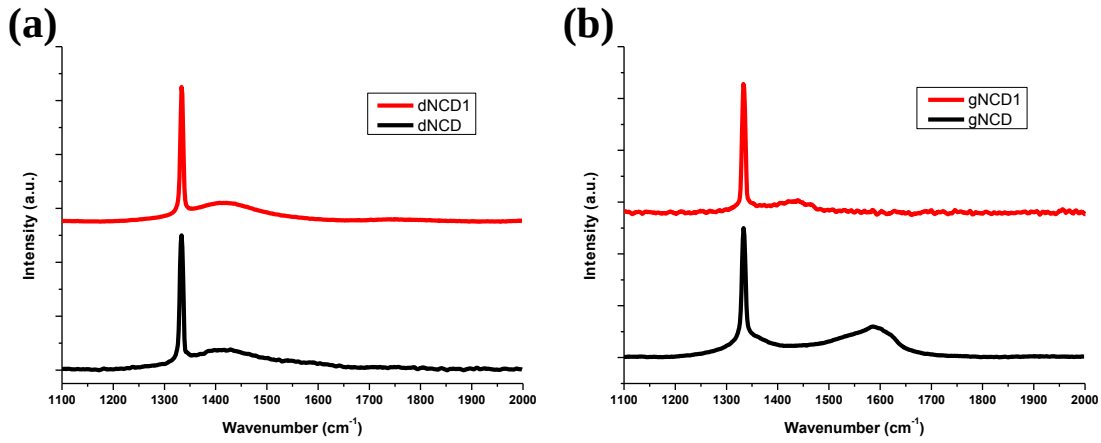

Fig. 3.14: Raman spectra, recorded using a 532 nm laser excitation, of (**a**) oxidized (red line, **dNCD1**) and pristine (black line, **dNCD**) diamond-rich nanocrystalline diamonds.

After the treatment in air ultrananocrystalline diamonds (**ANND2**) have shown a shift of the C=O stretching towards higher wavenumber values (Figure 3.15a) and the IR spectrum for the oxidized diamond-rich nanocrystalline diamonds (**dNCD1**, data not shown) have shown no differences with respect to the pristine ones. It has to be noticed that graphite-rich nanocrystalline diamonds after the oxidation (**gNCD1**) present the C=O stretching peak, not visible in the pristine sample (Figure 3.15b).

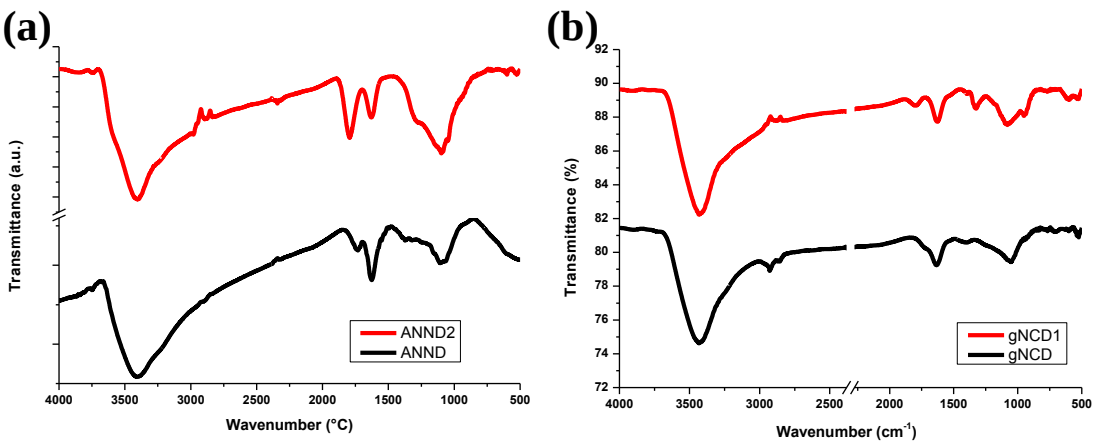

Fig. 3.15: IR spectra, using a KBr pellet, of (**a**) oxidized (red line) and pristine (black line) ultrananocrystalline diamonds **ANND** and (**b**) graphite-rich nanocrystalline diamonds **gNCD**.

3.3 Amidation

The procedure to functionalize NDs with amines via amide bond formation are generally similar to those used for CNTs,[12] and the same surface modification can be used for other nanoparticles, if in presence of carboxylic groups on their surface.
Mochalin and co-workers have synthetized hydrophobic blue fluorescent material by covalent linking of octadecylamine to 5 nm oxidized nanodiamonds, passing through the correspondent acyl chloride.[13] Similar reaction was performed on oxidized 5 nm and 60 nm nanodiamonds with ethylenediamine by Jee *et al.* but using 2-(7-aza-1H-benzotriazol-1-yl)-N,N,N',N'-tetramethylaminium hexafluorophosphate (HATU).[14]

3.3.1 Amidation on ultrananocrystalline and nanocrystalline diamonds

The amidation reaction was studied and optimized on detonation ultrananocrystalline diamonds synthetized in Rome **DND2**. The reaction was performed at first using thionyl chloride at 100 °C, changing the reaction time (24 h, 48 h, 72 h and 96 h) and using two kinds of amines, the N-Boc-amino-diethoxy-ethylamine and the N-Pht-amino-diethoxy-ethylamine (Scheme 3.3).

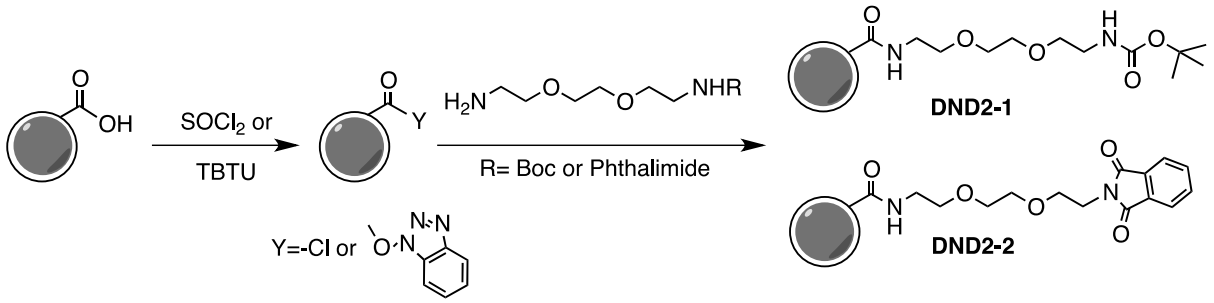

Scheme 3.3: Amide bond formation through the use of thionyl chloride or TBTU as coupling reagent.

Best results, in terms of reproducibility and degree of functionalization by TGA, were obtained using the amine with the Boc- as protecting group and allowing the mixture to react for 48 h.

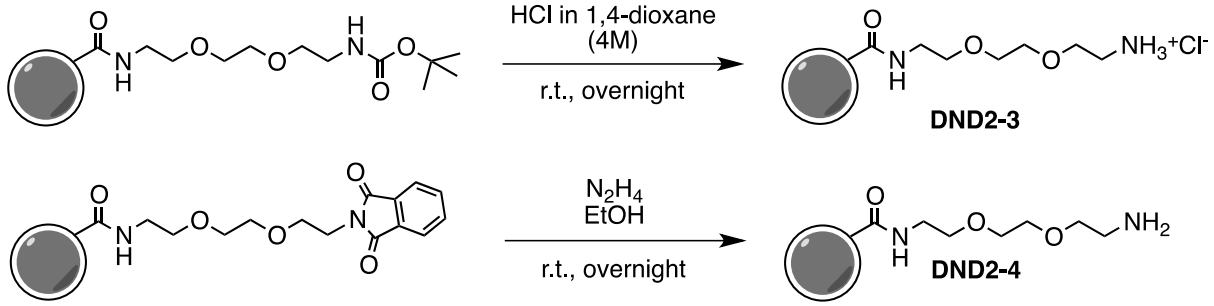

Scheme 3.4: Deprotection of the amine groups.

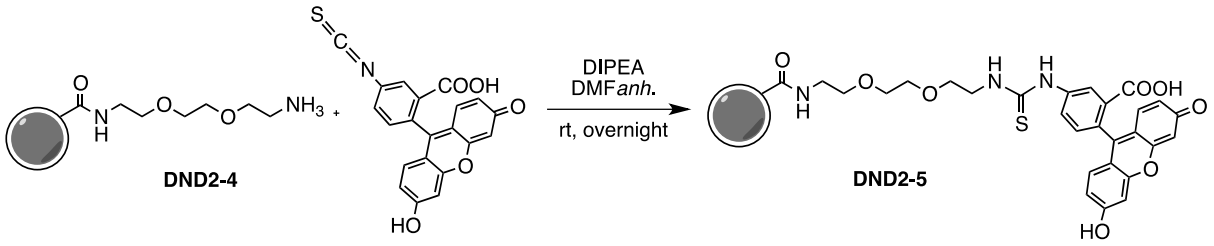

Scheme 3.5: Conjugation with FITC.

After removing the protecting groups (Scheme 3.4), the Kaiser test gave negative results but changes in IR spectra and thermogravigrams were obtained. The fluorescein isothiocyanate (FITC, Scheme 3.5) was used to functionalize the amino-grafted NDs and UV-visible absorbance and static fluorescence techniques were used to characterize the sample and to detect the presence of the dye. The fluorescein is commonly used as fluorescence label and it is known that its photophysical behaviour pH dependent.[15] Moreover, the FITC exhibits a reasonable overlap between its absorption and emission spectra and a critical energy transfer distance in the range of 42 to 56 Å have been reported.[16]

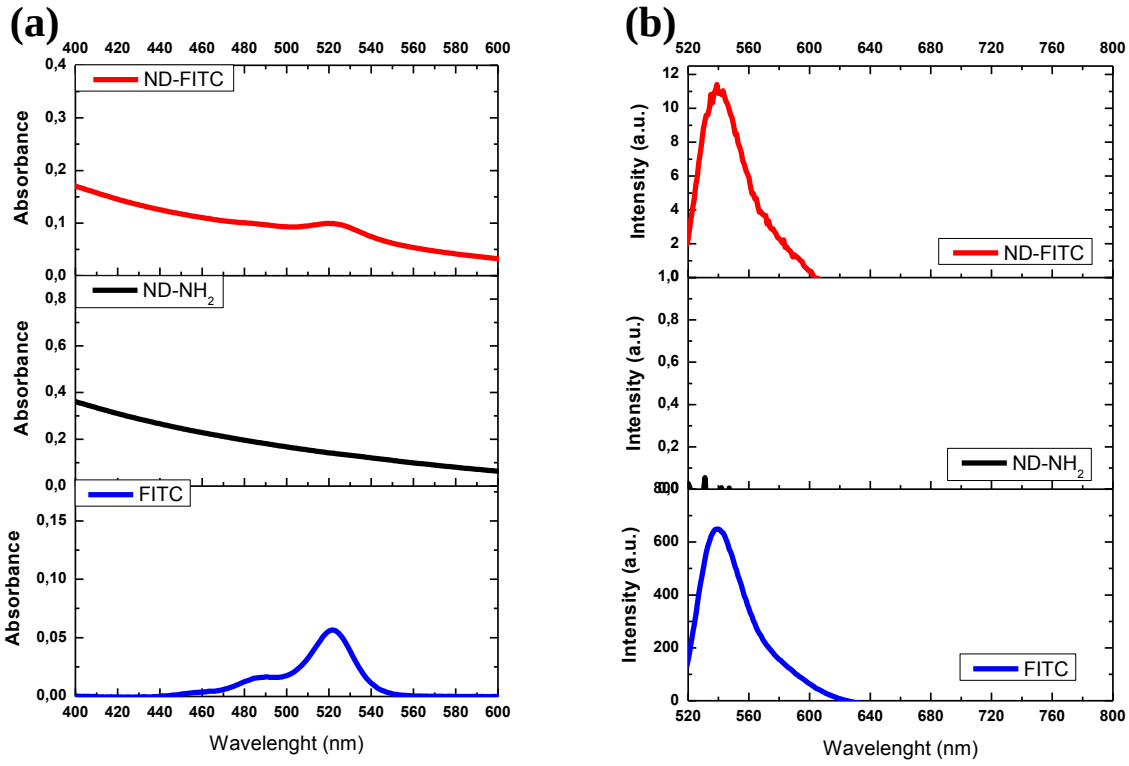

Fig. 3.16: (**a**) UV-visible absorbance spectra and (**b**) emission fluorescence spectra of FITC (blue line), **DND2-4** (black line) and **DND2-5** (red line).

Even if these results were promising, there was the necessity to further optimize the system and the same reaction was done on the same kind of DND, after their oxidation with sulfonitric mixture (**oDND2**, Scheme 3.6). By TGA (Figure 3.17) the degree of functionalization obtained for the product **oDND2-1** was higher with respect to the reaction

performed on **DND2** (167±11 μmol/g vs 33±7 μmol/g). This was expected considering that after the acid treatment an increase of the carboxylic groups should be present.

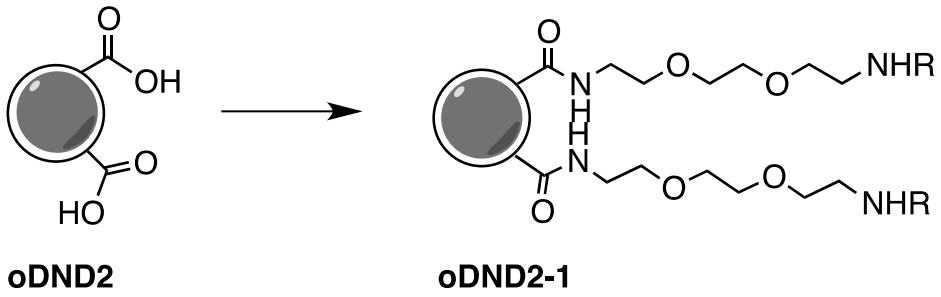

Scheme 3.6: Preparation of **oDND2-1**.

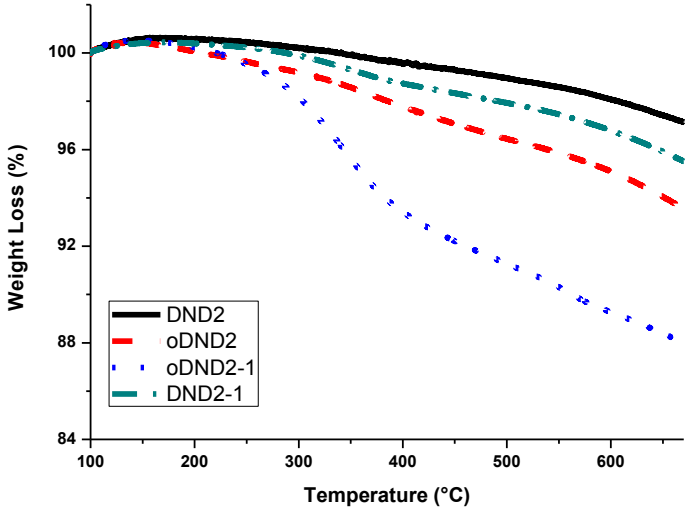

Fig. 3.17: TGA of **DND2** (black line), **oDND2** (red line), **DND2-1** (green line) and **oDND2-1** (blue line).

In order to compare the efficiency of coupling reagents, the reaction on pristine **DND2** with the *N,N,N′,N′*-Tetramethyl-*O*-(benzotriazol-1-yl)uronium tetrafluoroborate (TBTU) was also performed. A better degree of functionalization (169±6 μmol/g) was obtained with respect to the thionyl chloride, moreover the use of the TBTU requires milder conditions.

For these reasons the TBTU was chosen as coupling reagent for the amide coupling reactions performed on oxidized commercial detonation nanodiamonds by acid treatment **ANND1** and oxidation in air **ANND2,** and on pristine and oxidized diamond-rich (**dNCD** and **dNCD1**) and graphite-rich nanocrystalline diamonds (**gNCD** and **gNCD1**).

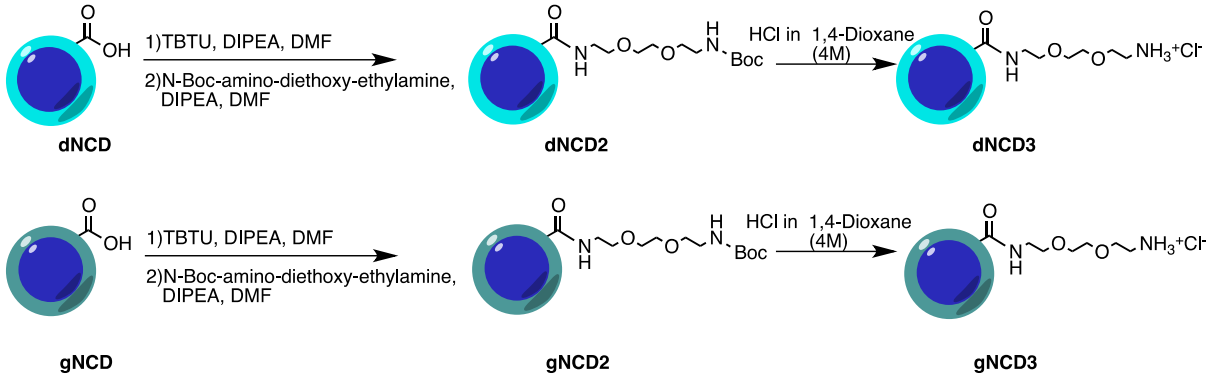

Scheme 3.7: Amide bond formation by using TBTU as coupling reagent on diamond-rich and graphite-rich nanocrystalline diamonds.

The samples were characterized by thermogravimetric analysis and infrared spectroscopy.

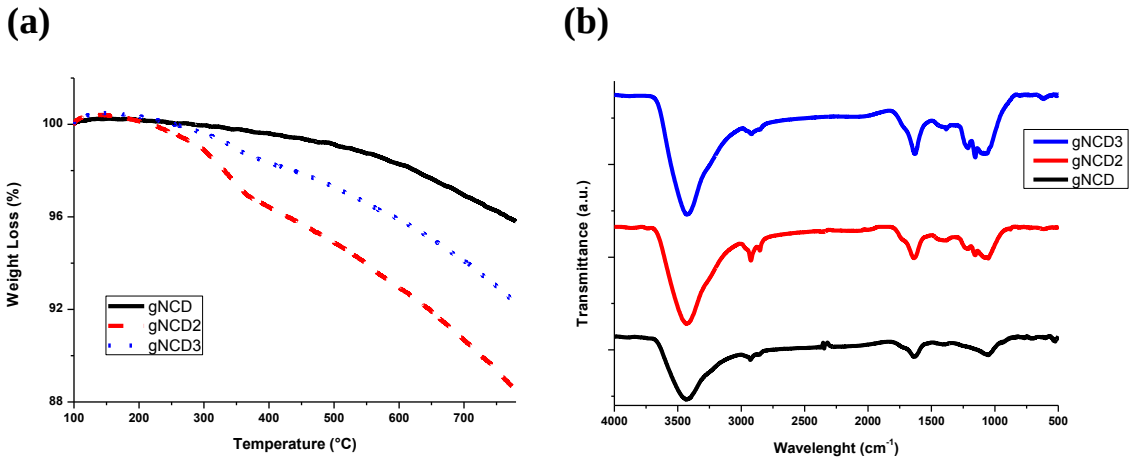

Fig. 3.18: (**a**) TGA and (**b**) IR spectra of pristine graphite-rich nananocrystalline diamond (black line), amide bond reaction with N-Boc-amino-diethoxy-ethylamine (red line) and deprotection of the Boc-function (blue line). The degree of functionalization obtained after the coupling is equal to 126 μmol/g.

3.4 Annealing

The removal of all the groups covalently bounded on the nanodiamonds surface could represent another option to uniform their external layers.
In fact, by thermal treatment or by irradiation with high-energy electrons, it is possible to have a fullerene-like surface on the nanodiamond and reactions usually applied on carbon nanotubes and fullerene can be performed.[4,17]
The partial or complete conversion of nanodiamond particles into "bulky diamonds" (multilayer graphitic shells) or carbon onions (multishell fullerene-like particles) can be so induced by different methods.[2,4,18]
The reactivity of nanodiamonds towards the annealing depends on their shape, size and initial amount of sp^2 carbon. In fact it was observed that smaller is the size of the nanodiamond and higher is the reactivity, moreover a spherical shape is usually more reactive than a material with several facets. For ultrananocrystalline diamonds, like detonation ones, the annealing temperature has to be chosen carefully in order to avoid the formation of carbon onions. In fact, Krueger and co-workers have found that a thermal annealing at 750 °C for 2 h under vacuum is sufficient for the complete removal of surface groups and the stability of the diamond core.[4] Moreover, recent studies suggested that below 900 °C the ND surface is reconstructed into graphite, but the diamond core is not altered.[19] Using the Raman spectroscopy Cebik *et al.* have studied the nanodiamond to carbon onion transformation.[2] It was observed that the transition of nanodiamond to carbon onion starts at 600 °C upon thermal annealing of 2 h in argon atmosphere. By XRD, TEM, TGA the sp^3-to-sp^2 conversion has been shown to start at lower temperatures (~600 °C) whereas the carbon onions formation is not observed below 1000-1100 °C.

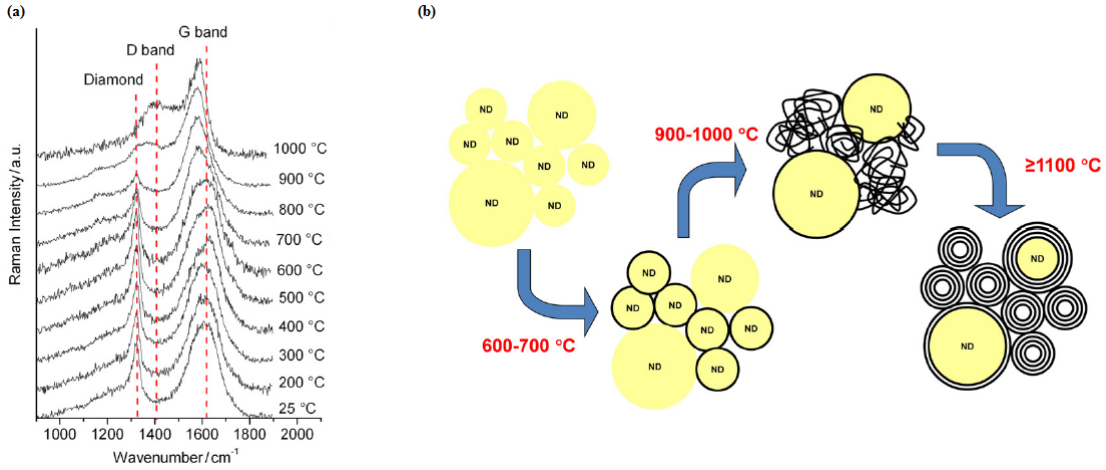

Fig. 3.19: (**a**) Raman spectra of ND measured at room temperature after annealing for 2 h at different temperatures between 25 °C and 1000 °C. It is possible to notice that increasing the temperature the diamond peak is disappearing while the D-band is becoming more visible. (**b**) Description of nanodiamond to carbon onion transformation. The transformation of nanodiamonds to sp^2 carbon begins at temperatures as low as 600 °C. At 1000 °C the majority of NDs is converted to sp^2 carbon but the sp^2 layers are highly disordered. At 1100 °C NDs are partially or fully converted to carbon onions. It was observed also that the rate of transformation is strongly dependent on the crystal size and it is higher for smallest NDs.[2]

3.4.1 Study of annealing on commercial detonation nanodiamond

The graphitization of commercially detonation nanodiamonds (**ANND**) was performed heating the sample for 2 h under argon atmosphere and choosing two different temperatures, 750 °C (**ANND3**) and 900 °C (**ANND4**).
The samples were studied by powder XRD in order to verify if the annealing process affected the diamond core. Two peaks were detected at 43.9° and 75.4°, attributed to (111) and (220) planes of the cubic structure, respectively. It was observed that even after the 900 °C annealing the diamond peak at 43.9 ° did not get broader so the core remained undamaged. From the line-width of the (111) diffraction peaks, the size of the pristine nanodiamonds (**ANND**) and annealed nanodiamonds (**ANND3**, **ANND4**) was estimated to be ~7 nm, indicating that the diamond core was not significantly reduced by the thermal treatment. In fact, based on the Scherrer equation if the peak gets broader the crystallite size gets smaller. For all the samples a broad peak at 25 ° was recorded, probably due to the graphitic (003) planes and no difference in intensity was obtained for this peak between the pristine and the annealed ones (Figure 3.20).
From the XPS analysis the presence of oxygen is confirmed by the presence of the O1s peak and a decrease of the percentage of this element was obtained for annealed NDs with respect to the pristine ones, with a better result at higher temperature.

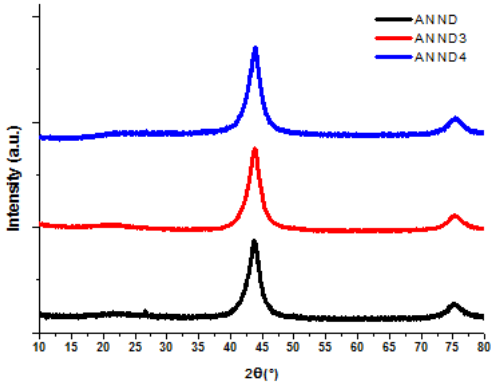

Atomic Concentration (%)

	ANND	*ANND3*	*ANND4*
C1s	90.9±0.3	92.6±0.2	93.8±0.1
N1s	0.71±0.06	1.28±0.07	1.30±0.09
O1s	8.4±0.3	6.1±0.2	4.93±0.09

Fig. 3.20: TGA of 900 °C annealed (blue line), 750 °C annealed (red line) and pristine (black line) ANND.
Tab. 3.4: Surface atomic percentages found by XPS spectroscopy on annealed and pristine ANND. A decrease of the oxygen percentage after the annealing process was obtained.

The TGA performed on annealed samples did not show an increase of the weight (Figure 3.21 a), as seen already for the annealed samples prepared in Rome. In this case the traces of oxygen present in the furnace are not oxidizing the surface and a higher stability up to 600 °C clearly indicates that the superficial functional groups were removed by the thermal treatment. The Raman spectra (Figure 3.21b) were in accordance with the results obtained by Cebik *at al.*[2] in fact increasing the annealing temperature a decrease of the intensity of the diamond peak was obtained.

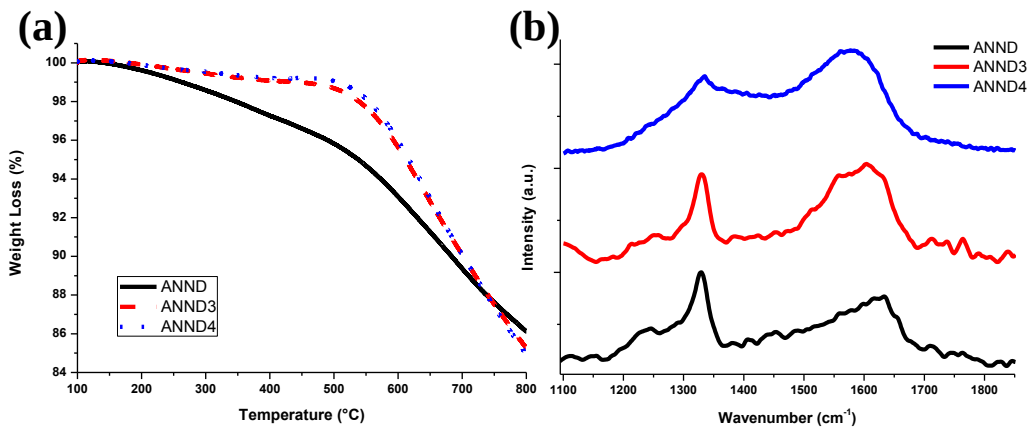

Fig. 3.21: (**a**) TGA and (**b**) Raman spectra of 900 °C annealed **ANND4** (blue line), 750 °C annealed **ANND3** (red line) and pristine **ANND** (black line).

3.5 Cycloaddition reactions

3.5.1 Study of 1,3-dipolar cycloaddition of azomethine ylides

The 1,3-dipolar cycloaddition of azomethine ylides on fullerene was reported for the first time in 1993[20] and used then for the functionalization of carbon nanomaterials like carbon nanotubes.[21,22] This kind of reaction occurs by the condensation of the amine in the α-amino acid and the carbonyl group of the aldehydes to form a dipole intermediate that is able to react with the double bounds present on the surface of the carbon nanostructure. In 2011 Krueger and co-workers have applied for the first time this kind of reaction on previously annealed NDs.[17] They used two types of azomethine ylides (aliphatic and pyridine derived) to show the broad applicability of the reaction for the surface modification of nanodiamonds.

In this work the 1,3-dipolar cycloaddition of azomethine ylides was performed on all the detonation nanodiamonds annealed in Rome (**DND4**, **DND5**, **DND6** and **DND7**, Scheme 3.8).

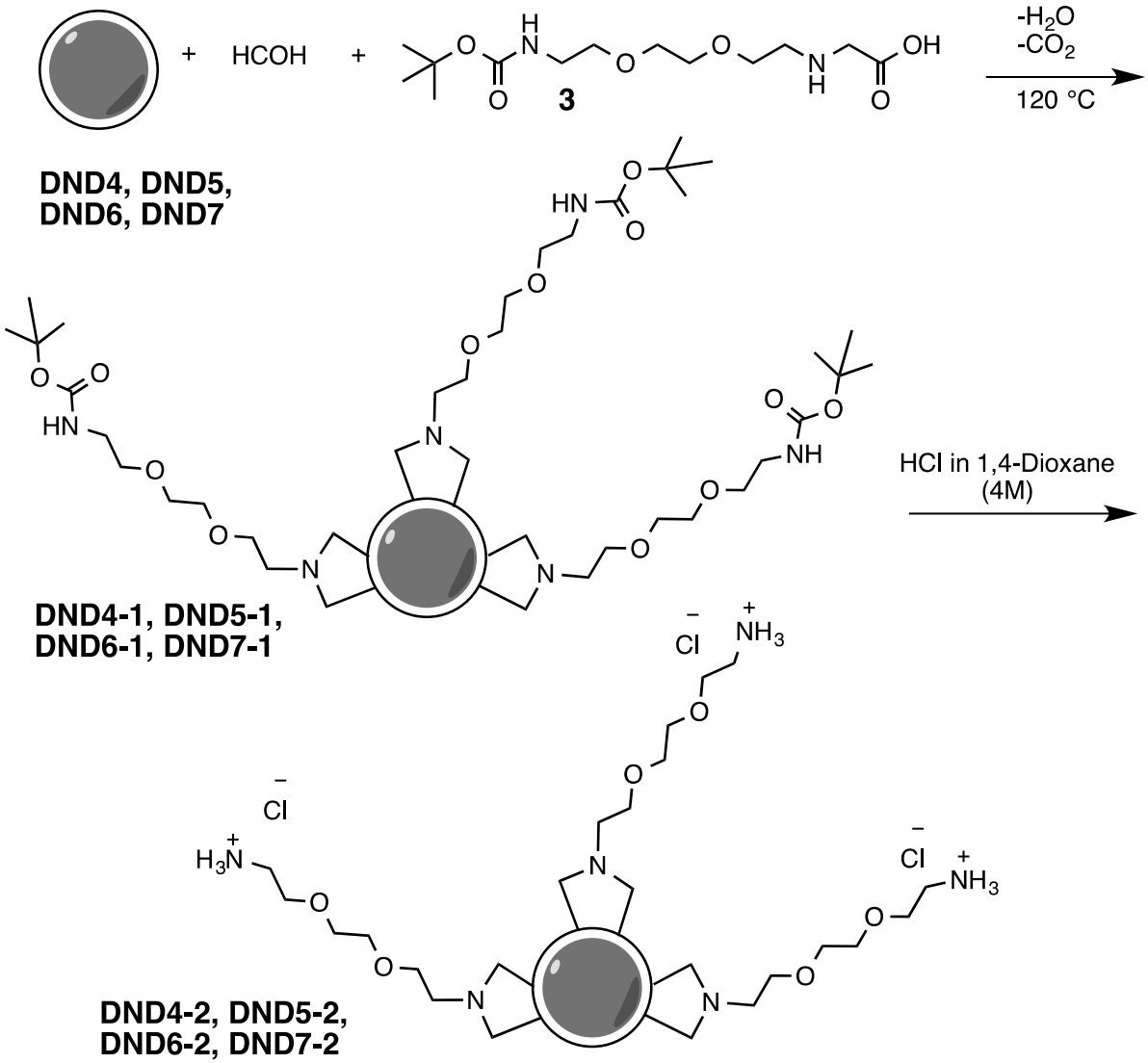

Scheme 3.8: 1,3-dypolar cycloaddition applied on annealed ultrananocrystalline diamonds **DND4**, **DND5**, **DND6**, **DND7** at 120 °C.

The reaction was firstly performed using an excess of paraformaldehyde and {2-[2-(2-*tert*-butoxycarbonylamino-ethoxy)-ethoxy]-ethylamino}-acetic acid **3**, in DMF at 120 °C and the mixture was allowed to react for 24 h.

The **DND4**, annealed using a hydrogen-plasma treatment in MW-RF-PECVD at 300 °C for 3 h, gave best results in terms of degree of functionalization (calculated by TGA) and reproducibility for all the cases, the value obtained in fact was 186±22 μmol/g.

The reactions performed on annealed NDs were repeated using the *o*-DCB at 120 °C, maintaining the other experimental conditions. Also in this case the reaction performed on **DND4**, to obtain product **DND4-3** and, after Boc deprotection in acidic condition, compound **DND4-4**, gave the bests results and the TGA value was 246±16 μmol/g.

The presence as protecting functional group of the *tert*-butyloxycarbonyl (which is not thermostable) did not allow to use higher temperatures so in order to perform the reactions at 180 °C the (2-{2-[2-(1,3-dioxo-1,3-dihydro-isoindol-2-yl)-ethoxy]-ethoxy}-ethylamino)-acetic acid **7** was used (Scheme 3.7).

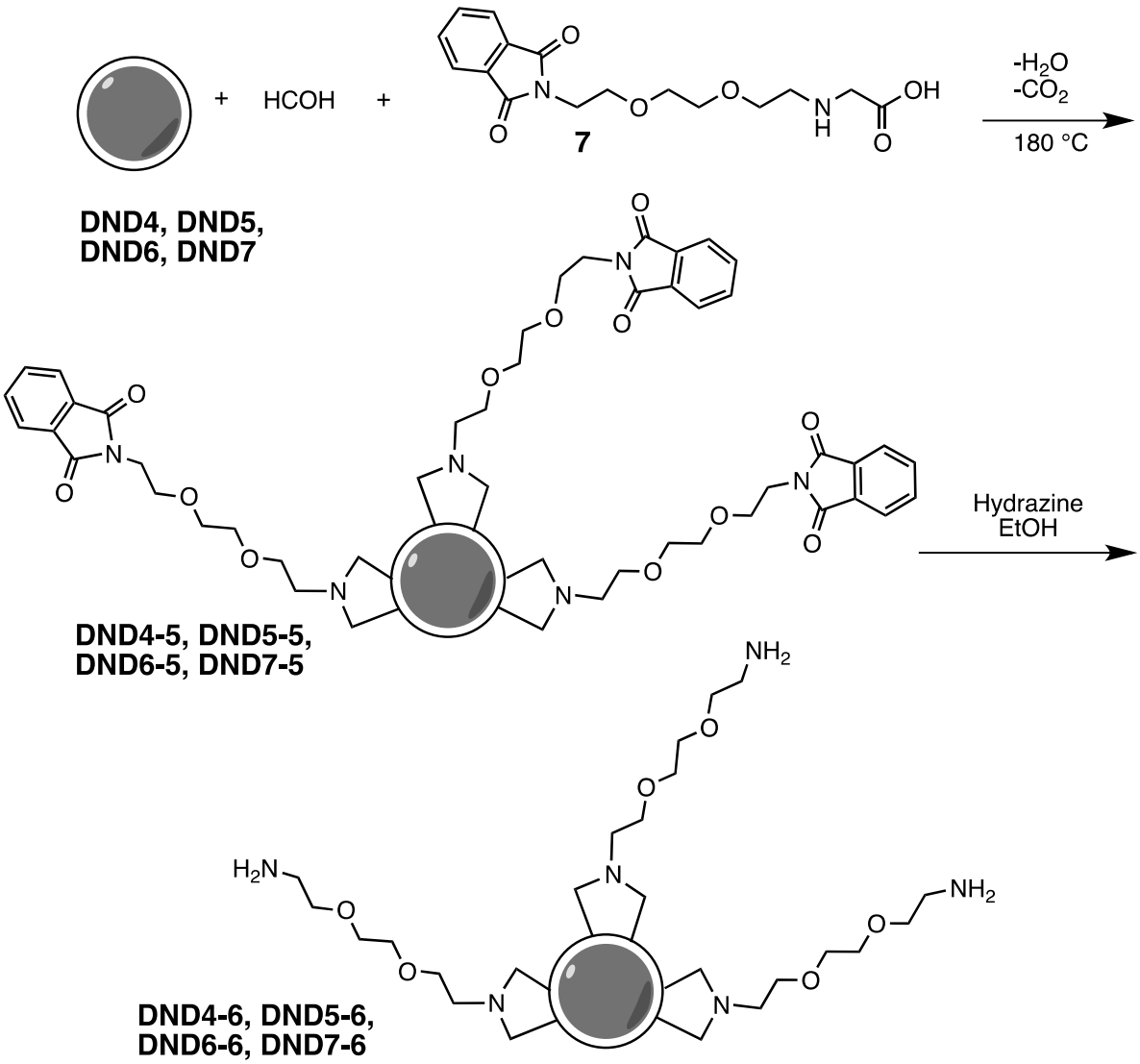

Scheme 3.7: 1,3-dypolar cycloaddition applied on annealed ultrananocrystalline diamonds **DND4**, **DND5**, **DND6**, **DND7** at 180 °C.

The degree of functionalization, calculated from thermogravimetric analysis, was 359±30 μmol/g (Figure 3.22a) and positive Kaiser test was obtained. For a resume of the used condition see Table 3.5.

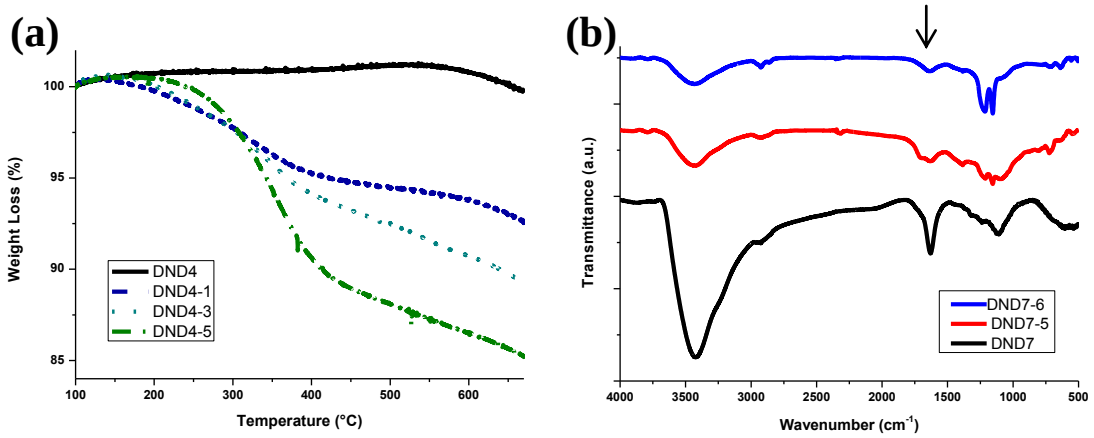

Fig. 3.22: (**a**) TGA of pristine **DND4** (black line), **DND4-1** obtained by cycloaddition at 120 °C in DMF (blue line), in o-DCB at 120 °C (**DND4-3**, light blue line) and at 180 °C (**DND4-5**, green line). (**b**) IR spectra of pristine **DND7** (black line), **DND7-5** obtained by cycloaddition at 180 °C in *o*-DCB (red line) and **DND7-6** (blue line). After the deprotection of the Pht-function the peak at 1710 cm^{-1} (arrow), due to the carboxylic group, disappeared.

Tab. 3.4: Resume table of the conditions used for the 1,3-dipolar cycloaddition.

Solvent	Temperature	Amino acid	Nanodiamond	Deprotected
DMF	120 °C	**3**	**DND4-1**	**DND4-2**
			DND5-1	**DND5-2**
			DND6-1	**DND6-2**
			DND7-1	**DND7-2**
o-DCB	120 °C	**3**	**DND4-3**	**DND4-4**
			DND5-3	**DND5-4**
			DND6-3	**DND6-4**
			DND7-3	**DND7-4**
o-DCB	180 °C	**7**	**DND4-5**	**DND4-6**
			DND5-5	**DND5-6**
			DND6-5	**DND6-6**
			DND7-5	**DND7-6**

The 1,3-dipolar cycloaddition of azomethine ylides was performed also using the MW irradiation for the first time. The **DND4** was chosen for this kind of study because using classical conditions it gave best results in terms of degree of functionalization (calculated by TGA and Kaiser test). In all the cases studied the paraformaldehyde and the α-amino acid **7** were added in excess to form the ylide. The first reaction (**DND4-5A**) was performed under

neat conditions for 90 minutes at 225W power, using a step-wise heating procedure. The degree of functionalization obtained by TGA was 174±10 μmol/g. It was observed that using a longer step-wise heating procedure the degree of functionalization did not increase as expected, in fact with 3 h of reaction the obtained value was 205±5 μmol/g (**DND4-5B**).
To study a possible role of the solvent, the reaction was repeated in *o*-DCB at 50W power with a 60 minutes step-wise procedure. The degree of functionalization obtained by TGA was 274±26 μmol/g, the highest one, and by XPS the appearance of the nitrogen peaks after the reaction confirmed the functionalization (**DND4-5C**).

Tab. 3.5: Resume table of the conditions used for the arylation of **DND4**.

Time	Temperature	System	Conditions	ND	μmol/g
90’	180 °C	MW/closed	**Neat**	**DND4-5A**	174±10
180’	180 °C	MW/closed	**Neat**	**DND4-5B**	205±5
60’	180 °C	MW/closed	***o*-DCB**	**DND4-5C**	274±26

Table 3.6 summarizes the values of binding energy and the surface atomic percentages found by XPS spectroscopy. The C1s peak is centered at 286 eV, the typical value of C-C sp^3. The two other components that are found by fitting are centered at 287 (hydroxyl and ether groups) and 288 eV (carbonyl and carboxyl groups). The presence of surface oxygen-containing groups is confirmed by the presence of the O1s peak that, in agreement with the assignment of the components of C, is composed of two components, a majority at 533 eV which is attributed to oxygen bound to C via single bond and a minority at 532 eV attributed to O associated with the double bond to carbon.
The functionalization is demonstrated by the presence in the samples of the N1s peak, this is fitted by two components 401 and 404 eV. The first is attributed to the amino group, the second (more oxidized nitrogen) is probably due to contamination.

	C1s	O1s	N1s	Surface Atomic Concentration
DND4	286.0 (75%)	531.3 (7%)	-	98% C; 2% O
	287.3 (15%)	533.3 (93%)	-	
	288.4 (10%)			
DND4-5C	286.0 (68%)	531.6 (11%)	401.2 (90%)	96% C; 3% O, 1%N
	287.2 (19%)	533.4 (89%)	404.1 (10%)	
	288.3 (13%)			

Tab. 3.6: Binding energy and the surface atomic percentages found by XPS spectroscopy.

3.6 Arilation

As already reported for carbon nanotubes (CNTs), sp^2 carbon can readily react with diazonium salts.[23] The thermal formation and reaction *in situ* of aryl diazonium species with CNTs was firstly reported in 2001.[24] Schmidt *et al.* proposed that after the generation of the diazonium compound, different events can take place: the reduction of the aryl diazonium salt to an aryl radical, the propagation of aryl radicals (generating new aryl and CNT radicals) and the coupling of radicals, forming in this way the desired C-C coupling between the CNT and the aryl radicals. In this reaction it is possible to obtain biaryl or multiaryl couplings, generating undesired byproducts.[25]
The annealed nanodiamond surface, presenting either isolated double bounds or extended conjugated π-systems, can be a suitable material for the C-C coupling with aryl diazonium salts. Krueger and co-workers have already shown the application of this chemical grafting to thermally annealed nanodiamonds.[4,26] They used different kinds of anilines and products were characterized by good improvement of their solubility in several solvents.
The possibility to simultaneously graft different moieties onto the same conjugate encourage us to explore more in detail also this kind of multivalent functionalization. This approach was already applied on other nanomaterials in order to have for example the simultaneous targeting and labeling in living cells.[27] Krueger and co-workers have already used different reactive moieties to orthogonally functionalize the nanodiamonds surface using the Tour reaction.[28] In particular, they combined alkyne and carboxylic acid groups using a mixture of anilines for the arylation procedure. The one-pot reaction was carried out at 80 °C, overnight.

In this work the so-called Tour reaction was applied various kind of ND, among which the thermally (750 °C, 900 °C) and plasma-treated annealed NDs. The arylation procedure was similar to the one published by Tour et al. for carbon nanotubes[23] The reaction is carried out in water and the diazonium salt was formed *in situ* in presence of aniline and isoamyl nitrite.

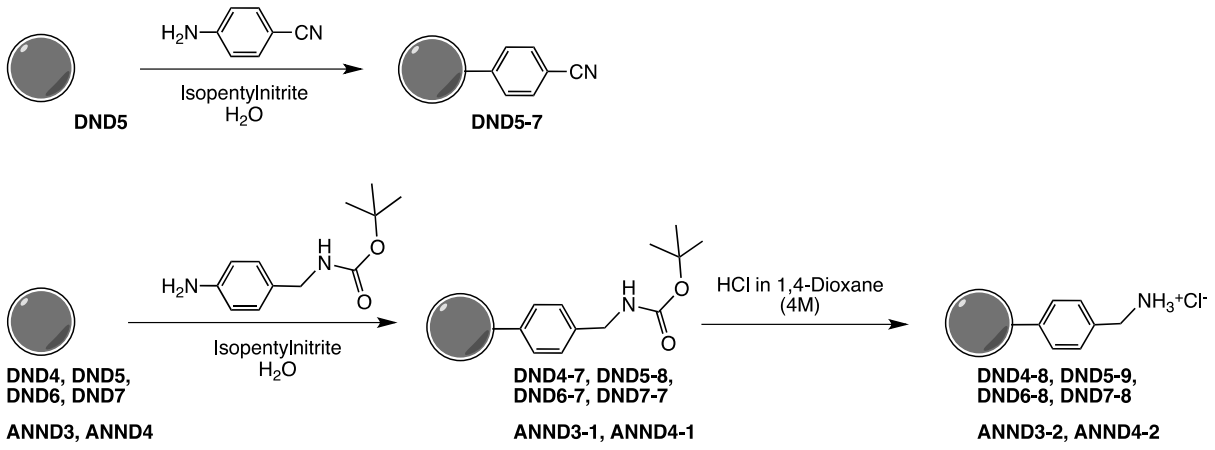

Scheme 3.8: Arylation of annealed NDs

Two different anilines were used as starting materials for the *in situ* formation of their diazonium salts: the 4-aminobenzonitrile and the 4-[(N-Boc)aminomethyl]aniline. The grafting was carried out at 80 °C, overnight, on annealed plasma-treated DNDs (**DND4**, **DND5**, **DND6**, **DND7**) and thermally annealed NDs (**ANND3**, **ANND4**). In the IR spectrum of **DND5-7**, the arylation was confirmed by the presence of the characteristic signal of the –CN group at 2225 cm^{-1} (Figure 3.24). The degree of functionalization obtained by TGA is 483±36 μmol/g.

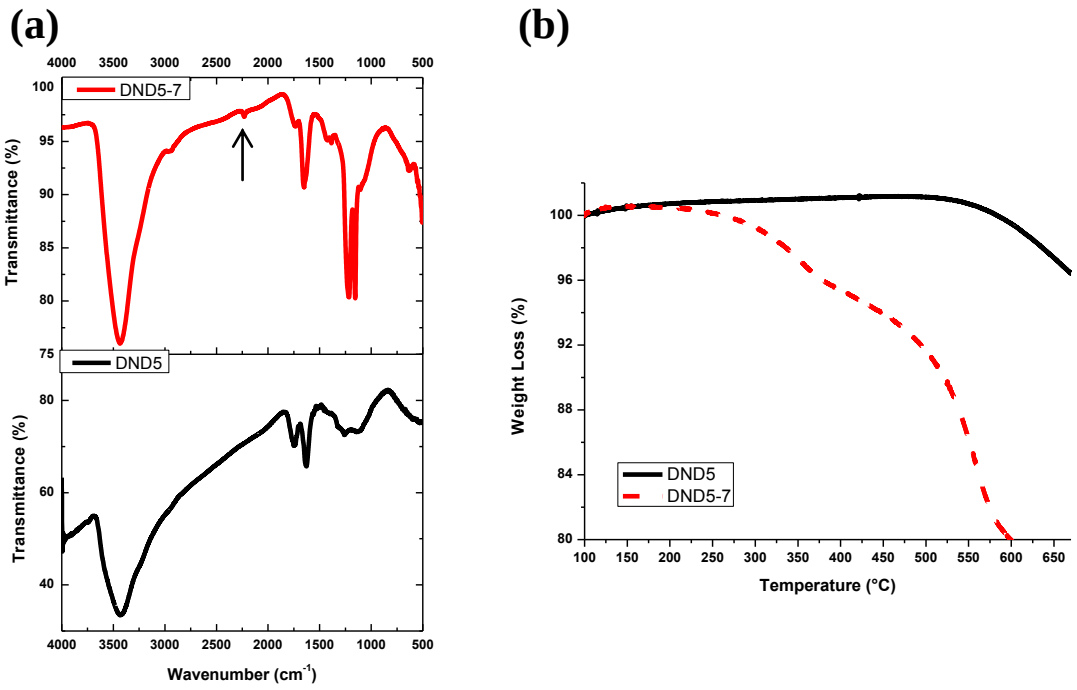

Fig. 3.24: (**a**) IR spectra, using KBr pellets, of annealed **DND5** and **DND5-7**. After the arylation it is possible to observe the characteristic signal of the –CN group at 2225 cm^{-1} (arrow). (**b**) TGA of **DND5** and **DND5-7**..

Also for the arylation with the 4-[(N-Boc)aminomethyl]aniline the **DND4** gave the best results in terms of degree of functionalization (520±23 μmol/g) and reproducibility. The deprotection of the Boc-function was performed in acids conditions and positive Kaiser tests were obtained.

Tab. 3.7: Resume table of the conditions used for the arylation of **DND4**.

Time	Temperature	System	ND	μmol/g	Deprotected
24 h	80 °C	Traditional	**DND4-7**	520	**DND4-8**
90’	80 °C	MW/open	**DND4-9**	500	**DND4-12**
35’	80 °C	MW/closed	**DND4-10**	449	**DND4-13**
15’	110 °C	MW/closed	**DND4-11**	528	**DND4-14**

On **DND4**, the reaction was also performed under microwave radiation, in order to decrease the reaction time and to avoid the presence of undesired byproducts. The reaction was at first performed using an open system for 90 min at 80 °C (**DND4-9**), a degree of functionalization

of 500 μmol/g was obtained, so differences in this sense if compared to the traditional heating previously reported. To further decrease the time, the same reaction was repeated using a closed system, for 35 min at 80 °C (**DND4-10**) and for 15 min at 110 °C (**DND4-11**). The TGA values obtained were 449 μmol/g and 528 μmol/g respectively (Figure 3.25). For all the cases after the Boc- deprotection (**DND4-12**, **DND4-13**, **DND4-14**, respectively) positive Kaiser tests were obtained.

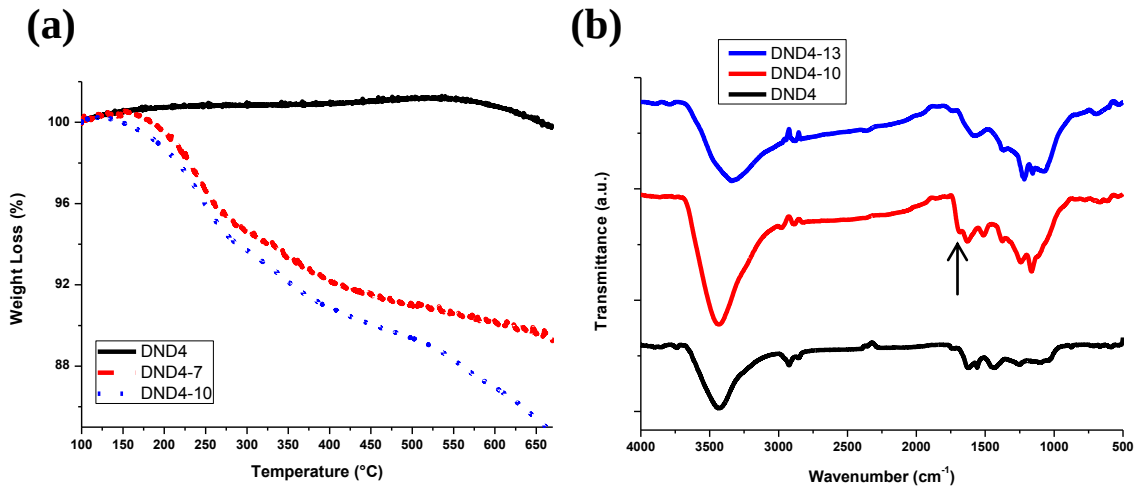

Fig. 3.25: (**a**) TGA of pristine **DND4** (black line), Tour reaction performed overnight at 80 °C in classical conditions (**DND4-7**, red line) and at 80 °C for 35 min under MW (**DND4-10**, blue line). (**b**) IR spectra, using KBr pellets, of annealed **DND4** (black line), **DND4-10** (red line), **DND4-13** (blue line). Only in the red line it is detected the peak of the C=O bond due to the presence of the Boc- group (arrow).

Considering that **DND4** were the annealed nanodiamonds giving the best results in all the experiments so far performed, these NDs were chosen to perform a double Tour reaction, using two different anilines: the 4-aminobenzenesulfonic acid and the 4-[(N-Boc)aminomethyl]aniline. The aim was to improve the water solubility of the nanomaterial, to decrease the reaction time and to achieve a high degree of functionalization. This covalent grafting of benzenesulfonic acid moieties and Boc-protected benzylamines on SWCNT was performed by Gonzalez-Dominguez *et al.*[29] Following the procedure previously reported, different approaches were used: double sequential functionalization (A+B or B+A) and one-pot reaction (AB, Scheme 3.9). Each step was performed both in classical condition (CC) and under MW irradiation. In the first case the grafting was performed at 80 °C for 1 h, in the second the reached temperature 110 °C was maintained for 15 min. The deprotection of the Boc- function was carried out using HCl in 1,4-dioxane (4M) at rt, overnight in all cases.
All the products were characterized by IR spectroscopy, TGA and Kaiser test.
For the single functionalization with 4-aminobenzenesulfonic acid both classical (**DND4-15**) and MW conditions (**DND4-16**) present in their IR spectra the peaks due to the presence of the sulfonic group (1635, 1230, 1190, 1037 and 1008 cm^{-1}) and from TGA the degree of functionalization was 473±15 μmol/g and 421±23 μmol/g, respectively (see Figure 3.26).

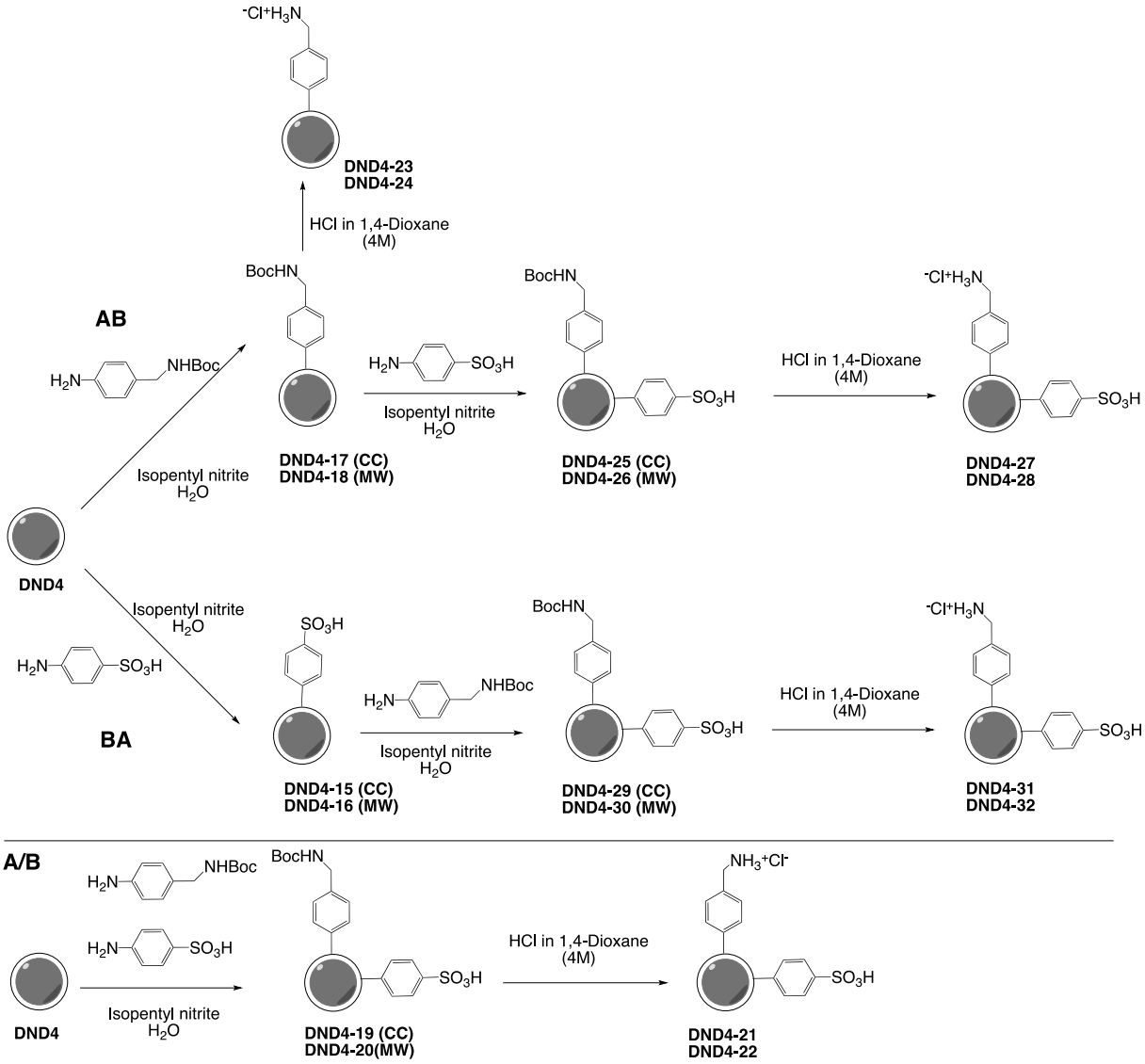

Scheme 3.9: Double Tour reaction. All the steps were performed using both classical conditions, at 80 °C for 1 h, and under MW irradiation for 15 min at 110 °C. The Boc- deprotection was performed using HCl in 1,4-dioxane (4M), rt, overnight.

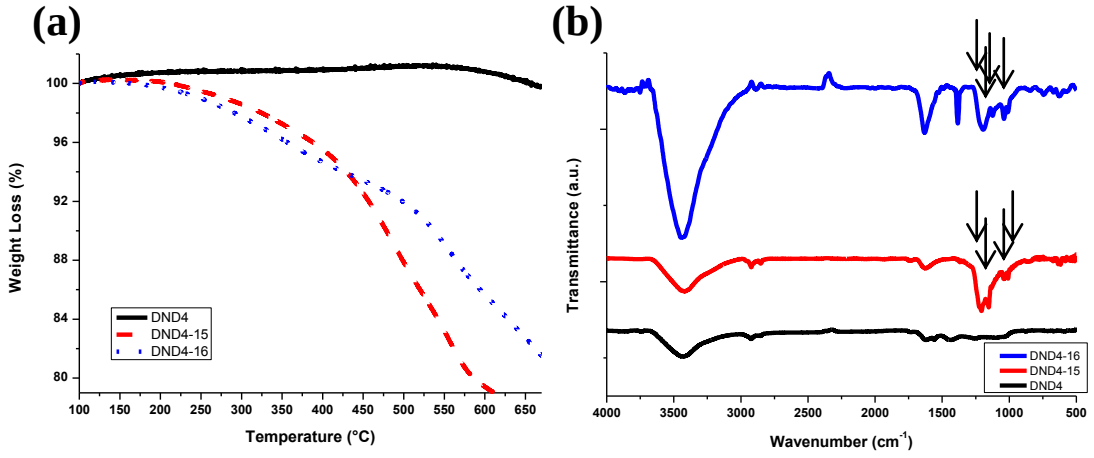

Fig. 3.26: (**a**) TGA and (**b**) IR spectra of pristine **DND4** (black line), **DND4-15** obtained in classical conditions (red line) and **DND4-16** under MW irradiation (blue line). Peaks due to the presence of the sulfonic group (1635, 1230, 1190, 1037 and 1008 cm^{-1}) are present in both cases (arrows).

For the reactions using the 4-[(N-Boc)aminomethyl]aniline both in classical conditions (1 h, 80 °C) and in MW (15 min, 110 °C) the IR spectra have shown the same features found for the reaction performed overnight. The degree of functionalization obtained for 1 h in classical conditions was 538±1 μmol/g.

Also the products obtained by the one-pot double Tour reaction using both classical conditions and MW irradiation (Path A/B, Scheme 3.9) were characterized by the presence in the IR spectra of the peaks due to the presence of the sulfonic group (1635, 1230, 1190, 1037 and 1008 cm^{-1}). The degree of functionalization due to the benzensulfonic moieties was determined by calculating the difference between the value corresponding to the total weight loss at 450 °C (from TGA), and the value calculated by Kaiser test after the Boc-deprotection, due to the free amino groups. For classical conditions the degree of functionalization obtained from Kaiser test was equal to 130 μmol/g so the value calculated for the benzenic sulfonic acid moiety was equal to 101 μmol/g.

For the MW system the difference between the two anilines is even bigger, in fact the value detected by Kaiser test was 170 μmol/g and the value for the benzenesulfonic acid moiety was equal to 34 μmol/g.

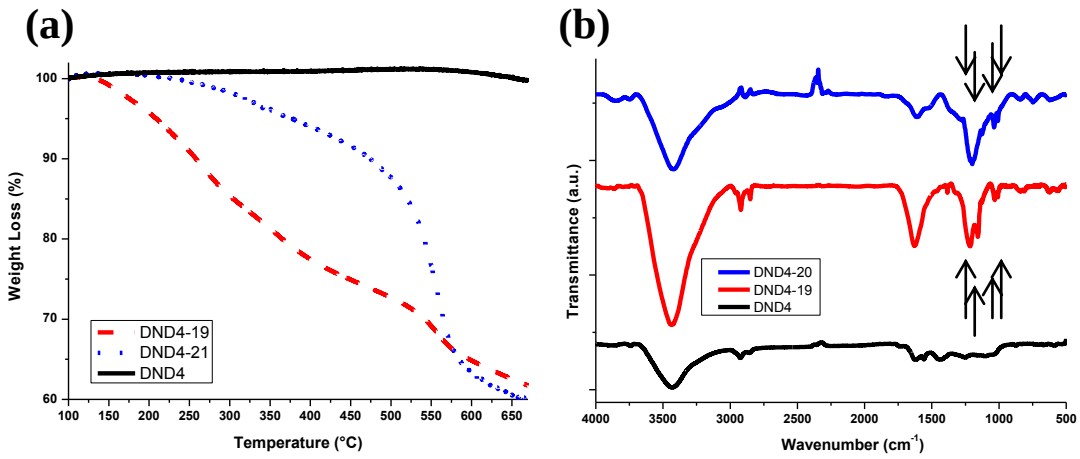

Fig. 3.27: (**a**) TGA and IR spectra (**b**) of pristine **DND4** (black line), one-pot reaction in classical condition (**DND4-19**, red line) and **DND4-21** (blue line). The degree of functionalization due to the benzenesulfonic acid moiety was 101 μmol/g.

The sequential reaction performed using first the 4-aminobenzenesulfonic then the aniline with Boc- function (BA steps) has given a better degree of functionalization for the first aniline with respect to the second (Figure 3.28). This is in agreement with the lower number of sites on NDs surface available for the second reaction. The same behavior, in fact, was obtained for the AB scheme.

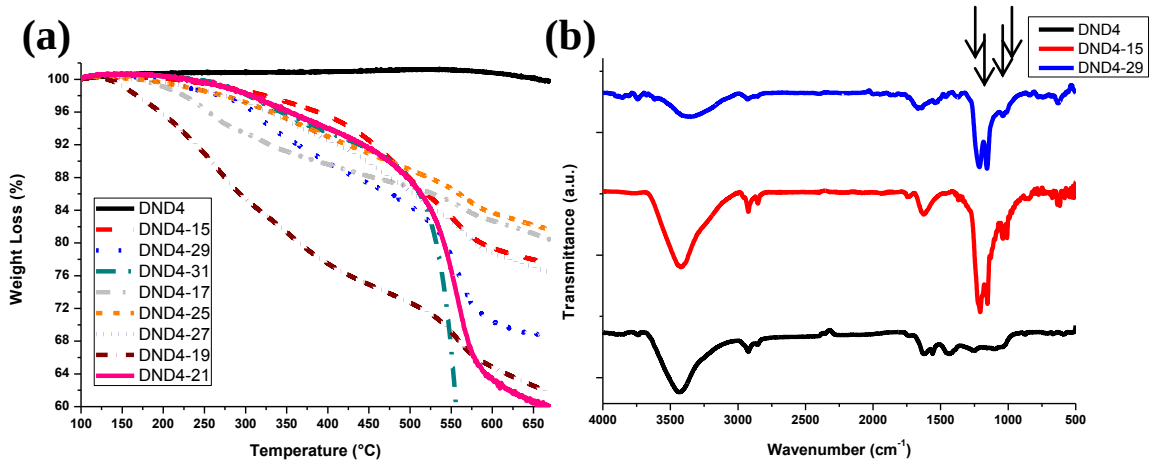

Fig. 3.28: (**a**) TGA of one-pot functionalization (A/B), of the consecutive double reaction AB and BA; (**b**) IR spectra of **DND4** (black line), and of **DND4-15** and **DND4-29**, obtained following the BA scheme. In both cases is possible to find the typical peaks due to the benzensulfonic moieties.

For all the double functionalizations performed (one-pot reaction A/B, AB or BA) the Kaiser test before and after the Boc-deprotection did not match the difference value. This was due to the partial or in some cases total Boc- deprotection in presence of the sulfonic acid moieties that gave a positive Kaiser test also before the intended removal as already reported for the CNTs.

A water dispersibility test was performed for all the samples in Milli-Q water. Functionalized NDs with benzenesulfonic acid or with benzylamine moieties showed an increase of dispersibility in several polar solvents with respect to the pristine **DND4** (Figure 3.29).

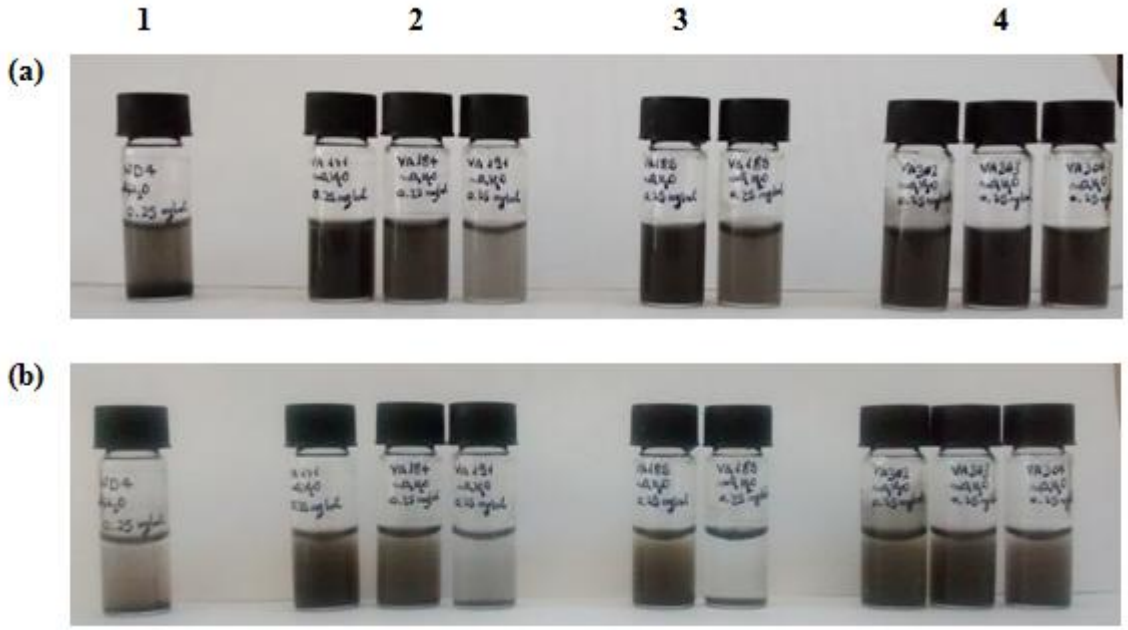

Fig. 3.29: (**a**) Suspensions in Milli-Q water (0.25 mg/ml) of (1) pristine **DND4**; (2) B-ND4 (**DND4-15**), BA-ND4 (**DND4-29**), Boc-deprotection of BA-ND4 (**DND4-31**); (3) one-pot AB-ND4 (**DND4-19**) and Boc-deprotection (**DND4-21**); (4) A-ND4 (**DND4-17**), AB-ND4 (**DND4-25**), Boc-deprotection of AB-ND4 (**DND4-27**). (**b**) Same samples after 24 h.

3.7 Nitrene reaction

Nitrenes (R-N:) can be considered as the nitrogen analogues of a carbenes.[30] They are formed as intermediates during the thermolysis or the photolysis of azides with expulsion of nitrogen gas, they cannot be isolated from the reaction system due to their extremely high reactivity. One of the well-known reactions of nitrene is the [2+1] cycloaddition to unsaturated bonds (present on CNTs, fullerenes, graphene, carbon onions) obtaining the aziridine compounds. The nitrene chemistry was applied on fullerene, where it was observed that mainly the monoadduct occurs, and on graphene nanosheets, where desired functional groups (i.e. –OH, -COOH, -Br), alkyl chains and polymers could be covalently and stably linked on.[31] The first work for the functionalization of CNTs via nitrene chemistry was performed by Holzinger *et al.* in 2001[32] and in a followed detailed study of nitrene functionalization, a variety of precursors were employed, containing alkyl chains, aromatic groups, dendrimers, crown ethers.[33] A further example of the [2+1] cycloaddition was the functionalization of carbon nano-onions using the 2-azidoethanol that gave an increase of solubility of the nanomaterial both in organic solvents and water.[34]

The nitrene reaction was carried out on annealed plasma-treated NDs (**DND4**, **DND5**, **DND6**, **DND7**) at 160 °C for 7 h. Also in this case the **DND4** gave best results, with positive Kaiser tests after the phthalimide deprotection. The cycloaddition was repeated at 180 °C and increasing the reaction time. The optimization condition studies were carried out on **DND6**.

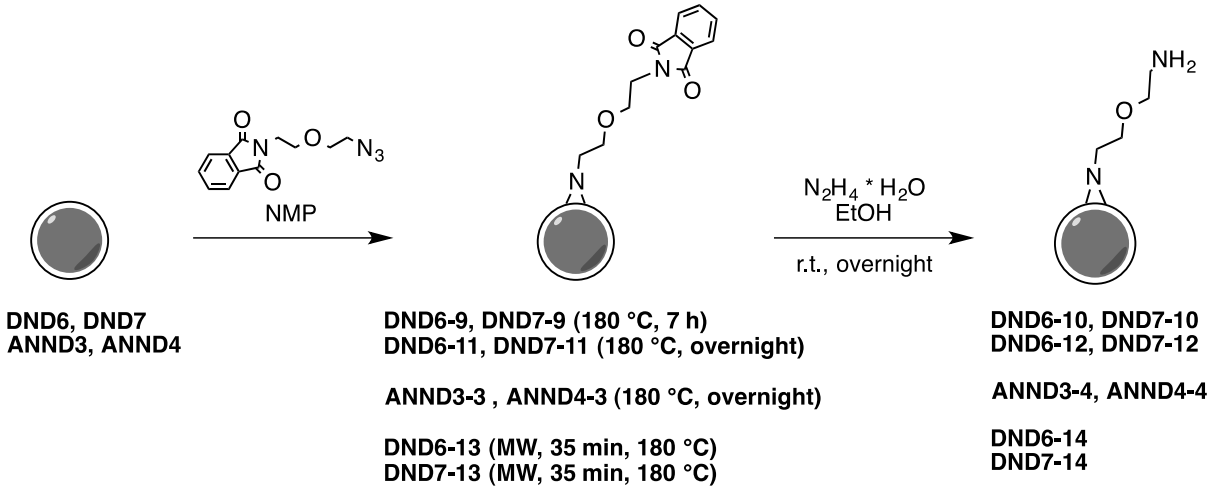

Scheme 3.10: Nitrene reaction on annealed NDs and deprotection of the phtalimide.

Best results were obtained for reactions carried out overnight at 180 °C, in fact the degree of functionalization obtained by TGA was 256±18 μmol/g for **DND6** (Figure 3.30a) and, after the deprotection, a positive Kaiser test was detected. After the [2+1] cycloaddition a peak at 1714 cm^{-1} was detected for all the samples, probably due to the C=O stretching of the Pht-function, in fact after the deprotection it was not anymore observed (Figure 3.30b).

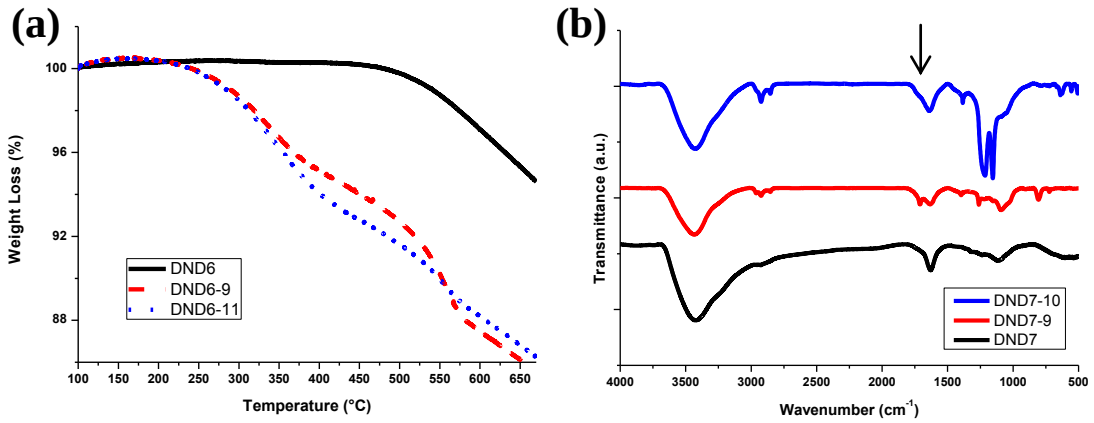

Fig. 3.30: (**a**) TGA of nitrene reaction performed on **DND6** at 180 °C for 7 h (red line) and overnight (blue line). (**b**) IR spectra, using KBr pellets, of pristine **DND7** (black line), **DND7-9** (red line) and after deprotection (**DND7-10,** blue line).

Tab. 3.8: Resume table of the conditions used for the nitrene on annealed NDs.

Time	Temperature	System	ND	µmol/g	Deprotected
7 h	180 °C	Traditional	**DND6-9**	**211±5**	**DND6-10**
			DND7-9	**207±12**	**DND7-10**
overnight	180 °C	Traditional	**DND6-11**	**256±18**	**DND6-12**
			DND7-11	**232±7**	**DND7-12**
			ANND3-3	**152±14**	**ANND3-4**
			ANND4-3	**198±6**	**ANND4-4**
35’	180 °C	MW/closed	**DND6-13**	**194±23**	**DND6-14**
			DND7-13	**170±5**	**DND7-14**

Optimized conditions (180 °C, overnight) were applied on thermally annealed NDs (**ANND3**, **ANND4**). In both cases after the coupling the peak at 1714 cm^{-1} was detected and the best degree of functionalization, calculated by TGA, was obtained for the 900 °C annealed ND (**ANND4**).

To decrease the reaction time, the [2+1] cycloaddition was carried out under MW irradiation at 180 °C. Also in this case the reaction was performed on all the annealed NDs, for 35 min. The best degree of functionalization was obtained for the **DND6** and decreasing the time to 5 min no changes were detected in terms of degree of functionalization, calculated by TGA. After deprotection, positive Kaiser tests were obtained.

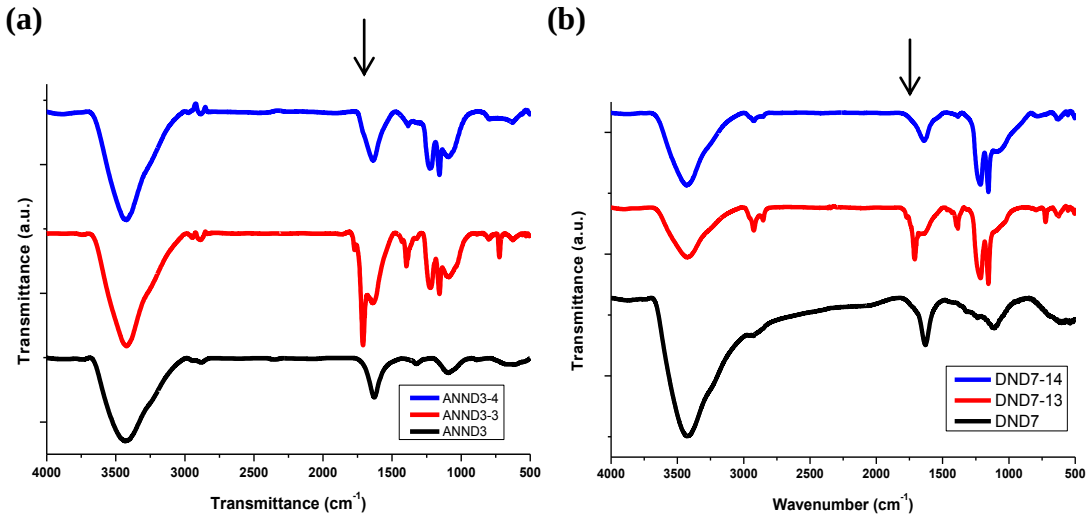

Fig. 3.31: IR spectra, using KBr pellets, (**a**) of pristine **ANND3** (black line), **ANND3-3** (nitrene reaction at 180 °C, overnight, red line) and deprotection (**ANND3-4**, blue line); (**b**) of pristine **DND7** (black line), **DND7-13** (nitrene reaction with MW irradiation, red line) and **DND7-14** (blue line).

3.8 Functionalization of nanodiamonds with tumor-homing peptide

Cancer is one of the leading causes of mortality worldwide. Despite the presence of several anticancer agents, cancer treatment is still not very effective. This is usually due to the lack of screening tests for early diagnosis and to the non-availability of tumor specific drug delivery system. Most of the current used anticancer drugs are not able to differentiate between cancerous and normal cells and this lead to a systematic toxicity and known adverse side effects. In order to solve this problem, a big progress has been done to identify peptides able to specifically bind tumor cells with respect to normal ones.[35]

Integrins, highly expressed in tumor cells, are membrane receptors able to mediate cell-cell and cell-matrix interactions, they play an important role in cell signaling, cell proliferation, apoptosis, invasion, metastasis, gene expression and tumor angiogenesis (Figure 3.32).[36]

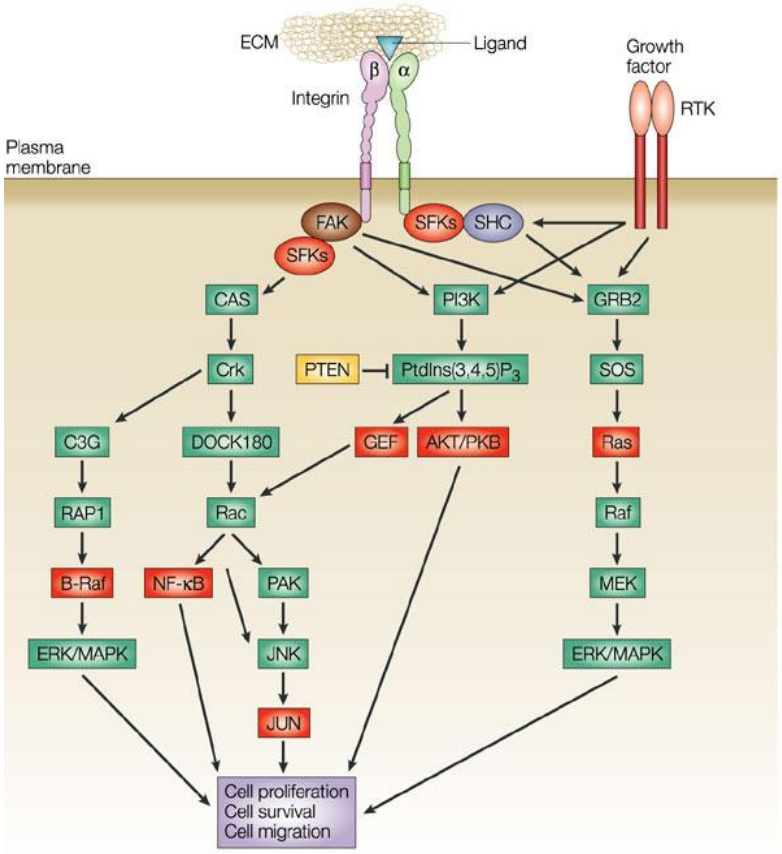

Fig. 3.32: Integrins through their interaction with extracellular matrix proteins as fibronectin, mediate the migration and survival of tumor cells and angiogenic endothelial cells. When triggered, integrins in turn trigger chemical pathways to the interior (signal transduction), such as the chemical composition and mechanical status of the ECM, which results in a response (activation of transcription) such as regulation of the cell cycle, cell shape, and/or motility. When a binding between tumor-homing peptides and specific integrins occurs, the unavailability of sites for ligands such as fibronectin are avoiding the triggering of chemical pathways responsible for cell proliferation, cell survival and cell migration.[36a]

Peptide sequences including NGR,[37] APRPG,[38] RGD[39] have been used for tumor and tumor-vasculature-targeting carrier. For example, RGD-modified liposomes,[40] nanoparticles,[41] dendrimers[42] and micelles[43] have been demonstrated to increase the intracellular delivery of chemotherapeutic agents or genes *in vitro* and *in vivo*.

Small RGD peptides derived from proteins of extracellular matrix have shown good bioactivity by binding to integrins receptors on the cell surface. In particular, cyclic RGD peptides exhibit a remarkable biological activity and it was observed that cyclization of the RGD motif stabilizes the bioactive conformation. The c(RGDfK), firstly designed and synthetized by Kessler and co-workers, was selected as delivery vehicle because the lysine side-chain provides a convenient handle for attaching specific groups or molecules, in fact the lysine residue is not involved in binding to the $\alpha_v\beta_3$ integrins.[44]

The NGR-peptide NGRSL, which is the ligand for aminopeptidase N, a marker of angiogenic endothelial cells, has proven useful for delivering various antitumor compounds to tumor vessels. In a work of Pastorino *et al.* the NGRSL peptide was coupled to the surface of liposomial doxorubicin and it was used to treat neuroblastoma in SCID mice. It was observed that the properties of the NGR-target liposomes may result in a higher and more durable anticancer effect than a strictly antiangiogenic approach.[45]

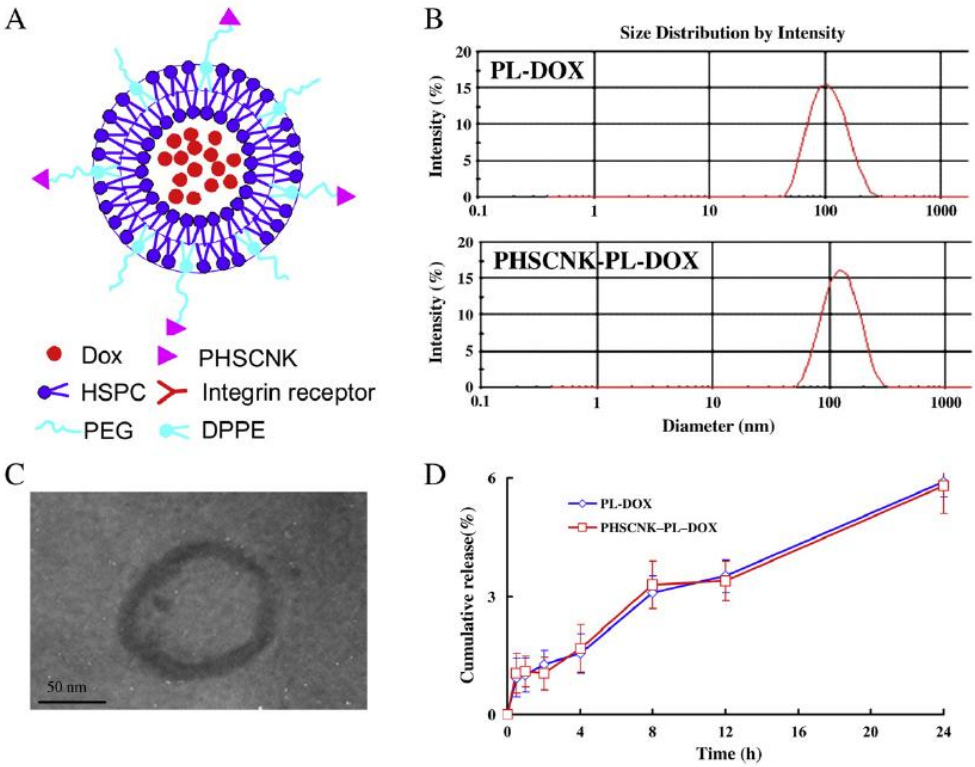

Fig. 3.33: Ac-PHSCNK-NH_2 was used as a novel homing peptide to prepare ligand-targeted liposomes loaded with doxorubicin (PHSCNK-PL-DOX), stealth liposomes loaded with doxorubicin (PL-DOX) were used as the control. PHSCNK-PL-DOX demonstrated an enhanced intracellular uptake and a greater cytotoxicity against melanoma B16F10 cells in comparison with PL-DOX. (**A**) Illustration of PHSCNK-modified and DOX-loaded PEGylated liposomes. (**B**) Size distribution of DOX-loaded PEGylated liposomes PL-DOX and PHSCNK-modified DOX-loaded PEGylated liposomes (PHSCNK-PL-DOX) by dynamic light scattering analysis. (**C**) TEM photomicrograph of PHSCNK-PL-DOX. (**D**) Cumulative release profiles of DOX from PL-DOX and PHSCNK-PL-DOX.[46]

The so-called ATN-161, currently in phase II trials for various cancer therapies, is a noncompetitive inhibitor of the human fibronectin in which a cysteine residue replaces an arginine in the original sequence (PHSCN) and it was observed that capping the ends of the peptide by acetylation and amidation yields a product with good pharmaceutical properties such as the stability and the bioactivity (Figure3.33).[46,47]
Unlike other integrin antagonists, ATN-161 does not block integrin-dependent adhesion, but may inhibit integrin-dependent signaling. Moreover, recent studies have shown that this peptide binds exclusively to integrin beta subunits. Disulphide interchange has been proposed to mediate integrin activation, and the hypothesis is that the free cystein thiol in ATN-161 blocks this interchange by forming a disulphide with the integrin target, thereby suppressing integrin function.

Nanomedicine could become a good solution for specificity and toxicity problems with current chemotherapy treatment regimens.[48] Currently, there are several clinically approved nanoparticle-based cancer drugs using liposomes, dendrimers, polymeric, and metal nanoparticles. These techniques have proven the importance of targeting for improved chemotherapeutic efficacy, but there can be limitations in biocompatibility, delivery and bioavailability, due to size. It was already observed that the use of nanoparticles confers several advantages over that of free drugs, including their capability to carry high payloads of therapeutic agents, confer increased half-life and reduced toxicity to the drugs, and provide means for selective targeting of the tumor tissue and vasculature.[49]
Over the past five years, nanodiamonds have been studied to be used in various drug delivery systems but minimal work has been done incorporating targeting molecules.

In this work, commercial detonation nanodiamond, oxidized by acid treatments, were used for their coupling with short tumor-homing peptides.

3.8.1 Synthesis of ND-c(RGDfK) and ND-AcPHSCNK-C(O)NH_2 conjugates

Oxidized **ANND1** were conjugated with c(RGDfK) and N-acetyl-PHSCNK-C(O)NH_2 peptides using the carbodiimide chemistry, as shown in scheme 3.11. The 1-Ethyl-3-(3-dimethylaminopropyl)-carbodiimide (EDC) was used to activate the carboxylic groups present on NDs surface. To increase the stability of the active ester, N-hydroxysuccinimide (NHS) was used, in fact the addition of NHS stabilizes the amine-reactive intermediate by converting it to an amine-reactive NHS ester, thus increasing the efficiency of EDC-mediated coupling reactions. The reaction was carried out in DMF for 48 h at room temperature.

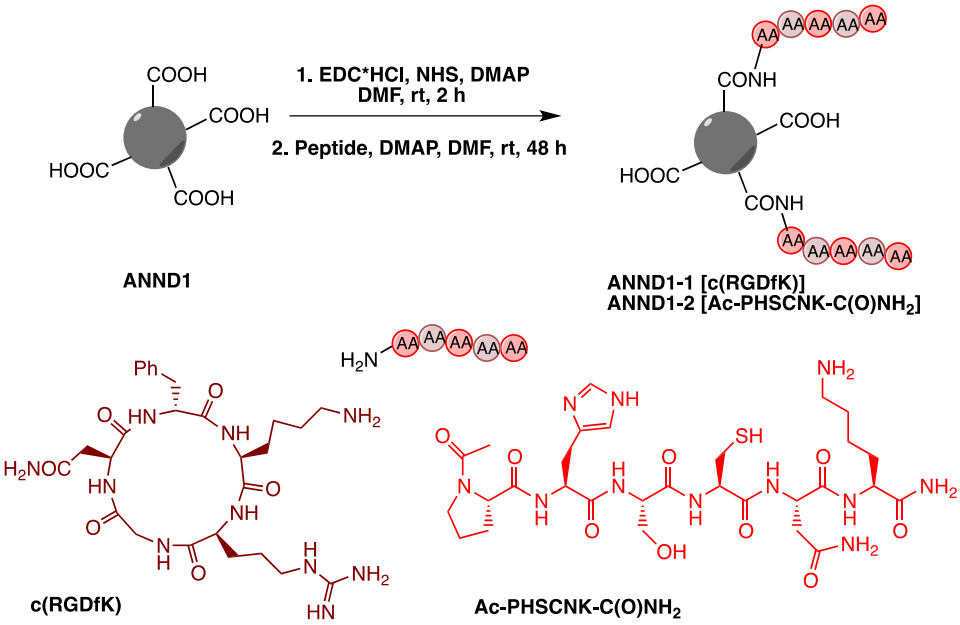

Scheme 3.11: ND-peptide conjugation with c(RGDfK) and Ac-PHSCNK-C(O)NH_2 peptides. The carbodiimide reaction used EDC and NHS to form a stable amide bond between the free amino group on the peptide and the carboxylic group on the ND surface.

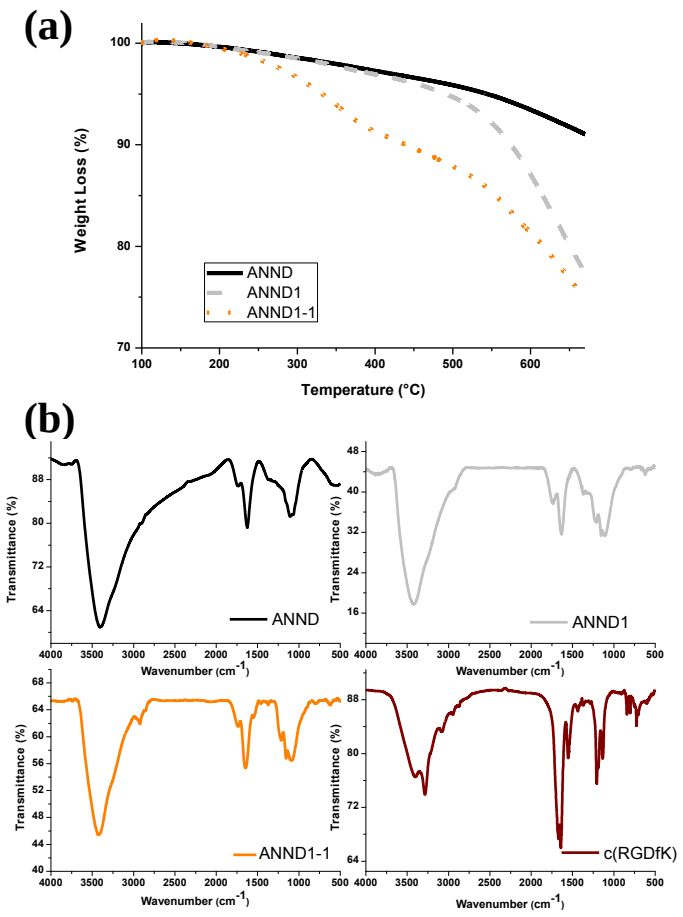

Fig. 3.34: (a) TGA and (**b**) IR spectra of pristine **ANND** (black line), oxidized **ANND1** (grey line) and coupling with c(RGDfK) peptide (**ANND1-1**, orange line). In the IR spectrum it was possible to detect the appearance of the peak at 1563 cm^{-1}, typical of the c(RGDfK) peptide (brown line).

After the purification, both ND-c(RGDfK) (**ANND1-1**) and ND-AcPHSCNK-C(O)NH_2 conjugates (**ANND1-2**) were characterized by TGA and IR spectroscopy (Figure 3.34, 3.35). The degree of functionalization obtained by TGA was for **ANND1-1** 115±8 μmol/g, while for **ANND1-2** was 86.2±0.8 μmol/g.

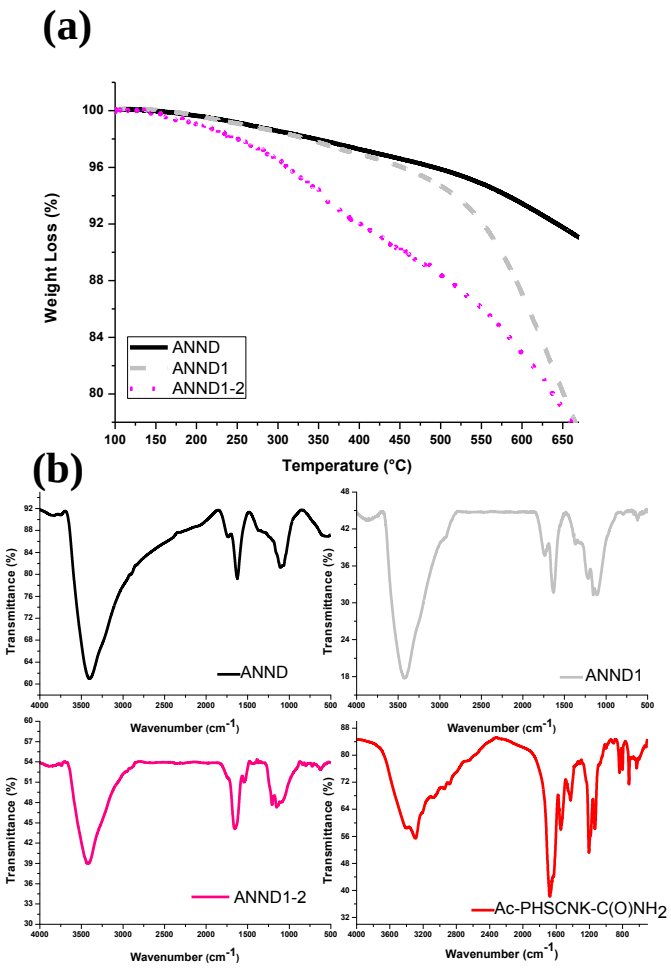

Fig. 3.35: (**a**) TGA and (**b**) IR spectra of pristine **ANND** (black line), oxidized **ANND1** (grey line) and coupling with Ac-PHSCNK-C(O)NH_2 peptide (**ANND1-2**, pink line). In the IR spectrum it was possible to detect the appearance of the peak at 1542 cm^{-1}, typical of the Ac-PHSCNK-C(O)NH_2 peptide (red line).

Tab. 3.9: Resume table of the coupling products

ND	**μmol/g**
ANND1	875±18
ANND1-1	115±8
ANND1-2	86.2±0.8

3.8.2 Synthesis of ND-peptide conjugates by maleimide function

Oxidized NDs were also conjugated to 3 peptides presenting a thiol group in their sequence. To do that, **ANND1** have been first amidated, as previously described, obtaining **ANND1-3**, the amine groups were deprotected (**ANND1-4**) and allowed to react with N-succinimidyl-3-maleimidopropionate, obtaining **ANND1-5**. The latter was then dispersed in DMF and allowed to undergo the Michael addition in presence of the different peptides (Scheme 3.12).

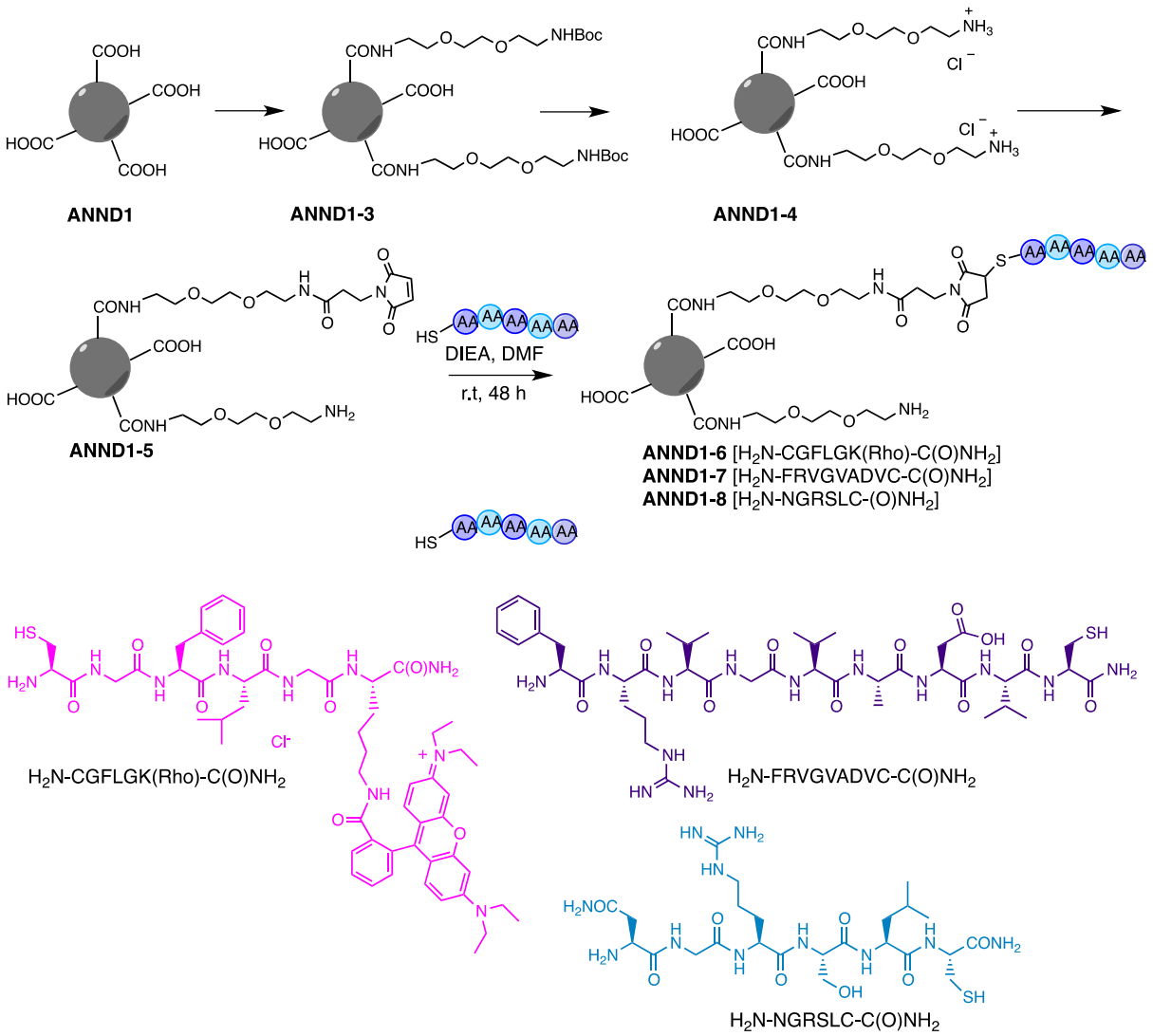

Scheme 3.12: ND-peptide conjugation with H_2N-FRVGVADVC-C(O)NH_2, H_2N-NGRSLC-C(O)$NH_2$and H_2N-CGFLGK(Rho)-C(O)NH_2 The coupling is based on the addition to the double bound of the maleimide group on NDs and the thiol group of cysteine residues in the peptides.

After the purification, all the NDs coupled with these peptides were characterized by TGA and IR spectroscopy (Figure 3.36-38). The degree of functionalization obtained by TGA was:
for ND-FRVGVADVC-C(O)NH_2 conjugated **ANND1-6** 51±4 μmol/g;
for ND-NGRSLC-C(O)NH_2 conjugated **ANND1-7** 53±11 μmol/g; and
for ND-CGLSLCK(Rho)-C(O)NH_2 conjugated **ANND1-8** 43±6 μmol/g.

The biological behavior of these conjugates will be studied.

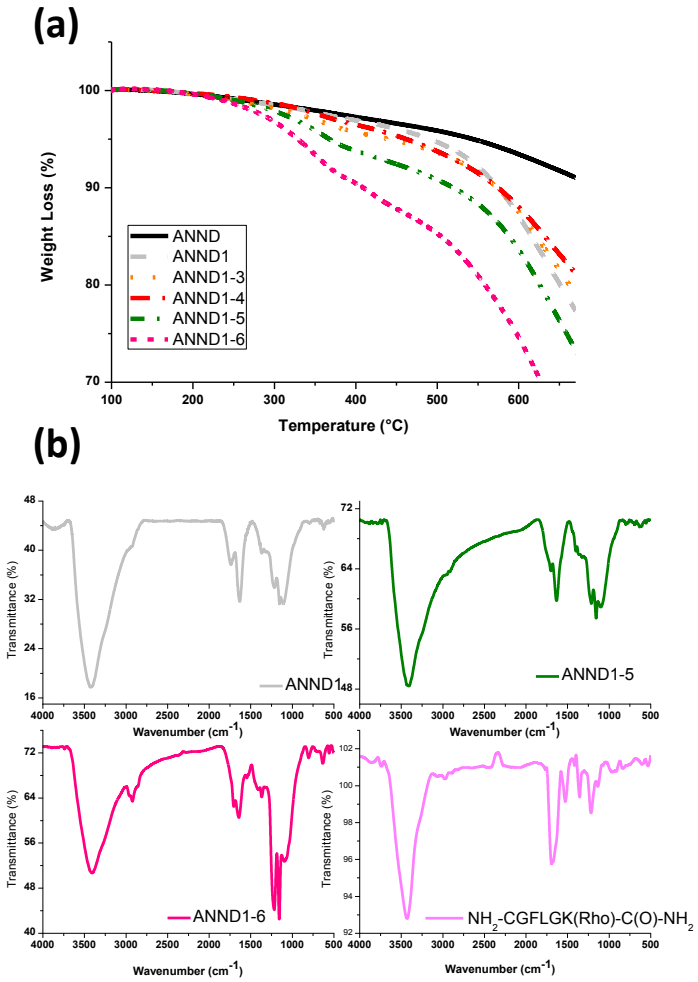

Fig. 3.36: (**a**) TGA and (**b**) IR spectra of pristine **ANND** (black line), oxidized **ANND1** (grey line) and coupling with NH_2-CGLSLCK(Rho)-C(O)NH_2 peptide (**ANND1-6,** fuchsia line). In the IR spectrum it was possible to detect the appearance of the peak at 1563 cm^{-1}, typical of the NH_2-CGLSLCK(Rho)-C(O)NH_2 peptide (pink line).

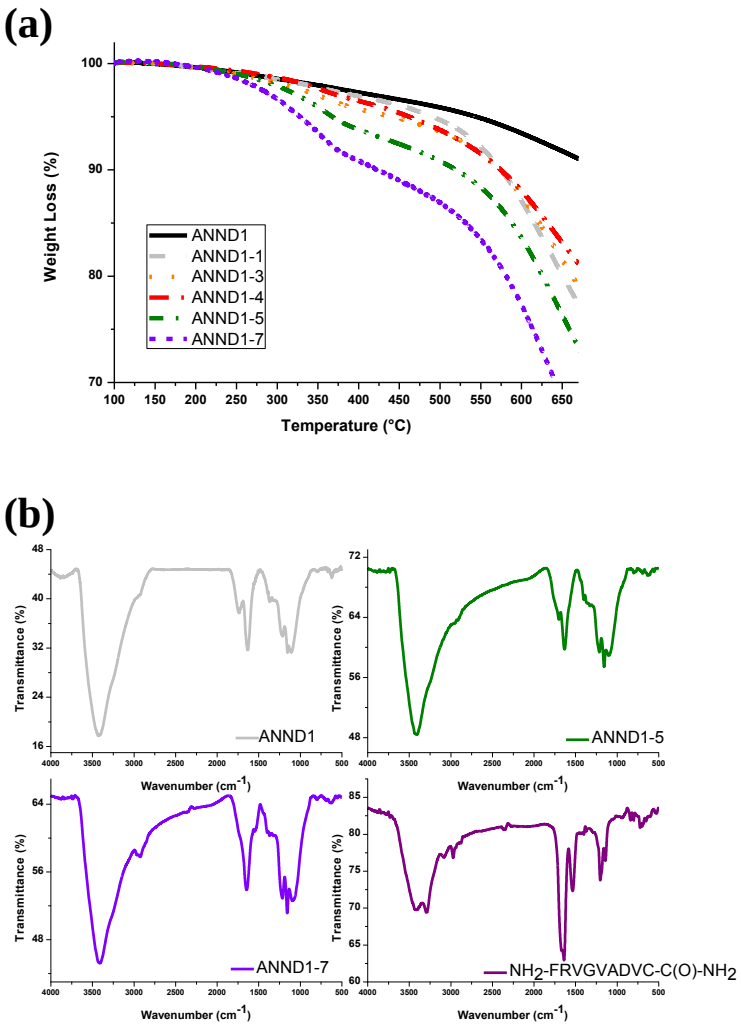

Fig. 3.37: (**a**) TGA and (**b**) IR spectra of pristine **ANND** (black line), oxidized **ANND1** (grey line) and coupling with NH_2-FRVGVADVC-C(O)NH_2 peptide (**ANND1-7**, violet line). In the IR spectrum it was possible to detect the appearance of the peak at 1563 cm^{-1}, typical of the NH_2-FRVGVADVC-C(O)NH_2 peptide (purple line).

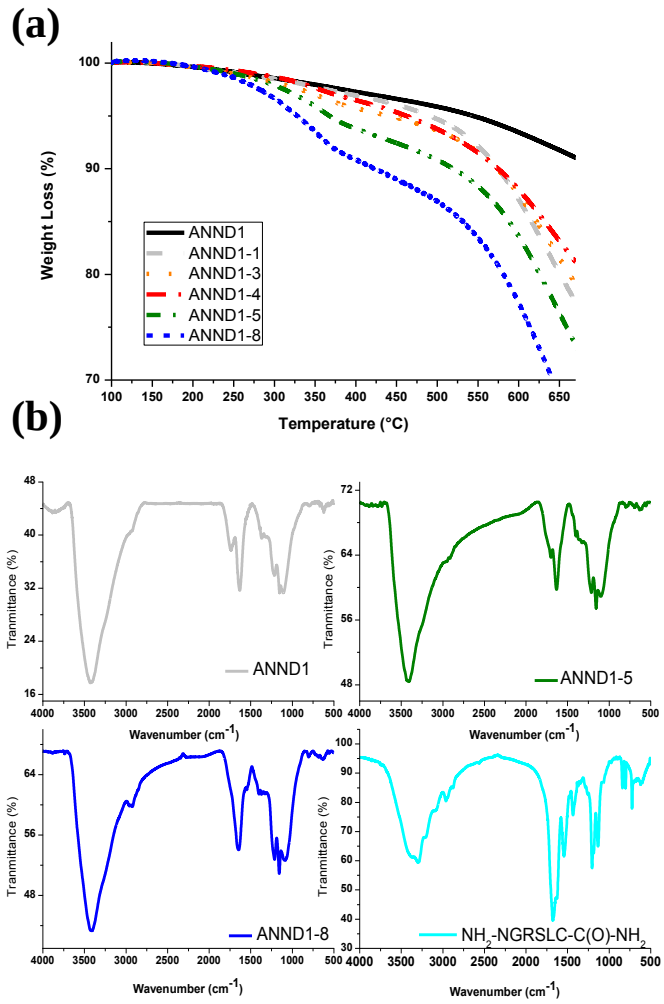

Fig. 3.38: (**a**) TGA and (**b**) IR spectra of pristine **ANND** (black line), oxidized **ANND1** (grey line) and coupling with NH_2-NGRSLC-C(O)NH_2 peptide (**ANND1-8**, blue line). In the IR spectrum it was possible to detect the appearance of the peak at 1563 cm^{-1}, typical of the NH_2-NGRSLC-C(O)NH_2 peptide (cyan line).

Tab. 3.10: Resume table of the coupling products

ND	µmol/g
ANND1	875±18
ANND1-3	50±20
ANND1-4	51±3
ANND1-5	119±17
ANND1-6	51±4
ANND1-7	53±11
ANND1-8	43±6

3.9 Study of biocompatibility of pristine and functionalized ultrananocrystalline diamonds

The study of biocompatibility of ultrananocrystalline diamonds was performed by Dr. Delogu group (University of Sassari).

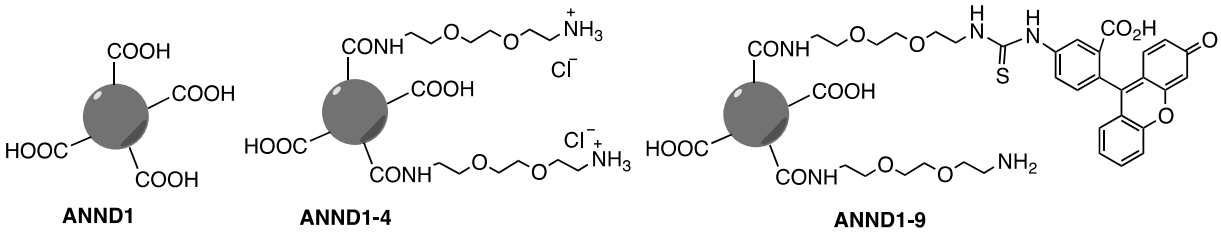

Fig. 3.39: Ultrananocrystalline diamonds used for biological tests.

The study was done on peripheral blood mononuclear cells (PBMC), consisting of lymphocytes (T cells, B cells, NK cells) and monocytes. These cells can be extracted from whole blood using ficoll, a hydrophilic polysaccharide that create a density gradient by centrifugation. In this was it is possible to separate the blood into a top layer of plasma, followed by a layer of PBMCs (a critical component in the immune system) and a bottom fraction of polymorphonuclear cells and erythrocytes.
The study of biocompatibility was performed using **ANND1** and **ANND1-4** samples and performing a MTT assay on this kind of cells. It was observed a dose-dependent decrease in viability, in fact increasing the concentration of nanodiamond suspensions, a lower cell viability was detected. Moreover, at higher concentrations NDs with free amino groups (**ANND1-4**) were found to be more toxic than oxidized NDs (**ANND1**). This is in accordance with literature.

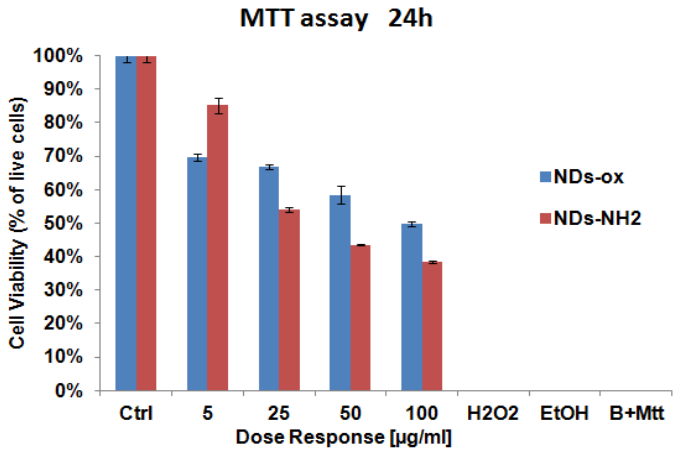

Fig. 3.40: MTT assay performed using ANND1 and ANND1-4 samples. Dose-dependent decrease in viability and different toxicity were observed.

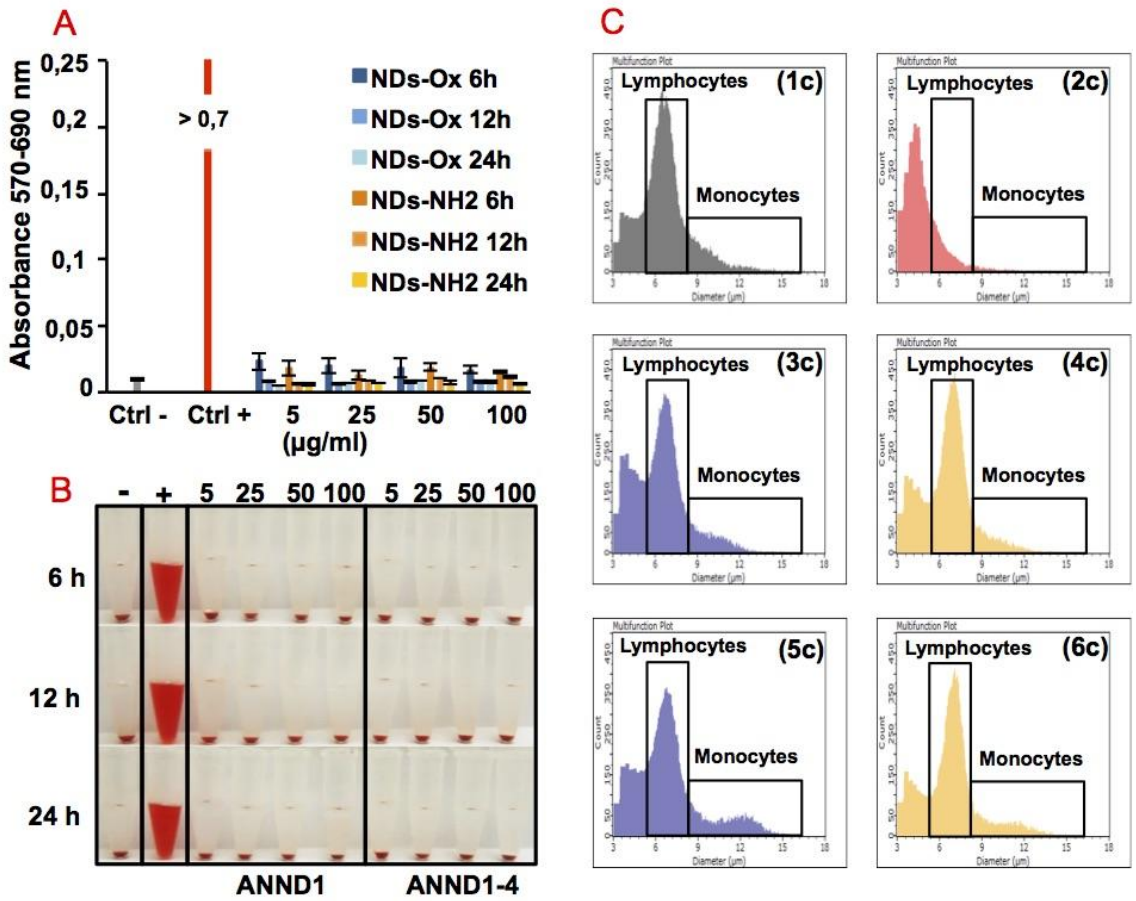

Fig. 3.41: Viability tests using **ANND1** and **ANND1-4**. **(A)** Samples were analysed by spectrophotometer. The haemolysis value is reported in Absorbance (570-690 nm). **(B)** Pictures of human RBCs treated with **ANND1**/ **ANND1-4** at the same dose response. Vitality test on human PBMCs (Lymphocytes and Monocytes) of dose 50 µg/ml treated with **ANND1** (blue, left side) and **ANND1-4** (orange, right side) incubated for 6 h (3c and 4c) and 24 h (5c and 6c). PBMCs is the negative (1c) control and PBMCs/EtOH 70% the positive (2c) one. PBMCs: Periferal Blood Mononuclear Cells; RBCs: Red Blood Cells; CTRL: control; PBS: Phosphate Buffered Saline; DDW: Distilled Deionized Water.

Also haemolysis test on RBCs were performed using increasing doses (5, 25, 50 and 100 µg/ml) of **ANND1** and **ANND1-4** incubated for 6, 12, 24 h. The samples were analysed by spectrophotometer (Figure 3.41A). The haemolysis value is reported in Absorbance (570-690 nm) and it is evident that no significant haemolytic effect was found at the used concentration. Another indication of the lack of haemolytic effect is evident from Figure 3.41B where pictures of human RBCs treated with **ANND1** and **ANND1-4** at the same dose response are reported. The red colour of solution in the case of the positive control shows the release of haemoglobin from RBCs and the pellet at the bottom of the Eppendorf tubes are intact RBCs precipitated by centrifugation.

Vitality test on human PBMCs (Lymphocytes and Monocytes) were performed using 50 µg/ml of **ANND1** and **ANND1-4**. The behaviours of the population are shown in Figure 3.41C at different incubation time: 6 h (3c and 4c) and 24 h (5c and 6c). The graphics show

that PBMCs treated with NDs are healthy after incubation 6 and 24 hours. The graphics after 24 h (5c and 6c) show the monocytes activation.

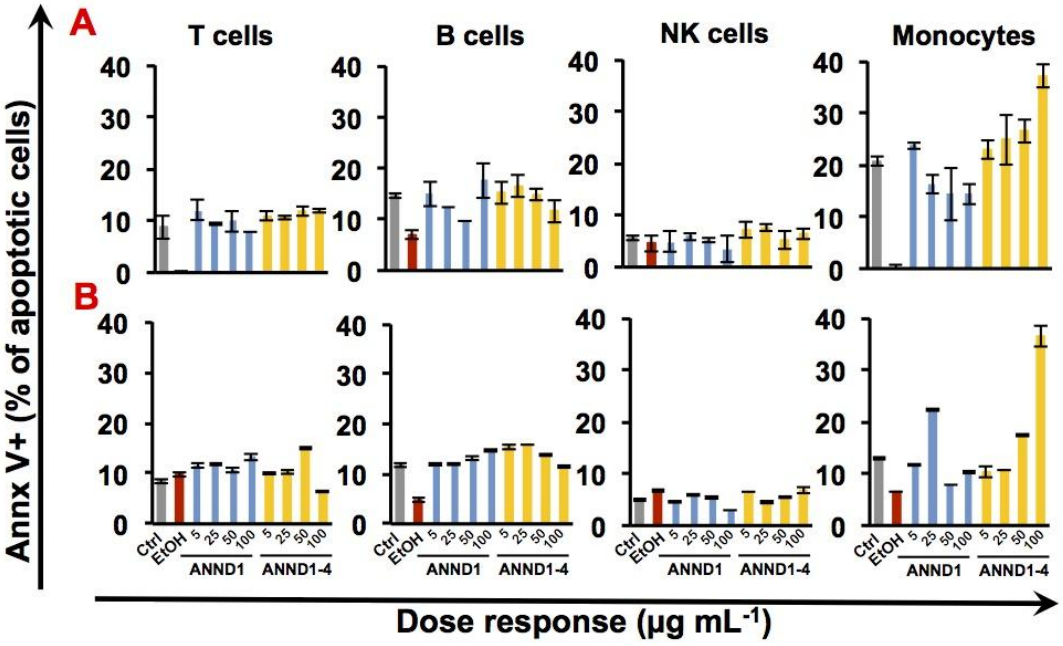

Fig. 3.42: **ANND1** (blue) and **ANND1-4** (orange). The graphics were shown the percentage of Annexin V positive cells after incubation 6 h (A) and after 24 h (B). Annx V: Annexin V.

To study the apoptotic response of PBMCs, these cells were treated with increasing doses (5, 25, 50, 100 µg/ml) of **ANND1** (blue) and **ANND1-4** (orange). Apoptotic cells were stained with Annexin V and with specific antibodies for each population (T, B, NK cells and Monocytes). The analyses were performed with flow cytometry and in the graphics (Figure3.42) were shown the percentage of Annexin V positive cells after incubation 6 h (A) and after 24 h (B). A certain effect was reported for both NDs in the case of monocytes, while for B, T and NK cells the populations were not significantly affected by the treatment.

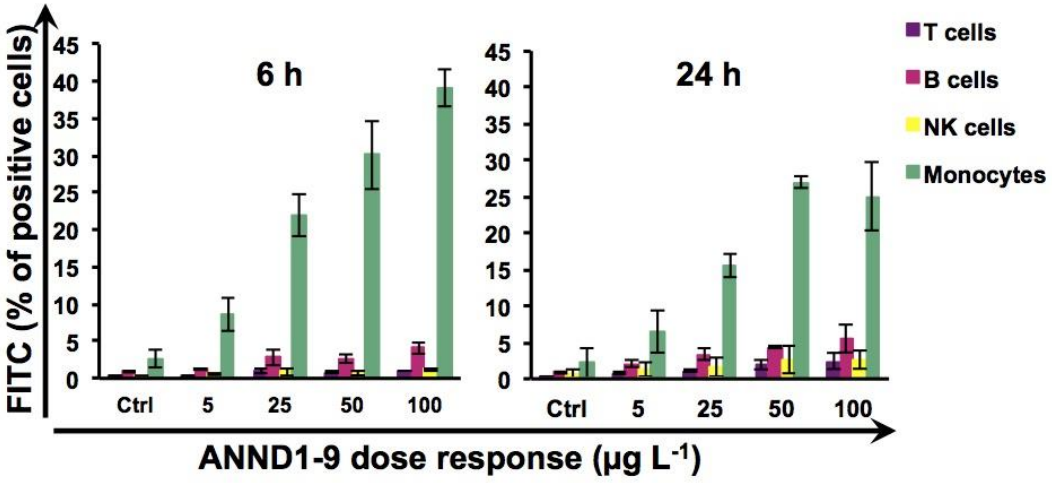

Fig. 3.43: NDs uptake dose response performed on PBMCs at 6 and 24 h

The NDs uptake was studied on PBMCs using fluorescent labeled-NDs (**ANND1-9**). The uptake observed on both kinds of cells was dose-dependent. Internalization of increasing doses of fluorescent NDs was investigated into T cells, B cells, NK cells and monocytes after 6 h (Figure 3.43, left side) and 24 h incubation (Figure 3.43, right side). The best uptake was detected at 50 µg/ml concentration and time point 6 h.

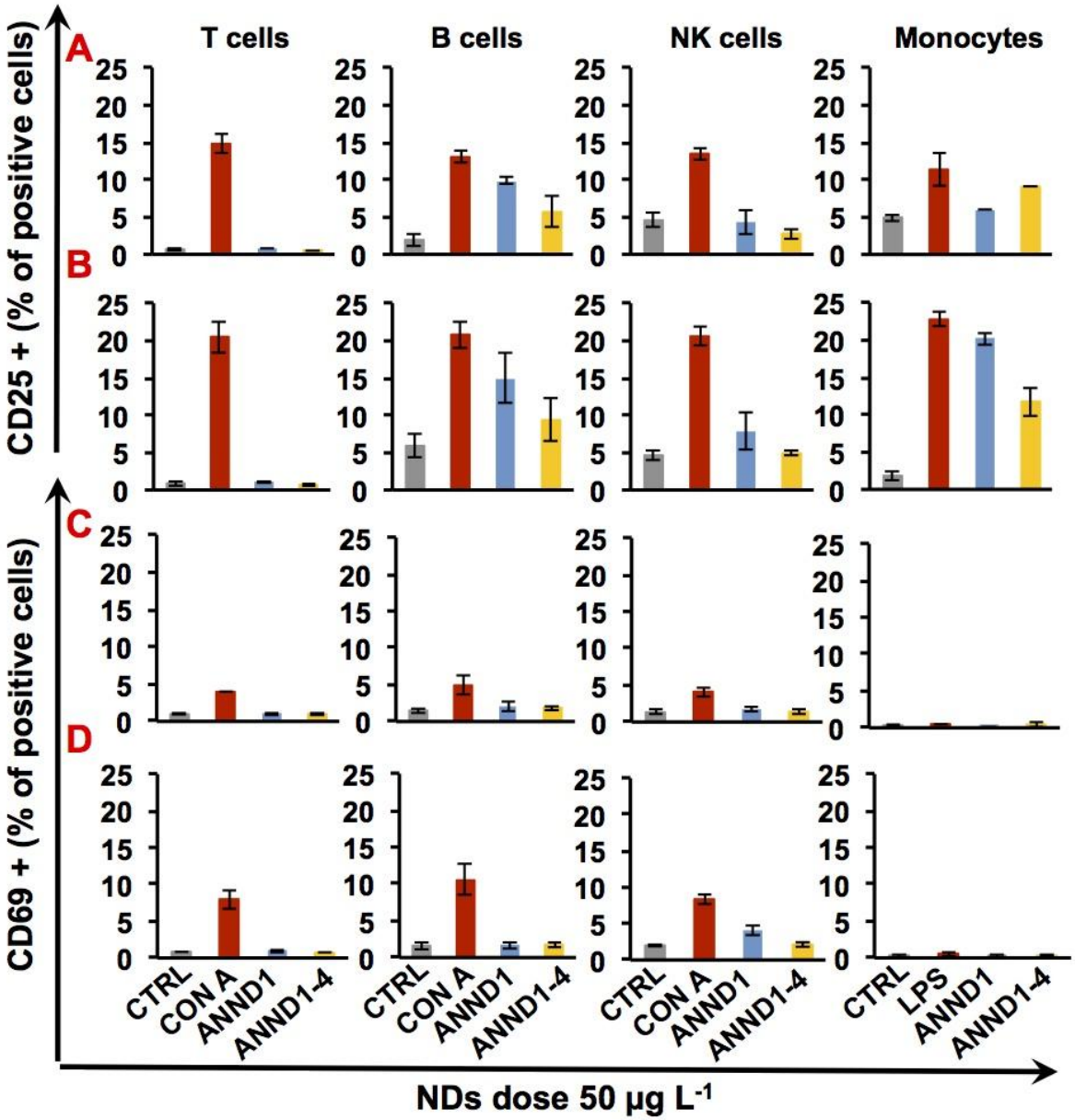

Fig. 3.44: Impact of Nanodiamonds on human Peripheral Blood Mononuclear Cells activation. PBMCs were the negative control (gray), Concanavalin A (CON A, 10 µg/ml) and lipopolysaccharides (LPS, 8 µg/ml) were used as positive controls (red) for T cells, B cells, NK cells and monocytes, respectively.

Human PBMCs activation was investigated into T cells, B cells, NK cells and monocyte by treating the cells with a dose of 50 µg/ml of **ANND1** (Figure 3.44, blue) and **ANND1-4** (Figure 3.44, orange). Cell activation was assessed looking at the expression of CD25 and

CD69. Their expression on different cell subsets was assessed by flow cytometry. The graphics show the activation marker CD25 after incubation 6 h (Figure 3.44A) and after 24 h (Figure 3.44B) and activation marker CD69 after incubation 6 h (Figure 3.44C) and after 24 h (Figure 3.44D). In the case of CD25, the major effect has been demonstrated by ANND1, especially on B cells and monocytes, while in the case of CD69 the nanodiamonds do not show any significant difference with respect to the negative control.

3.10 Bibliography

[1] P. H. Chung, E. Perevedentseva, C. L. Cheng, *Surf. Sci.* **2007**, *601*, 3866
[2] J. Cebik, J. K. McDonough, F. Peerally, R. Medrano, I. Neitzel, Y. Gogotsi, S. Osswald, *Nanotechnology* **2013**, *24*, 205703
[3] J.-S. Tu, E. Perevedentseva, P.-H. Chung, C.-L. Cheng, *J. Chem. Phys.* **2006**, *125*, 174713
[4] A. Krueger, D. Lang, *Adv. Funct. Mater.* **2012**, *22*, 890
[5] L. Rondin, G. Dantelle, A. Slablab, F. Grosshans, F. Treussart, P. Bergonzo, S. Perruchas, T. Gacoin, M. Chaigneau, H.-C. Chang, V. Jacques, J.-F. Roch, *Phys. Rev. B* **2010**, *82*, 115449
[6] D. Mitev, R. Dimitrova, M. Spassova, Ch. Minchev, S. Stavrev, *Diamond Relat. Mater.* **2007**, *16*, 776
[7] J. Cheng, J. He, C. Li, Y. Yang, *Chem. Mater.* **2008**, *20*, 4224
[8] S. Osswald, G. Yushin, V. Mochalin, S. O. Kucheyev, Y. Gogotsi, *J. Am. Chem. Soc.* **2006**, *128*, 11635
[9] C. Desai, S. Mitra, *Diam. Relat. Mater.* **2013**, *34*, 65
[10] V. N. Mochalin, O. Shenderova, D. Ho, Y. Gogotsi, *Nat. Nanotechnol.* **2011**, *7*, 11
[11] S. Osswald, G. Yushin, V. Mochalin, S. O. Kucheyev, Y. Gogotsi, *J. Am. Chem. Soc.* **2006**, *128*, 11635
[12] J. Chen, M. A. Hamon, H. Hu, Y. S. Chen, A. M. Rao, P. C. Eklund, R. C. Haddon, *Science* **1998**, *282*, 95
[13] V. N. Mochalin, Y. Gogotsi, *J. Am. Chem. Soc.* **2009**, *131*, 4594
[14] A.-Y. Jee, M. Lee, *Curr. Appl. Phys.* **2009**, *9*, e144
[15] a) G. Hungerford, J. Benesch, J. F. Mano, R. L. Reis, *Photochem. Photobiol. Sci.* **2007**, *6*, 152; b) R. Sjoback, J. Nygren and M. Kubista, *Spectrochim. Acta*, **1995**, *A51*, L7
[16] a) A. Kawski, *Photochem. Photobiol.* **1983**, *38*, 487; b) J. N. Miller, *Analyst* **2005**, *130*, 265; c) R. S. Knox, *Physica* **1968**, *39*, 361
[17] D. Lang, A. Krueger, *Diam. Relat. Mater.* **2011**, *20* (2), 101
[18] J. Xiao, G. Ouyang, P. Liu, C. X. Wang, G. W. Yang, *Nano Lett.* **2014,** *14*, 3645
[19] T. Petit, J.-C. Arnault, H. A. Girard, M. Sennour, P. Bergonzo, *Phys. Rev. B* **2011**, *84*, 233407
[20] M. Maggini, G. Scorrano, M. Prato, *J. Am. Chem. Soc.* **1993**, *115*, 9798
[21] N. Tagmatarchis, M. Prato, *J. Mater. Chem.* **2004**, *14*, 437
[22] G. Pastorin, W. Wu, S. Wieckowski, J.-P. Briand, K. Kostarelos, M. Prato, M. Bianco, *Chem. Comm.* **2006**, 1182
[23] B.K. Price, J.M. Tour, *J. Am. Chem. Soc.* **2006**, *128*, 12899
[24] J. L. Bahr, J. M. Tour, *Chem. Mater.* **2001**, *13*, 3823
[25] G. Schmidt, S. Gallon, S. Esnouf, J.-P. Bourgoin, P. Chenevier, *Chem. Eur. J.* **2009**, *15*, 2101
[26] Y. Liang, T. Meinhardt, G. Jarre, M. Ozawa, P. Vrdoljak, A. Schöll, F. Reinert, A. Krueger, *J. Colloid Interface Sci.* **2011**, *354* (1), 23
[27] a) N. Rubio, M. A. Herrero, A. De la Hoz, M. Meneghetti, M. Prato, *Org. Biomol. Chem.* **2010**, *8*, 1936; b) R. Sardar, J. S. Shumaker-Perry, *Nano Lett.* **2008**, *8*, 731; c) W. Liu, M. Howarth, A. B. Greytak, Y. Zheng, D. G. Nocera, A. Y. Ting, M. G. Bawendi, *J. A. Chem. Soc.* **2008**, *130*, 1274
[28] T. Meinhardt, D. Lang, H. Dill, A. Krueger, *Adv. Funct. Mater.* **2011**, *21*, 494
[29] J. M. Gonzalez-Dominguez, A. Santidrian, A. Criado, C. Hadad, M. Kalbac, T. Da Ros, *Chem. Eur. J.* **2015**, *21*, 18631
[30] a) W. Lwowski, *Nitrenes*, Interscience, **1970**; b) J. Han, C. Gao, *Nano-Micro Lett.* **2010**, *2*, 213
[31] a) M. Prato, Q. C. Li, F. Wudl, *J. Am. Chem. Soc.* **1993**, *115*, 1149; b) H. K. He, C. Gao, *Chem. Mater.* **2010**, *22*, 5054
[32] M. Holzinger, O. Vostrowsky, A. Hirsch, F. Hennrich, M. Kappes, R. Weiss, F. Jellen, *Angew. Chem. Int. Ed.* **2001**, *40*, 4002
[33] M. Holzinger, J. Abraham, P. Whelan, R. Graupner, L. Ley, F. Hennrich, M. Kappes, A. Hirsch, *J. Am. Chem. Soc.* **2003**, 125, 8566

[34] a) L. Zhou, C. Gao, D. Zhu, W. Xu, F. F. Chen, A. Palkar, L. Echegoyen, E. S.-W. Kong, *Chem. Eur. J.* **2009**, *15*, 4419; b) J. Bartelmess, S. Giordani, *Beilstein J. Nanotechnol.* **2014**, *5*, 1980

[35] a) A Gaiutam, P. Kapoor, K Chaudhary, R. Kumar, G. P. Raghava, *Curr. Med. Chem.* **2014**, *21*, 2367; b) P. Laakkonen, K. Vuorinen, *Integr. Biol.* **2010**, *2*, 326

[36] a) W. Guo, F. Giancotti, *Nature* **2004**, *5*, 816; b) W. Dai, T. Yang, Y. Wang, X. Wang, J. Wang, X. Zhang, Q. Zhang, *Nanomedicine Nanotechnology, Biol. Med.* **2012**, *8* (7), 1152

[37] S. V. Garde, A. J. Forte, M. Ge, E. A. Lepekhin, C. J. Panchal, S. A. Rabbani, *Anti-Cancer Drug* **2007**, *18*, 1189

[38] N. Maeda, Y. Takeuchi, M. Takada, Y. Sadzuka, Y. Namba, N. Oku, *J. Control Release* **2004**, *100*, 41

[39] R. M. Schiffelers, G. A. Koning, T. L. Hagen, M. H. Fens, A. J. Schraa, A. P. Janssen, *J. Control Release* **2003**, *91*, 115

[40] H. Zhao, J. C. Wang, Q. S. Sun, C. L. Luo, Q. Zhang, *J. Drug Target* **2009**, *17*, 10

[41] S. R. Singh, H. E. Grossniklaus, S. J. Kang, H. F. Edelhauser, B. K. Ambati, U. B. Kompella, *Gene Ther.* **2009**, *16*, 645

[42] I. Dijkgraaf, A. Y. Rijnders, A. Soede, A. C. Dechsne, G. V. Esse, A. J. Brouwer, *Org. Biomol. Chem.* **2007**, *5*, 935

[43] Y. G. Wang, X. Wang, Y. F. Zhang, S. J. Yang, J. C. Wang, X. Zhang, *J. Drug Target* **2009**, *7*, 459

[44] a) X. D. Dai, Z. Su, J. O. Liu, *Tetrahedron Lett.* **2000**, *41*, 6295; b) C. F. McCusker, P. J. Kocienski, F. T. Boyle, A. G. Schätzlein, *Bioorganic Med. Chem. Lett.* **2002**, *12*, 547; c) R. Hassert, P.- G. Hoffmeisater, M. Pagel, M. Hacker, M. Schulz-Siegmund, A. G. Beck-Sickinger, *Chem. Biodiv.* **2012**, *9*, 2648

[45] F. Pastorino, C. Brignole, D. Marimpietri, M. Cilli, C. Gambini, D. Ribatti, R. Longhi, T. M. Allen, A. Corti, M. Ponzoni, *Cancer Res.* **2003**, *63*, 7400

[46] W. Dai, T. Yang, Y. Wang, X. Wang, J. Wang, X. Zhang, Q. Zhang, *Nanomedicine Nanotechnology, Biol. Med.* **2012**, *8*, 1152

[47] a) M. E. Cianfrocca, K. A. Kimmel, J. Gallo, T. Cardoso, M. M. Brown, G. Hudes, N. Lewis, L. Weiner,G. N. Lam, S. C. Brown, D. E. Shaw, A. P. Mazar, R. B. Cohen, *Brit. J. Cancer* **2006**, *94*, 1621; b) F. Donate, G. C. Parry, Y. Shaked, *Clin. Cancer Res.* **2008**, *14*, 2137

[48] a) E. K. Chow, D. Ho, *Sci. Transl. Med.* **2013**, *5*, 2016; b) O. C. Farokhzad, R. Langer, *ACS Nano* **2009**, *3*, 16; c) A. Z. Wang, R. Langer, O. C. Farokhzad, *Annu. Rav. Med.* **2012**, *63*, 185; d) M. Ferrari, *Nat. Rev. Cancer* **2005**, *5*, 161

[49] D. Banerjee, R. Harfouche, S. Sengupta, *Vascular Cell* **2011**, *3*, 1

4. Experimental Part

4.1 Materials

Reagents and solvents were purchased from *Sigma Aldrich, VWR Prolabo, Acros Organics, Thermo Scientific, ABCR, Carbosynth, TCI* and were used as received. Resins for solid phase synthesis were purchased from *Peptides International*. Deuterated solvents were purchased by *Sigma-Aldrich,* and anhydrous solvents from *Acros Organics*. Anhydrous conditions were achieved by drying 2- or 3-neck flasks by flaming with a heat gun under vacuum and then purging with Argon. The inert atmosphere was maintained using Argon filled balloons equipped with a syringe and needle that was used to penetrate the silicon stoppers used to close the flasks' necks. Additions of liquid reagents were performed using dried plastic or glass syringes. Kaiser test kit was purchased by *Sigma-Aldrich*.

4.2 Instrumentation

4.2.1 Thermogravimetric analysis

TGA was recorded using a Q500 (TA Instruments). The equilibration at 100 °C for 20 minutes was followed by a ramp of 10 °C/min up to 830 °C. About 1 mg of compound was used for each analysis.

4.2.2 UV-visible spectra

UV-vis spectra were recorded using a *Varian Cary 5000* spectrophotometer with quartz cuvettes (path length = 1 cm).

4.2.3 IR spectra

IR spectra were recorded on a *Perkin-Elmer spectrum RX I FT-IR System,* pellets were prepared mixing about 1 mg of the sample with the KBr, previously dried.

4.2.4 Raman spectra

Raman spectra were recorded using a *Via Renishaw* spectrometer equipped with a 532 nm laser. For the analysis about 0.5 mg of each sample were dispersed in 1 ml of DMF and 3 drops of the suspension were deposited on a silicon wafer and let them dry.

4.2.5 X-Ray Photoelectron Spectroscopy (XPS)

XPS analyses were performed on different spots using an *ESCA SPECTROMETER* with a monochromatised Al Ka line ($h\nu$ = 1486.6 eV), applied with a take-off angle of 35°, as photon source. The survey spectra were the result of the accumulation of 5 scans where the EV $Step^{-1}$ was equal to 0.08. The C1s core level peak was taken as reference at 284.7 eV.

4.2.6 Transmission electron microscopy (TEM)

TEM analyses were performed using a *TEM Philips EM208* with an accelerating voltage of 100 kV. For the analysis 0.5 mg of each sample were dispersed in 1 ml of DMF and one drop of the suspension was deposited on a TEM grid (200 mesh, Nichel).

4.2.7 X-Ray Diffraction analysis (XRD)

X-Ray measurements were performed on a Gelmini Ultra R system (4-circle kappa platform, Ruby CCD detector) using Cu K radiation (l=1.54178Å) at Université de Namur in Belgium. Analysis were solved with SHELXS-86 program and refined on F2 using SHELXL-97 software.

4.2.8 Solid phase peptide synthesis (SPPS)

According to the conditions required for the orthogonal removal of protecting groups, Rink-amide MBHA resin (loading 0.32 mmol/g) was used as solid support for the growing peptides, in a 250 mg scale. HATU was chosen as coupling reagent. A qualitative Kaiser test was applied to a sample of the resin to determine if the Fmoc- deprotection had been successful.

4.2.9 MALDI-TOF mass spectrometry

MALDI-TOF mass spectrometry analyses were carried at the Centre de spectrométrie de masse - Université de Mons. They were recorded using a *Waters QToF Premier mass spectrometer* equipped with a nitrogen laser, operating at 337 nm with a maximum output of 500 mW delivered to the sample in 4 ns pulses at 20 Hz repeating rate. Time-of-flight mass analyses were performed in the reflectron mode at a resolution of about 10.000. The matrix solution (1 μL) was applied to a stainless steel target and air-dried. Analyte samples were dissolved in a suitable solvent to obtain 1 mg mL^{-1} solutions. 1 μL aliquots of those solutions were applied onto the target area already bearing the matrix crystals, and air dried. For the recording of the single-stage MS spectra, the quadrupole (rf-only mode) was set to pass ions from 100 to 1000 Th, and all ions were transmitted into the pusher region of the time-of-flight analyser where they were mass analysed with 1s integration time.

4.2.10 Reverse Phase-High Pressure Liquid Chromatography (RV-HPLC)

Analyses and purifications of peptides were performed on a *Varian 940*-LC liquid chromatograph system. The analytical HPLC column used was a *Varian Pursuit C18, 5 μm, 4.6 × 250 mm* column. The preparative HPLC column used was *a Varian Pursuit C18, 5 μm, 21.2 × 250 mm column*. 0.1% TFA in H_2O and 0.1% TFA in CH_3CN were used as eluents in all cases.

4.2.11 Thin layer chromatography

TLC assessments were performed on *Merck* pre-coated aluminium plates with silica gel 60 F254.

4.2.12 Flash column chromatography

Flash column chromatography was carried out using *Merck* silica gel 60 (particle size 40-63 μm).

4.2.13 Fluorescence spectroscopy

Fluorescence spectra were recorded on a Cary Eclipse Fluorescence Spectrophotometer (Agilent Technologies), using quartz cuvettes (path length = 1 cm).

4.2.14 ^{1}H-Nuclear Magnetic Resonance (^{1}H-NMR)

NMR spectra were obtained on a *Varian* (270MHz) or a *Varian* (400MHz). Chemical shifts were reported in ppm using the solvent residual peak as an internal reference. The resonance multiplicity was described as *s* (singlet), *d* (doublet), *t* (triplet), *m* (multiplet), *bs* (broad singlet).

4.3 Methods

4.3.1 Thermogravimetric analysis

The thermogravimetric analysis (TGA) is a useful technique to determine the quantity of functional groups that are present on the surface of the nanomaterial, with sensitivity in the nanograms range. It can measure weight changes in a material as a function of temperature (or time) under a controlled atmosphere. Its principal uses include measurement of a material thermal stability and composition. The TGA of nanodiamonds is generally performed in inert atmosphere (argon or nitrogen) and temperature range from 25 to 900 °C routinely. The degree of functionalization, expressed in μmol/g, is generally calculated from the percentage loss of weight of the system, for an *ensemble* of different derivatives obtained progressively starting from the pristine material.

$$Degree\ of\ functionalization\ \left(\mu mol/g\right) = \frac{Loss\ of\ weight\ (\%) * 10^4}{Molecular\ Weight\ of\ the\ functional\ group}$$

4.3.2 Kaiser test

The test was introduced for the first time in 1970 and it is generally used for the quantification of free amino groups in the solid phase peptide synthesis.
It is based on the following reaction that takes place at 100 °C:

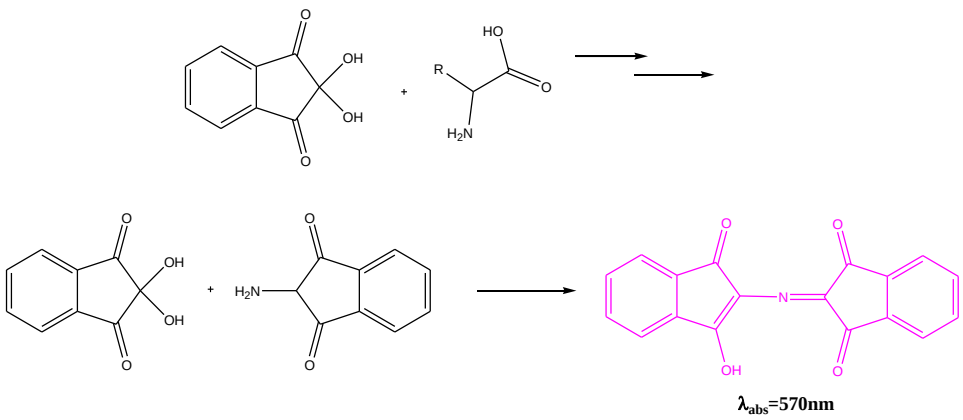

Scheme 4.1: Formation of the ninhydrin complex in presence of free amino groups.

Based on the Lambert-Beer law the absorbance value detected at 570 nm, due to the ninhydrin complex, can be generally correlated to the concentration of free amino groups.

This method is generally applied on amino-grafted nanomaterials, for example functionalized carbon nanotubes. Unfortunately, only in 2015 Krueger and co-workers have reported a modified Kaiser test with which is possible to determine the concentration of free amine groups eventually present on the NDs surface and this procedure is not still optimized.

4.3.3 Raman spectroscopy

The Raman spectroscopy can be applied to the qualitative and quantitative analysis of inorganic, organic and biological systems.[1]

By irradiating a sample with a powerful source of monochromatic beam, the radiation can be inelastically scattered (*Raman* scattering) and elastically scattered (*Rayleigh* scattering).

The *Rayleigh* scattering, whose wavelength is that of the excitation source, produces the most intense signal and at lower and higher wavenumber values it is possible to detect *Stokes* and *anti-Stokes* lines, respectively. In fact, the vibrational energy of a bound can be added to or subtracted from the photons energy and this can change its frequency. Energy changes that produce *Stokes* and *anti-Stokes* emission differ from the Rayleigh radiation by frequencies that correspond to the energy of the first vibrational level of the ground state.

If the bond is infrared active, the Raman frequency shift and the infrared absorption peak frequency are coincident.

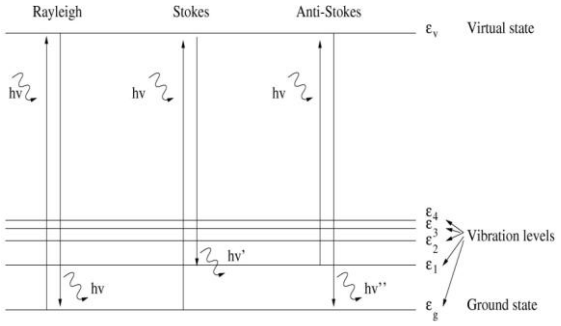

Fig. 4.1: Schematic representation of elastic (*Rayleigh*) and inelastic (*Stokes* and *anti-Stokes*) scattering.[11]

4.3.4 Transmission electron microscopy

Electron microscopy is generally used to investigate the structure of a wide range of biological and inorganic specimens including cells, large molecules, metals, crystals and, industrially, for quality control of materials. The electron microscopy has a resolution thousands times higher than an optical microscope. In fact, in accordance to the Broglie principle, electrons have a wavelength inversely proportional to the their energy. In the electron microscope electrons are extracted from a hot filament and accelerated to energies correspondent to wavelength down to tenths of nanometers.

The transmission electron microscopy is a useful tool for the investigation of the nature and structure of materials, giving crystallographic information and composition at the nanometer scale.[2] The technique is based on the detection of a high-energy electron beam (~ 200 keV) that is transmitted through a thin specimen (~ 100-150 nm). The contrast, in the bright-field imaging mode, is due to the different absorption of different portions of the sample. For

crystalline samples, rays are diffracted and diffraction peaks positions are detected and they can provide a contrast image.

4.3.5 X-ray photoelectron spectroscopy (XPS)

In the X-ray photoelectron spectroscopy the sample is illuminated with soft (1.5 kV) X-radiation in ultrahigh vacuum conditions. The photoelectric effect leads to the production of photoelectrons with kinetic energies that are then measured. The obtained energy spectrum, recorded in a beta-ray spectrometer, permits to determine the composition of the sample.
Knowing the binding energies related to the electron orbitals of the atoms, from the positions of the peaks obtained in the spectrum it is possible to identify the atomic composition of the sample surface. Moreover, measurements of relative areas of photoelectron peaks allow the quantitative analysis of the sample composition. The information usually obtained come from the sample surface (sampling depth = 5-10 nm), this is due to the attenuation of photoelectrons by passing through the material.[3]

4.3.6 X-ray powder diffraction (powder-XRD)

X-ray powder diffraction is mostly used for the characterization of crystalline materials, measurement of sample purity, identification of unknown crystalline materials (i.e. minerals, inorganic compounds).[4] X-rays are generated in a cathode ray tube, heating a filament to have electrons that are then accelerated by applying a specific voltage. Electrons arrive with a sufficient energy to dislodge inner shell electrons of the target material that usually is copper with a radiation equal to 1.5418 Å. The intensity of the reflected X-rays is detected when sample and detector are rotated. When the geometry of the incident X-ray follows the Bragg equation, constructive interference occurs and a peak in intensity occurs. In an X-ray diffractometer, the sample rotates in the path of the collimated X-ray beam with an angle θ, while the X-ray detector is mounted on an arm to collect the diffracted X-rays and rotates with an angle of 2θ. The instrument used to maintain the angle and rotate the sample is termed *goniometer*. Typically, data are collected at 2θ from ~5° to 80°, angles that are preset in the X-ray scan.[5]

4.3.7 Solid-phase peptide synthesis (SPPS)

The solid-phase peptide synthesis (SPPS) was described for the first time in 1963 by B. Merrifield for the synthesis of the Leu-Ala-Gly-Ala peptide.[6] In the Merrifield method the C-terminal end amino acid is bounded to the polymeric support as benzyl ester and the polypeptidic chain is then grown by starting from the N-terminus. The strength of this technique is due to the insolubility of the polymeric particles (with bounded polypetidic chains) in the common solvents used for the synthesis and this allows the easily removing of the not-reacted reagents or undesired products by washing the solid particles with various solvents.[7] The α-NH_2 group and reactive side-chain moieties have to be blocked. α-NH2-modifications are necessary to temporary block the tail and they can be removed specifically after each successful coupling step, whereas side-chain protecting groups and resin allow a permanent protection against unwanted side reactions. Moreover, it is necessary to activate the carboxyl group by a special auxiliary to increase the electrophilicity for the coupling. All

the alternating steps of N_α-deprotection, activation and coupling are repeated until the desired peptide is obtained. The last step of SPPS should be carried out in presence of scavengers to trap highly reactive carbocations formed during the cleavage procedure and that could react with the peptide.[8] For the protection of the N_α-amino function two protecting groups were established: the Boc (*tert*-butyloxycarbonyl) and the Fmoc (fluorenylmethoxycarbonyl) groups. In the Merrifield's method the Boc- was used for the temporary protection of the amino function and benzyl group (Bn) or related protecting groups for the side chains. The Boc/Bn protecting group strategy is then based on graded acid lability of these protecting groups. The method that is based on the use of the Fmoc group, removable under basic conditions, for the protection of the N_α-amino function and of the *t*-Bu (*tert*-butyl), removable under acid conditions, for the protection of side-chain groups offers the great advantage of orthogonality. This concept is very important because it allows the selective removal of different protecting groups using completely different chemical conditions. Moreover, the Fmoc strategy, that does not require repeated uses of TFA, has a lower impact on sensitive peptide bonds and does not require the use of special vessels.

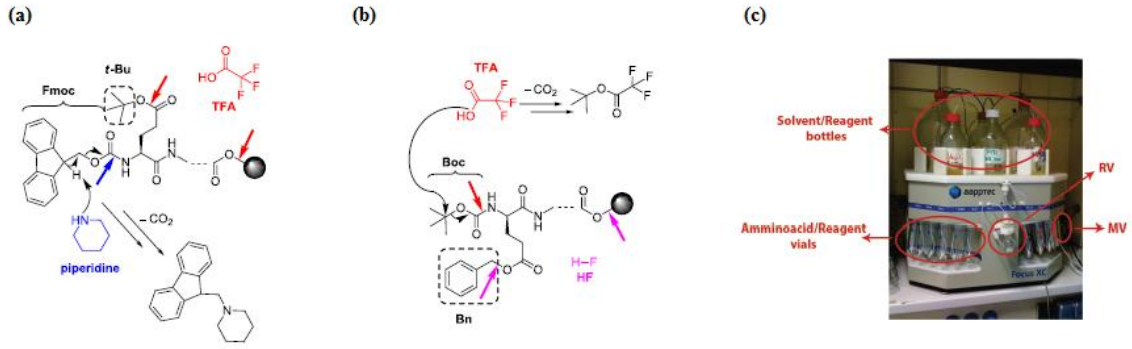

Fig. 4.2: (**a**) Fmoc/*t*-Bu and (**b**) Boc/Bn protecting group strategies. Blue arrows indicate basic conditions and red arrows acid conditions. (**c**) Image of the solid-phase peptide synthesizer. RV are reaction vessels where activation, coupling and deprotection steps take place.[8c].

Actually, a great variety of coupling reagents are commercially available, in fact it is possible to use traditional carbodiimides (DCC, DIC), classical auxiliary nucleophiles (HOBt, HOAt) and uranium reagents (HATU, TBTU) and phosphonium salts (PyBOP).

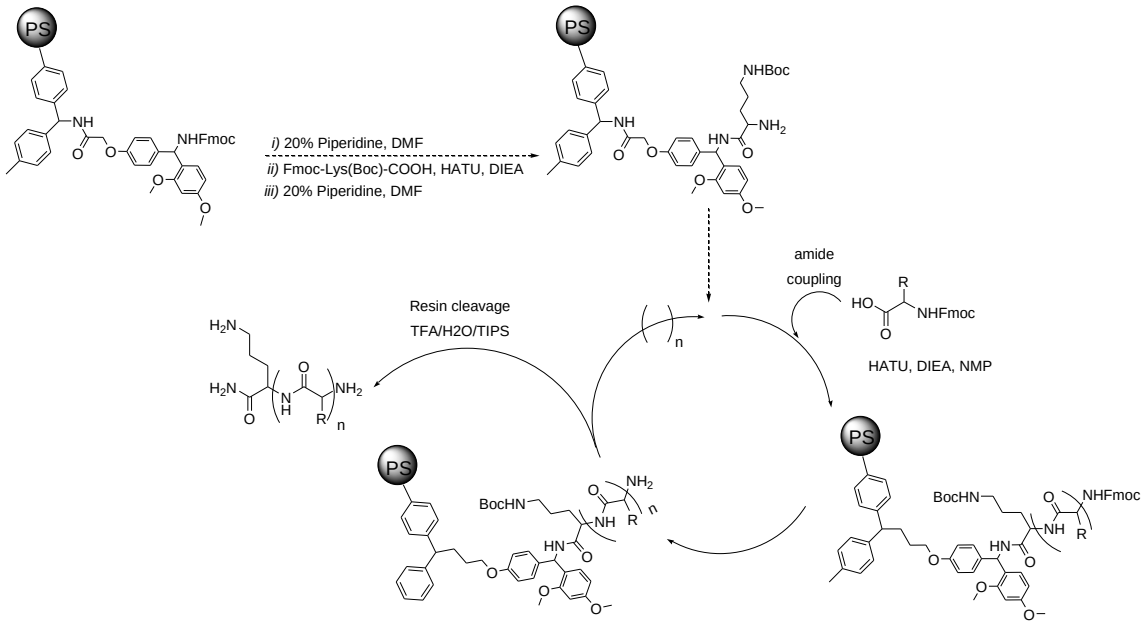

Scheme 4.2: Schematic solid phase peptide synthesis process. The resin is the Rink-amide MBHA, the deprotection of the Fmoc- group is carried out using 20% piperidine in DMF, HATU is the coupling reagent.

Resins and linkers for peptide synthesis have to meet few essential requirements. The resin has to be - insoluble in all the solvents, - chemically resistant and - mechanically stable to allow the filtration steps. Moreover, an appropriate solvation and good swelling properties are key features for a good synthesis. The linker represents the connection between the solid support and the peptide. It affects the loading of the resin, chemical conditions for the coupling and the space between resin and the assembling peptide. Among all the resins and linkers the Rink-amide MBHA is one of the most used.

4.4 Experimental procedures

4.4.1 Amino acids synthesis

The α-amino acid N-Boc-amino-diethoxy-ethylamino-acetic acid **3** was synthetized in 3 steps. First, the 2,2'-(ethylenedioxy)bis(ethylamine) was mono-protected with di-*tert*-butyldicarbonate and purified from the bis-protected and the unreacted bis-amine with ethyl acetate/water extractions, obtaining the 56% of the desired product. Compound **1** was alkylated using benzyl 2-bromoacetate and the reaction crude was purified by flash chromatography from the bis-alkylated product to obtain 55% of the desired α-amino ester **2**. Finally, compound **2** was deprotected by catalytic hydrogenation to obtain the α-amino acid **3** in quantitative yield.

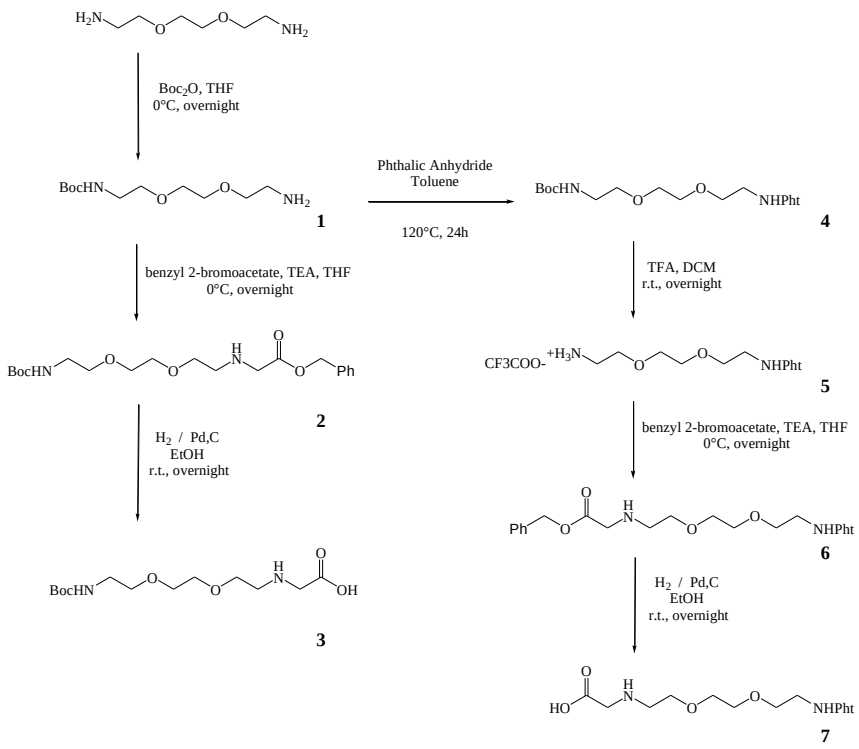

Scheme 4.3: Synthesis of amino acids **3** and **7**

For the synthesis of the α-amino acid N-Pht-amino-diethoxy-ethylamino-acetic acid **7** firstly the free amino group of compound **1** was protected using phthalic anhydride, the crude was purified by flash chromatography obtaining the desired product **4**. The deprotection of the Boc function was carried out in acid conditions, quantitatively giving the salt **5**. Compound **5** was alkylated using benzyl 2-bromoacetate and the reaction crude was purified by flash chromatography from the bis-alkylated product to obtain 55% of the desired α-amino ester **6**. Finally, compound **6** was deprotected by catalytic hydrogenation to obtain the α-amino acid **7** in quantitative yield.

4.4.1.1 Synthesis of compound 1

A solution of di-*tert*-butyldicarbonate (25.07 g, 0.11 mol, 1 eq) in THF (250 ml) was added dropwise to a THF (250 ml) solution of 2,2'-(ethylenedioxy)bis(ethylamine) (34.05 g, 0.23 mol, 2 eq), cooled to 0 °C. The mixture was stirred overnight at r.t. The solvent was removed under reduced pressure. After the addition of water (200 ml) the mixture was filtered over celite, in order to remove the diprotected diamine that is not water-soluble. Extractions with dicloromethane were made to recover the product. The organic layers were dried on anhydrous Na_2SO_4 and the solvent was removed. Product **1** was then dried under vacuum, resulting in 16.00 g (0.06 mol) of viscous oil. $C_{11}H_{24}N_2O_4$ (MW 248.32). Yield = 56%.
^{1}H-NMR (200 MHz, $CDCl_3$): δ 5.15 (bs, 1H), 3.65-3.45 (m, 8H), 3.31 (t, J = 5.1 Hz, 2H), 2.85 (t, J = 5.2 Hz, 2H), 1.42 (s, 9H). The characterization is in agreement with literature.[9]

4.4.1.2 Synthesis of compound 2

A THF solution (133 ml) of benzyl 2-bromoacetate (7.2 ml, 0.04 mol, 0.33 eq) and triethylamine (10.2 ml, 0.05 mol, 0.40 eq) was added dropwise to a solution of compound **1** (10.0 g, 0.04 mol, 0.33 eq) in THF (200 ml), cooled to 0 °C. The mixture was stirred

overnight at r.t. The solvent was evaporated and the product was purified by column chromatography (eluent AcOEt/MeOH 9.5:0.5). Product **2** was dried under vacuum to obtain 9.82 g (0.025 mol) of yellow oil. $C_{20}H_{32}N_2O_6$ (MW396.48). Yield = 62%.
^{1}H-NMR (200 MHz, $CDCl_3$): δ 7.36 (s, 5H), 5.22 (bs, 1H), 5.15 (s, 2H), 3.36-3.42 (m, 10H), 3.30 (m, 2H), 2.80 (t, J = 5.2 Hz, 2H), 1.43 (s, 9H). The characterization is in agreement with literature.[9]

4.4.1.3 Synthesis of compound 3

10% Pd/C was added to a deoxygenated EtOH solution (250 ml) of compound **2** (9.82 g, 0.025 mol). The reaction flask was purged with H_2 several times and then stirred at r.t. overnight. The catalyst was removed by filtration over celite and the solvent removed under reduced pressure. The product was dried under vacuum to give a white solid in quantitative yield (8.00 g). $C_{13}H_{26}N_2O_6$ (MW=306.36).
^{1}H-NMR (200 MHz, $CDCl_3$): δ 5.57 (bs, 1H), 3.82 (m, 2H), 3.69-3.44 (m, 10H), 3.36-3.16 (m, 4H), 1.43 (s, 9H). The characterization is in agreement with literature.[9]

4.4.1.4 Synthesis of compound 4

A toluene solution (317 ml) of compound **1** (16.0 g, 68.0 mmol) and phthalic anhydride (10.0 g, 68.0 mmol) was stirred at 120 °C in a Dean-Stark apparatus for 24 h. The solvent was then evaporated under vacuum and chromatographic column purification (toluene/AcOEt 7:3) afforded the pure product (14.6 g, 38.5 mmol, yield 57%) as colourless oil.
^{1}H-NMR (200 MHz, $CDCl_3$): δ 7.86 (m, 2H), 7.72 (m, 2H), 5.06 (s, 1H), 3.96-3.44 (m, 8H), 3.25 (t, J = 4.9 Hz, 2H), 1.43 (s, 9H). The characterization is in agreement with literature.[9]

4.4.1.5 Synthesis of compound 5

The N-phthalimido-N-Boc-amino-diethoxy-ethyl amine (7.4 g, 19.5 mmol) was dissolved in CH_2Cl_2 (30 mL) and TFA (15 mL) was slowly added to the solution while stirring at 0 °C. The reaction mixture was then allowed to reach r.t. and it was stirred for 3 h. The solvent was removed under vacuum and the resulting product, as trifluoroacetic acid salt, was triturated in diethyl ether to give a white solid **5** in quantitative yield.
^{1}H-NMR (200 MHz, $CDCl_3$): δ 8.25 (s, 2H), 7.86 (m, 2H), 7.72 (m, 2H), 3.90 (t, J = 5.2 Hz, 2H), 3.75 (m, 4H), 3.60 (m, 4H), 3.25 (t, J = 4.9 Hz, 2H). The characterization is in agreement with literature.[9].

4.4.1.6 Synthesis of compound 6

A THF solution (150 ml) of benzyl 2-bromoacetate (3.3 ml, 18.0 mmol, 1 eq) and triethylamine (4.2 ml, 21.6 mol, 1.2 eq) were added dropwise to a solution of compound **5** (10.0 g, 0.04 mol, 0.33 eq) in THF (200 ml), cooled to 0 °C. The mixture was stirred overnight at r.t. The solvent was evaporated and the product was purified by column chromatography (eluent AcOEt/MeOH 9.5:0.5). Product **6** was dried under vacuum to obtain 4.26 g (0.010 mol) of yellow oil. $C_{20}H_{32}N_2O_6$ (MW426.46). Yield = 56%.

^{1}H-NMR (200 MHz, $CDCl_3$): δ 7.86 (m, 2H), 7.72 (m, 2H), 7.35 (m, 5H), 5.20 (s, 2H), 3.90 (t, J = 5.2 Hz, 2H), 3.75 (t, J = 5.1 Hz, 2H), 3.70-3.55 (m, 10H), 2.90 (t, J = 5.2 Hz, 2H), 2.42 (s, 1H). The characterization is in agreement with literature.[9]

4.4.1.7 Synthesis of compound 7

10% Pd/C was added to a deoxygenated EtOH solution (25 ml) of compound **6** (1.19 g, 2.7 mmol). The reaction flask was purged with H_2 several times and then stirred at r.t. overnight. The catalyst was removed by filtration over celite and the solvent removed under reduced pressure. The product was dried under vacuum to give a white solid in quantitative yield (0.9 g). $C_{13}H_{26}N_2O_6$ (MW=336.34). Yield = 96%.

^{1}H-NMR (200 MHz, $CDCl_3$): δ 7.86 (m, 2H), 7.72 (m, 2H), 3.90 (t, J = 5.2 Hz, 2H), 3.75-3.50 (m, 12H), 2.90 (t, J = 5.2 Hz, 2H), 2.62 (s, 1H). The characterization is in agreement with literature.[9]

4.4.2 Synthesis of the azide derivative

The synthesis of the azide compound **10** was carried out in 3 steps. The free amino group in the 2-(2-aminoethoxy)ethanol was mono-protected with the Pht- function, with quantitative yield. The compound **8** was then reacted with methanesulfonyl chloride, in presence of triethylamine, obtaining product **9** (yield 94%). The last step was the substitution of the methanesulfonyl group with sodium azide, giving **10** in quantitative yield.

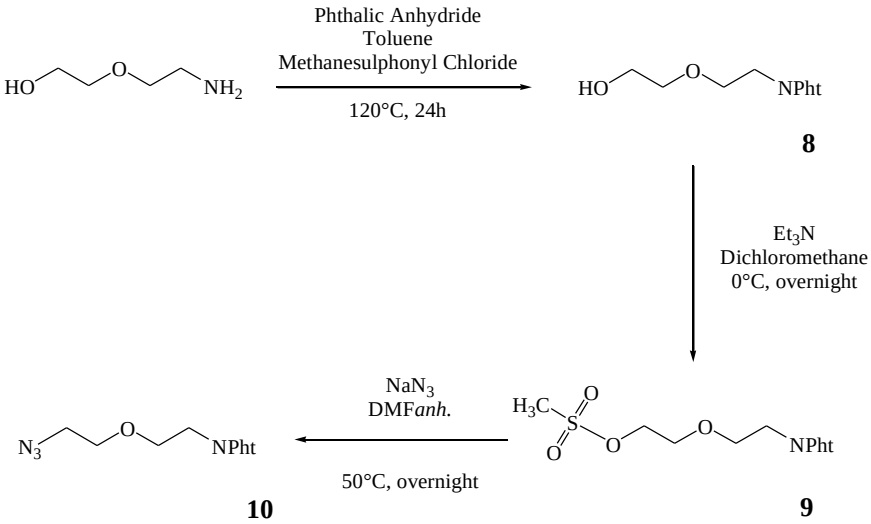

Scheme 4.4: Synthesis of compound **10**.

4.4.2.1 Synthesis of compound 8

A toluene solution (150 ml) of 2-(2-aminoethoxy)ethanol (10.3 g, 98.3 mmol) and phthalic anhydride (14.6 g, 98.3 mmol) was stirred at 120 °C in a Dean-Stark apparatus for 24 h. The solvent was then evaporated under vacuum, and the pure product was recovered (23.1 g, 97.3 mmol, 99%) as a white solid.

^{1}H-NMR (200 MHz, $CDCl_3$): δ 7.86 (m, 2H), 7.72 (m, 2H), 3.90 (t, J = 5.2 Hz, 2H), 3.74 (t, J = 5.2 Hz, 2H), 3.67 (t, J = 4.9 Hz, 2H), 3.59 (t, J = 5.1 Hz, 2H), 3.65 (s, 1H). The characterization is in agreement with literature.[10]

4.4.2.2 Synthesis of compound 9

Methanesulfonyl chloride (4.24 ml, 51.8 mmol, 1.2eq) was added slowly to a DCM solution (20 ml) of compound **8** (10.0 g, 42.2 mmol, 1 eq) and triethylamine (8.8 ml, 63.2 mmol, 1.5 eq), cooled at 0 °C. The mixture was stirred overnight at r.t. The solvent was evaporated and the product was purified by extractions with 1 M HCl solutions and water. The product **9** was dried under vacuum to obtain 12.4 g (39.6 mmol) of yellow solid. $C_{13}H_{15}NO_6S$ (MW313.33). Yield = 94%.

^{1}H-NMR (200 MHz, $CDCl_3$): δ 7.86 (m, 2H), 7.72 (m, 2H), 4.30 (t, J = 4.9 Hz, 2H), 3.90 (t, J = 5.2 Hz, 2H), 3.75 (t, J = 5.2 Hz, 4H), 3.01 (s, 3H). The characterization is in agreement with literature.[10]

4.4.2.3 Synthesis of compound 10

Sodium azide (0.8 g, 3.2 mol, 2 eq) was added slowly to a DMF anhydrous solution (200 ml) of compound **9** (2.0 g, 1.6 mmol, 1 eq), under argon atmosphere, at 50 °C. The mixture was stirred for 48 h. The solvent was evaporated and the product was purified by extractions with petroleum ether and water. The product **10** was dried under vacuum to obtain 0.3 g (1.2 mmol) of white solid. $C_{12}H_{12}N_4O_3$ (MW260.33). Yield = 68%.

^{1}H-NMR (200 MHz, $CDCl_3$): δ 7.86 (m, 2H), 7.72 (m, 2H), 3.93 (t, J = 5.2 Hz, 2H), 3.77 (t, J = 4.9 Hz, 2H), 3.66 (t, J = 5.2 Hz, 2H), 3.31 (t, J = 5.1 Hz, 2H). The characterization is in agreement with literature.[10]

4.4.3 Synthesis of peptides

4.4.3.1 Synthesis of c(RGDfK)

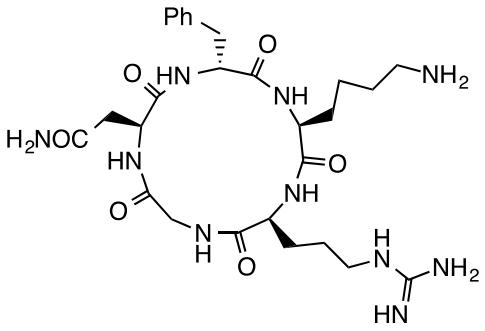

C(RGDfK) was synthetized in a 0.10 mmol scale using a five-fold excess of protected amino acids (AA, 0.5 mmol) relative to the Rink-amide MBHA resin (300 mg, 0.32 mmol g^{-1}). Before starting the synthesis, all the AA were dissolved in NMP (2.4 ml, 0.26 M), and HATU (0.4 M in DMF), DIEA (2.5 M in NMP) and 20% piperidine in DMF solutions were freshly prepared. The resin was kept in the synthesizer and swelled in NMP (6 ml) at r.t. for 15 min. Fmoc deprotection was obtained by using 20% piperidine in DMF (6 ml) three times for 4 minutes each. Afterwards, the downloading of the resin was performed by coupling reaction using Fmoc-Asp(OAll)-OH (2.4 ml of 0.26 M), HATU (2 ml of 0.4 M) and DIEA (1 ml of 2.5 M). All the reagents were mixed at r.t. for 1 min and then added to the resin. The reaction was mixed at r.t. for 25 min and the resin was after washed (6 ml NMP x 2, 15 ml DMF x 2). After Fmoc removal on the α-NH_2, the deprotected resin was then coupled with G, R(Pbf), K(Boc), f [(2.4 ml of 0.26M of each AA starting from L to C), HATU (2 ml of 0.4 M) and

DIEA (1 ml of 2.5 M)], washed and deprotected in automatic way to obtain the DGRKf sequence.

At this step, Alloc deprotection of the β-CO_2H was performed in manual mode, adding to the resin first phenylsilane (1.9 mmol) at r.t. for 5 min and after [$Pd(PPh_3)_4$] (0.032 mmol) at r.t for 30 min, both of them previously dissolved in CH_2Cl_2. The last step was the deprotection of the Fmoc group on the α-NH_2 of the f residue, performed as described before.

The cyclization was successfully performed in manual mode adding to the resin a solution of PyBop (0.14 mmol), HOBt (0.14 mmol), DIEA (0.48 mmol) in DMF (4 ml). The reaction was performed at r.t. for 6 h and then the resin was washed with DMF and NMP.

Resin Cleavage. When the synthesis was completed, a freshly prepared cleavage solution of TFA, TIPS, water and EDT (94:1:2.5:2.5) was added to the resin (3 ml) and the cleavage reaction was allowed to proceed at r.t. for 5 h. The product was precipitated with Et_2O (50 ml) and isolated by centrifugation to form a white solid (23 mg, 40% after RP-HPLC purification).

RP-HPLC analysis and purification. Crude peptide was analysed and purified by RP-HPLC. The gradient was from 0.1% TFA in water to 0.1% TFA in CH_3CN over 38 min. The flow rates for analytical and preparative HPLC were 1 ml min^{-1} and 21 ml min^{-1}, respectively. According to these parameters, c(RGDfK) detected at 220 nm was eluted at 15 min retention time.

MS (MALDI-HRMS): found 603.3351 $[M+H]^+$, [$C_{27}H_{43}N_{10}O_6$] requires = 603.3367; found 641.3 $[M+K]^+$, [$C_{22}H_{34}N_6O_5K$] requires = 641.3

a)

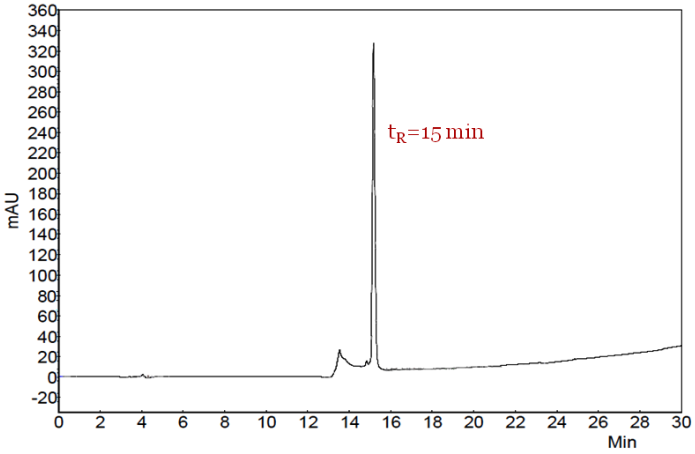

b)

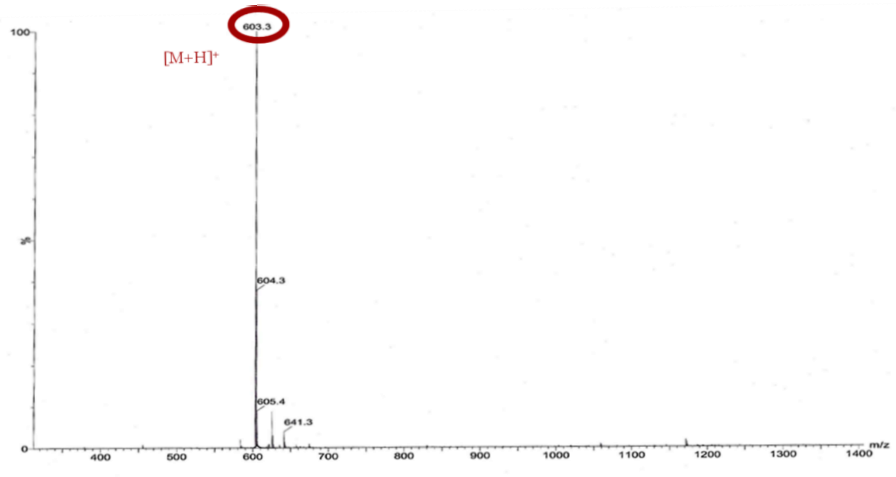

Fig. 4.3: (**a**) HPLC chromatogram and (**b**) MALDI-TOF analysis of purified c(RGDfK). HPLC conditions: Agilent Zorbax SBC18, 5 µm, 4.6×250 mm, eluents from 0.1% TFA in H_2O to 0.1% TFA in CH_3CN, flow 1 mL min-1, r.t. The eluents were monitored at 220 nm.

4.4.3.2 Synthesis of NH_2-NGRSLC-C(O)NH_2

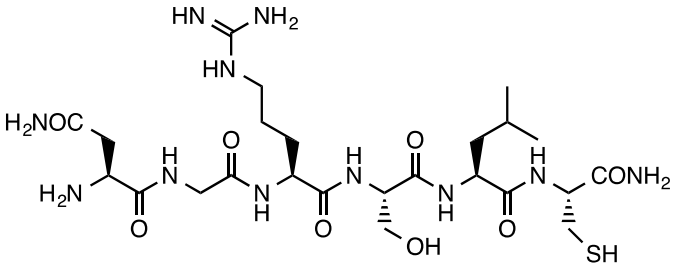

NH_2-NGRSLC-C(O)NH_2 was synthetized in a 0.10 mmol scale using a five-fold excess of protected amino acids (AA, 0.5 mmol) relative to the Rink-amide MBHA resin (300 mg, 0.32 mmol g^{-1}). Before starting the synthesis, all the AA were dissolved in NMP (2.4 ml, 0.26 M), and HATU (0.4 M in DMF), DIEA (2.5 M in NMP) and 20% piperidine in DMF solutions were freshly prepared. The resin was kept in the synthesizer and swelled in NMP (6 ml) at r.t. for 15 min. Fmoc deprotection was obtained by using 20% piperidine in DMF (6 ml) three times for 4 minutes each. Afterwards, the downloading of the resin was performed by coupling reaction using Fmoc-Cys-OH (2.4 ml of 0.26 M), HATU (2 ml of 0.4 M) and DIEA (1 ml of 2.5 M). All the reagents were mixed at r.t. for 1 min and then added to the resin. The reaction was mixed at r.t. for 25 min and the resin was after washed (6 ml NMP x 2, 15 ml DMF x 2). A double coupling process was performed. After Fmoc removal on the α-NH_2, the deprotected resin was coupled (double coupling) with L, S, R, G, N [(2.4 ml of 0.26M of each AA starting from L to C), HATU (2 ml of 0.4 M) and DIEA (1 ml of 2.5 M)], washed and deprotected in automatic way to obtain the NGRSLC.

Resin Cleavage. When the synthesis was completed, a freshly prepared cleavage solution of TFA, TIPS, water and EDT (92.5:2.5:2.5:2.5) was added to the resin (3 ml) and the cleavage reaction was allowed to proceed at r.t. for 3.5 h. The product was precipitated with Et_2O (50 ml) and isolated by centrifugation to form a white solid.

RP-HPLC analysis and purification: Crude peptide was analyzed and purified by RP-HPLC. The gradient was from 0.1% TFA in water to 0.1% TFA in CH_3CN over 38 min. The flow rates for analytical and preparative HPLC were 1 ml min^{-1} and 21 ml min^{-1}, respectively.

According to these parameters, NGRSLC detected at 220 nm was eluted at 16 min retention time.

MS (MALDI-HRMS): found 648.3256 $[M+H]^+$, $[C_{24}H_{46}N_{11}O_8S]$ requires = 647.3252.

a)

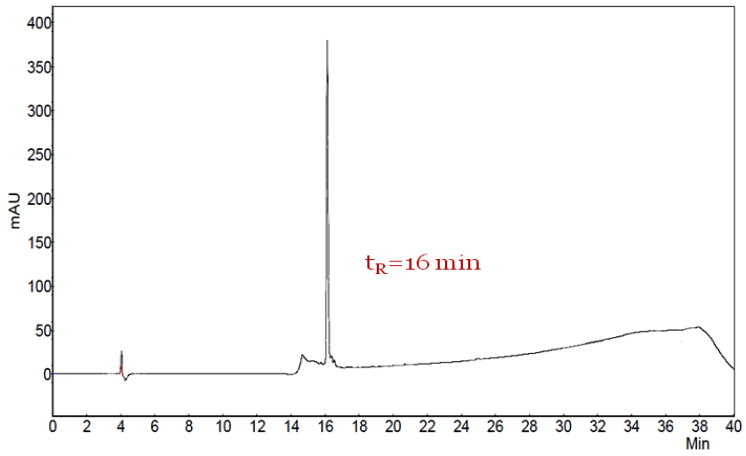

b)

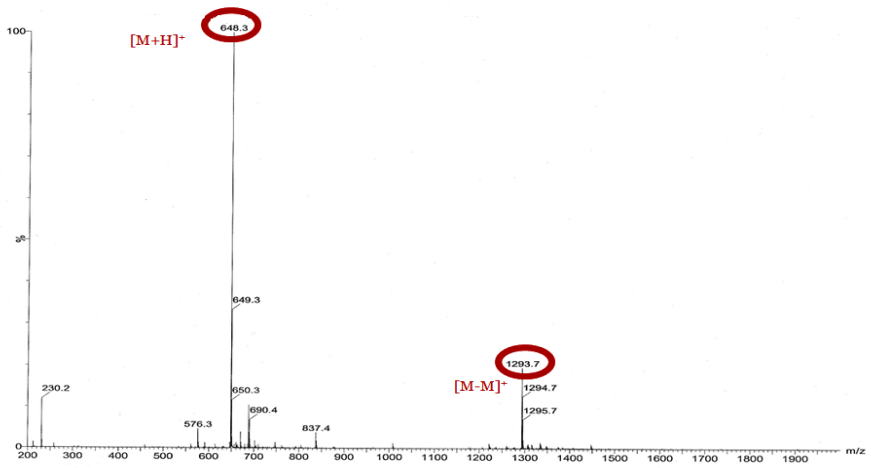

Fig. 4.4: (**a**) HPLC chromatogram and (**b**) MALDI-TOF analysis of purified NH_2-NGRSLC-C(O)NH_2. HPLC conditions: Agilent Zorbax SBC18, 5 µm, 4.6×250 mm, eluents from 0.1% TFA in H_2O to 0.1% TFA in CH_3CN, flow 1 mL min-1, r.t. The eluents were monitored at 220 nm.

4.4.3.3 Synthesis of compound NH_2-FRVGVADVC-C(O)NH_2

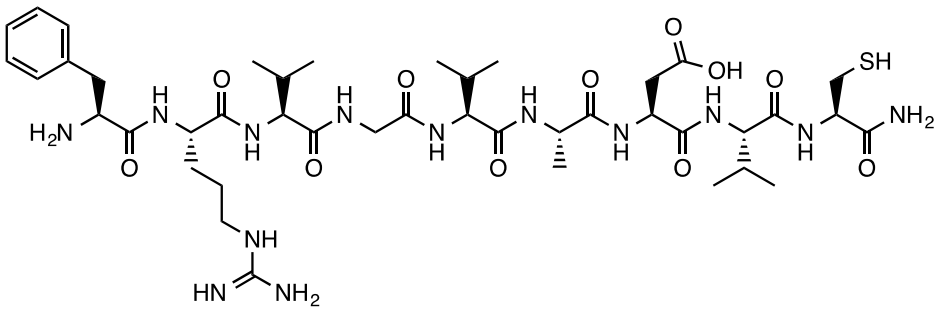

NH_2-FRVGVADVC-C(O)NH_2 was synthetized in a 0.10 mmol scale using a five-fold excess of protected amino acids (AA, 0.5mmol) relative to the Rink-amide MBHA resin (300 mg, 0.32 mmol g^{-1}). Before starting the synthesis, all the AA were dissolved in NMP (2.4 ml, 0.26

M), and HATU (0.4 M in DMF), DIEA (2.5 M in NMP) and 20% piperidine in DMF solutions were freshly prepared. The resin was kept in the synthesizer and swelled in NMP (6 ml) at r.t. for 15 min. Fmoc deprotection was obtained by using 20% piperidine in DMF (6 ml) three times for 4 minutes each. Afterwards, the downloading of the resin was performed by coupling reaction using Fmoc-Cys-OH (2.4 ml of 0.26M), HATU (2 ml of 0.4 M) and DIEA (1 ml of 2.5 M). All the reagents were mixed at r.t. for 1 min and then added to the resin. The reaction was mixed at r.t. for 25 min and the resin was after washed (6 ml NMP x 2, 15 ml DMF x 2). A double coupling process was performed. After Fmoc removal on the α-NH_2, the deprotected resin was then coupled (double coupling) with V, D, A, V, G, V, R, F [(2.4 ml of 0.26 M of each AA starting from L to C), HATU (2 ml of 0.4 M) and DIEA (1 ml of 2.5 M)], washed and deprotected in automatic way to obtain the FRVGVADVC.

Resin Cleavage. When the synthesis was completed, a freshly prepared cleavage solution of TFA, TIPS, water and EDT (92.5:2.5:2.5:2.5) was added to the resin (3 ml) and the cleavage reaction was allowed to proceed at r.t. for 4 h. The product was precipitated with Et_2O (50 ml) and isolated by centrifugation to form a white solid (57 mg, Yield = 62%).

RP-HPLC analysis and purification: Crude peptide was analyzed and purified by RP-HPLC. The gradient was from 0.1% TFA in water to 0.1% TFA in CH_3CN over 38 min. The flow rates for analytical and preparative HPLC were 1 ml min^{-1} and 21 ml min^{-1}, respectively. According to these parameters, NGRSLC detected at 220 nm was eluted at 17 min retention time.

MS (MALDI-HRMS): found 964.5034 $[M+H]^+$, $[C_{42}H_{70}N_{13}O_{11}S]$ requires = 964.5038

a)

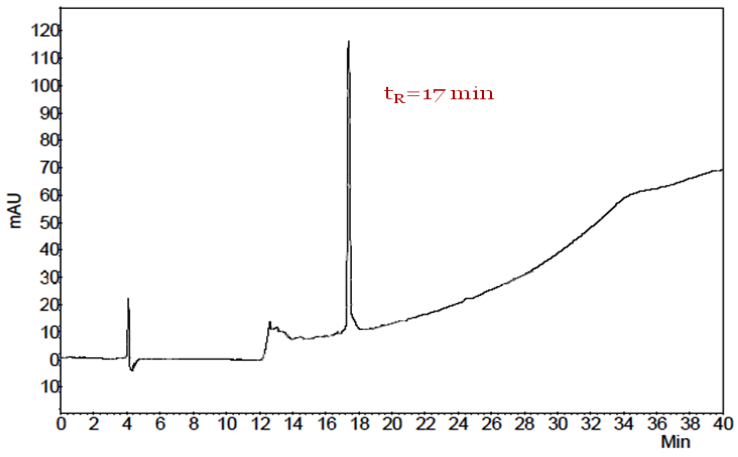

b)

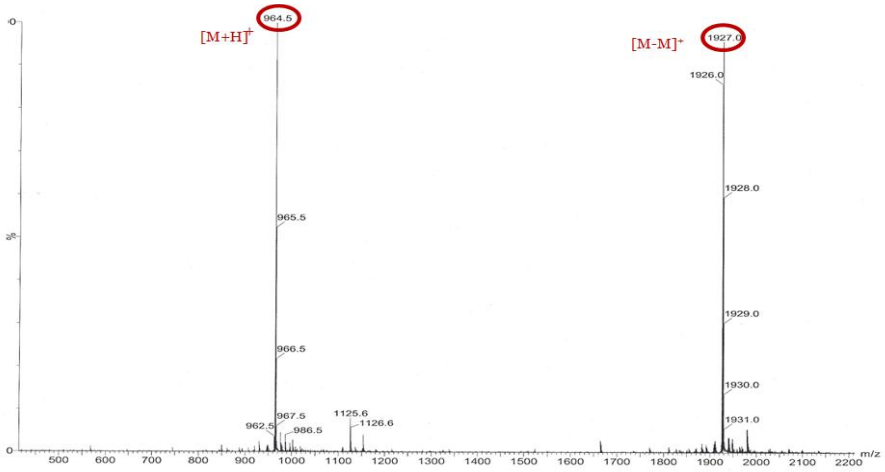

Fig. 4.5: (**a**) HPLC chromatogram and (**b**) MALDI-TOF analysis of purified NH_2-FRVGVADVC-C(O)NH_2. HPLC conditions: Agilent Zorbax SBC18, 5 µm, 4.6×250 mm, eluents from 0.1% TFA in H_2O to 0.1% TFA in CH_3CN, flow 1 mL min-1, r.t. The eluents were monitored at 220 nm.

4.4.3.4 Synthesis of N-acetylPHSCNK-C(O)NH_2

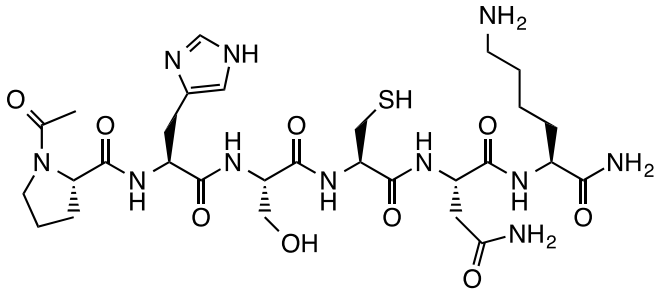

N-acetylPHSCNK-C(O)NH_2 was synthetized in a 0.10 mmol scale using a five-fold excess of protected amino acids (AA, 0.5 mmol) relative to the Rink-amide MBHA resin (300 mg, 0.32 mmol g^{-1}). Before starting the synthesis, all the AA were dissolved in NMP (2.4 ml, 0.26 M), and HATU (0.4 M in DMF), DIEA (2.5 M in NMP) and 20% piperidine in DMF solutions were freshly prepared. The resin was kept in the synthesizer and swelled in NMP (6 ml) at r.t. for 15 min. Fmoc deprotection was obtained by using 20% piperidine in DMF (6 ml) three times for 4 minutes each. Afterwards, the downloading of the resin was performed by coupling reaction using Fmoc-Lys-OH (2.4 ml of 0.26 M), HATU (2 ml of 0.4 M) and DIEA (1 ml of 2.5 M). All the reagents were mixed at r.t. for 1 min and then added to the resin. The reaction was mixed at r.t. for 25 min and the resin was after washed (6 ml NMP x 2, 15 ml DMF x 2). After Fmoc removal on the α-NH_2, the deprotected resin was then coupled (double coupling) with N, C, S, H, P [(2.4 ml of 0.26 M of each AA starting from L to C), HATU (2 ml of 0.4 M) and DIEA (1 ml of 2.5 M)], washed and deprotected in automatic way to obtain the PHSCNK. The acetylation of the N-terminal function was performed adding dropwise 6 ml of a mixture of Ac_2O:pyridine:NMP (1:2:2) and repeating this step a second time.

Resin Cleavage. When the synthesis was completed, a freshly prepared cleavage solution of TFA, TIPS, water and EDT (92.5:2.5:2.5:2.5) was added to the resin (3 ml) and the cleavage reaction was allowed to proceed at r.t. for 3 h. The product was precipitated with Et_2O (50ml) and isolated by centrifugation to form a white solid (63%).

a)

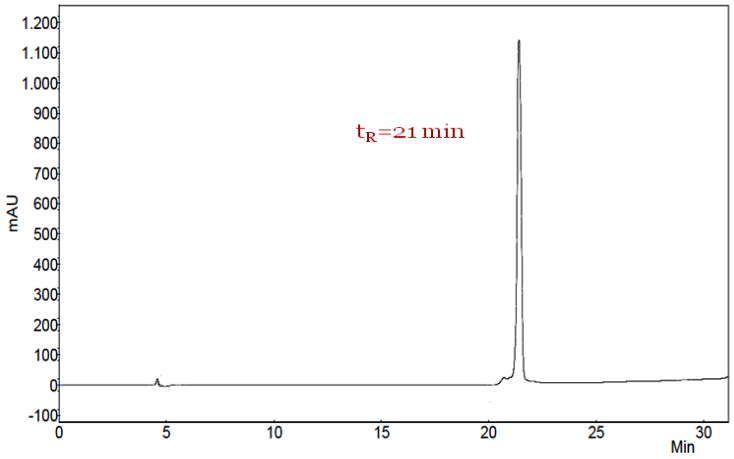

b)

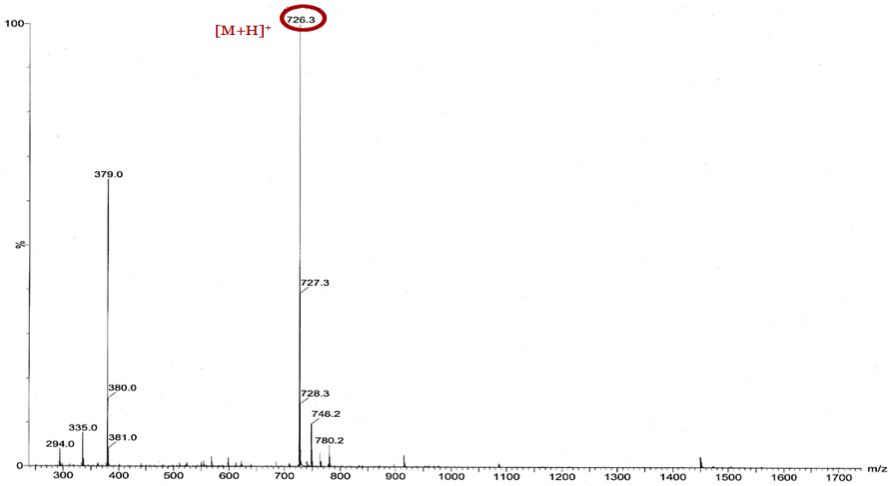

Fig. 4.6: (**a**) HPLC chromatogram and (**b**) MALDI-TOF analysis of purified N-acetylPHSCNK-C(O)NH_2. HPLC conditions: Agilent Zorbax SBC18, 5 µm, 4.6×250 mm, eluents from 0.1% TFA in H_2O to 0.1% TFA in CH_3CN, flow 1 mL min-1, r.t. The eluents were monitored at 220 nm.

RP-HPLC analysis and purification: Crude peptide was analyzed and purified by RP-HPLC. The gradient was from 0.1% TFA in water to 0.1% TFA in CH_3CN over 38 min. The flow rates for analytical and preparative HPLC were 1 ml min^{-1} and 21 ml min^{-1}, respectively. According to these parameters, N-acetylPHSCNK detected at 220 nm was eluted at 21 min retention time.

MS (MALDI-HRMS): MS (MALDI-HRMS): found 726.3362 $[M+H]^+$, $[C_{29}H_{48}N_{11}O_9S]$ requires = 726.3357; found 748.2 $[M+Na]^+$, [C29H47N11O9NaS] requires = 748.2; found 780.2 $[M+K]^+$, [C29H47N11O9KS] requires = 780.2

4.4.3.5 Synthesis of NH_2-CGFLGK(Rho)-C(O)NH_2

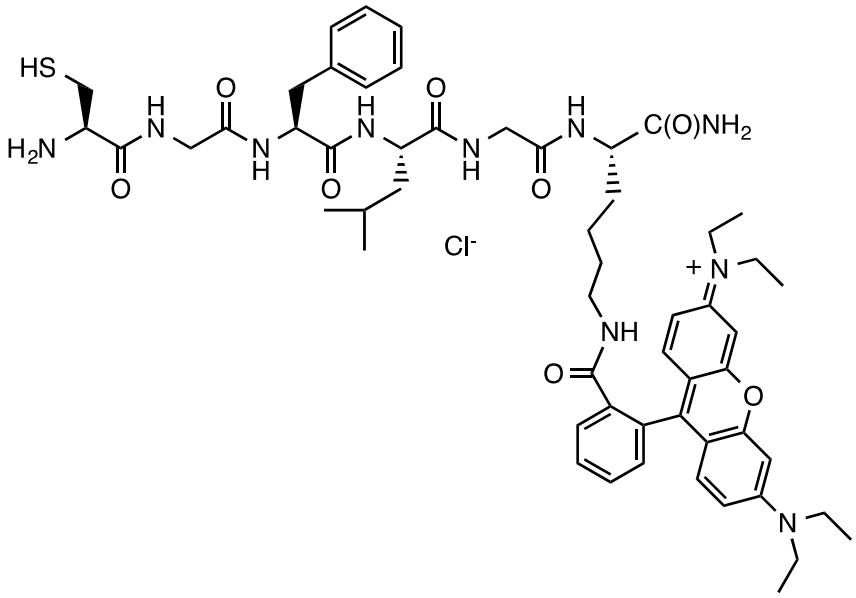

NH_2-CGFLGK(Rho)-C(O)NH_2 was synthetized in a 0.10 mmol scale using a five-fold excess of protected amino acids (AA, 0.5 mmol) relative to the Rink-amide MBHA resin (300 mg, 0.32 mmol g^{-1}). Before starting the synthesis, all the AA were dissolved in NMP (2.4 ml, 0.26 M), and HATU (0.4 M in DMF), DIEA (2.5 M in NMP) and 20% piperidine in DMF solutions were freshly prepared. The resin was kept in the synthesizer and swelled in NMP (6 ml) at r.t. for 15 min. Fmoc deprotection was obtained by using 20% piperidine in DMF (6 ml) three times for 4 minutes each. Afterwards, the downloading of the resin was performed by coupling reaction using Fmoc-Lys(OAll)-OH (2.4 ml of 0.26 M), HATU (2 ml of 0.4 M) and DIEA (1 ml of 2.5 M). All the reagents were mixed at r.t. for 1 min and then added to the resin. The reaction was mixed at r.t. for 25 min and the resin was after washed (6 ml NMP x 2, 15 ml DMF x 2).

At this step, Alloc deprotection of the ε-NH_2 was performed in manual mode, adding to the resin first phenylsilane (1.9 mmol) at r.t. for 5 min and after [$Pd(PPh_3)_4$] (0.032 mmol) at r.t for 30 min, both of them previously dissolved in CH_2Cl_2. The amide bond formation between the free γ-amino group and the carboxylic group of the Rhodamine B was performed introducing dropwise into the reactor vessel a solution of Rhodamine B (230 mmol, 0.5 mmol), 1.8 ml of HATU (0.4M in DMF) 1 ml of pyperidine (20% in DMF) in NMP (2.4ml).

After Fmoc removal on the α-NH_2, the deprotected resin was then coupled with G, L, F, G, C [(2.4 ml of 0.26 M of each AA starting from G to C), HATU (2 ml of 0.4 M) and DIEA (1 ml of 2.5 M)], washed and deprotected in automatic way to obtain the CGFLGK.

The last step was the deprotection of the Fmoc group on the α-NH_2 of the last residue, performed as described before.

Resin Cleavage. When the synthesis was completed, a freshly prepared cleavage solution of TFA, TIPS, water and EDT (92.5:2.5:2.5:2.5) was added to the resin (3 ml) and the cleavage reaction was allowed to proceed at r.t. for 2 h. The product was precipitated with Et_2O (50 ml) and isolated by centrifugation to form a pink solid (26mg).

RP-HPLC analysis and purification: Crude peptide was analyzed and purified by RP-HPLC. The gradient was from 0.1% TFA in water to 0.1% TFA in CH_3CN over 50 min. The flow rates for analytical and preparative HPLC were 1 ml min^{-1} and 21 ml min^{-1}, respectively.

According to these parameters, CGFLGK(Rho) (detected at 220 nm and 540 nm for the Rhodamine emission) was eluted at 38 min as retention time.
MS (MALDI-HRMS): found 1049.6 $[M]^+$, $[C_{56}H_{77}N_{10}O_8S]^+$ requires = 1049.6

a)

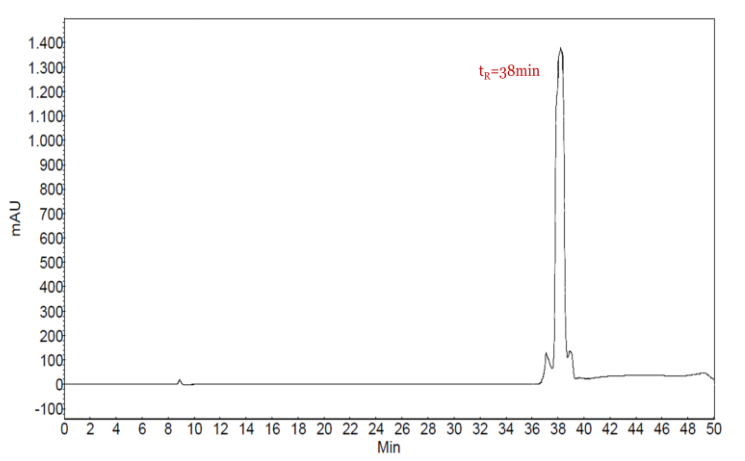

b)

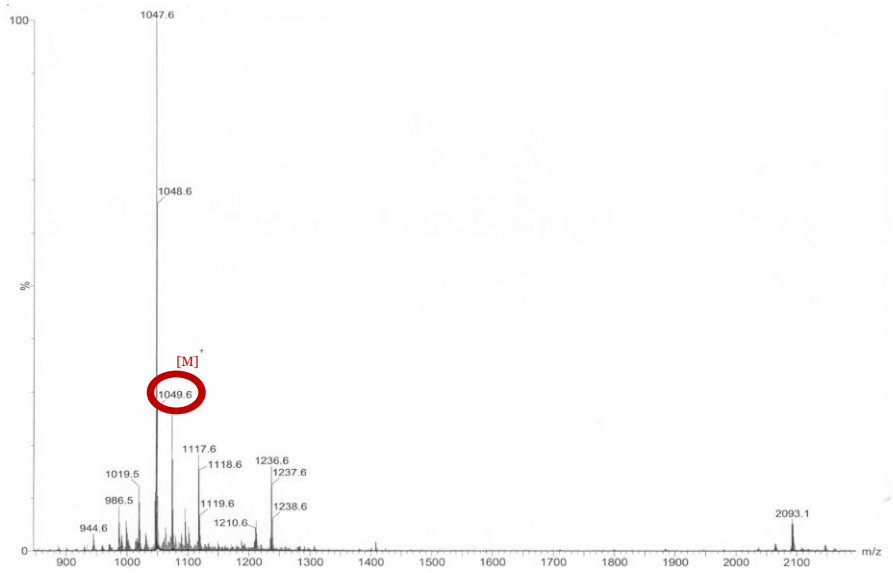

Fig. 4.7: (**a**) HPLC chromatogram and (**b**) MALDI-TOF analysis of purified NH_2-CGFLGK(Rho)-C(O)NH_2. HPLC conditions: Agilent Zorbax SBC18, 5 µm, 4.6×250 mm, eluents from 0.1% TFA in H_2O to 0.1% TFA in CH_3CN, flow 1 mL min-1, r.t. The eluents were monitored at 540 nm (Rhodamine B $\lambda_{emission}$).

4.4.4 NDs functionalization

4.4.4.1 Oxidation with sulfonitric mixed acid

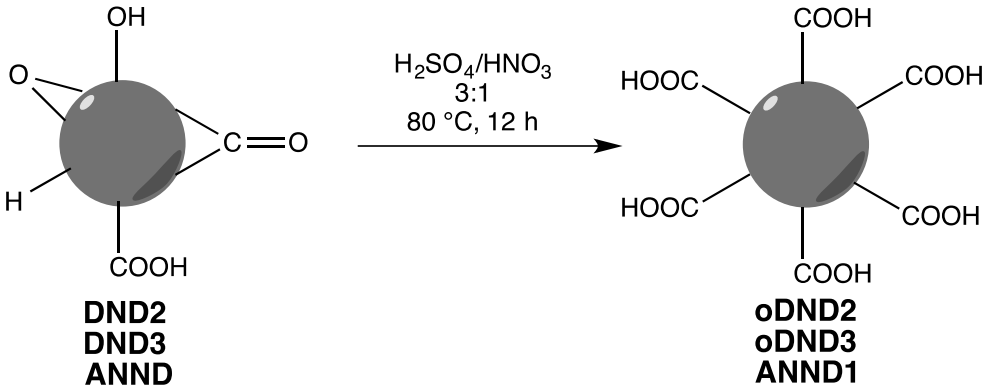

A H_2SO_4/HNO_3 (3:1) mixture (30 ml) was introduced very slowly into a round-bottom flask containing 30 mg of NDs. After a short sonication, the reaction mixture was stirred at 80 °C. After 12 h the mixture was filtrated and the nanodiamonds were washed with water (until the neutral pH value) DMF, MeOH, AcOEt and Et_2O. The product was then dried, resulting in 26 mg.

4.4.4.2 Synthesis of DND2-1 and DND2-3

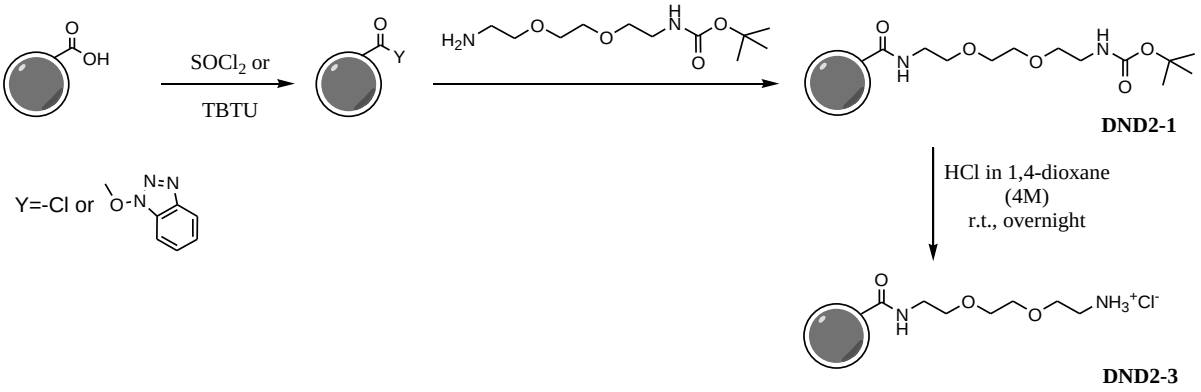

Using $SOCl_2$:

NDs (15 mg) were refluxed with 25 ml of $SOCl_2$ and 0.5 ml of anhydrous N,N-dimethylformamide (DMF) at 70 °C for 24 h, the yellow-colored liquid was removed under vacuum. The acyl chloride derivative was stirred in the flask with 0.5 g of N-Boc-amino-diethoxy-ethylamine **1** and 1 ml of pyridine, using DMF anhydrous as solvent (15 ml). After 48 h the reaction mixture was filtrated and then washed with DMF, water, MeOH, AcOEt and Et_2O. The product was then dried, resulting in 10 mg. For the deprotection of the Boc- group, a sonicated solution of the obtained compound (4 mg) in 4 ml of HCl 4M in dioxane was stirred overnight at r.t.. Nanodiamonds were filtrated and then washed with H_2O, DMF, MeOH, AcOEt and Et_2O. The product was then dried, resulting in 3 mg.

Using TBTU:

10 mg of NDs were dispersed in 5 ml of dicloromethane in a flask. The system was cooled down to 0 °C and the solution was purged with nitrogen for few minutes. TBTU (0.026 g,

0.08 mmol) and DIPEA (0.103 ml, 0.59 mmol) were dissolved in a separate round bottom flask with 5 ml of dicloromethane and they were transferred into the ice-cold solution of NDs. The reaction was left for 1 h at 0 °C. The compound N-Boc-amino-diethoxy-ethylamine **1** was added into the suspension of NDs and the reaction mixture was stirred at r.t. overnight. After 16 h the reaction mixture was filtrated and then washed with DMF, water, MeOH, AcOEt and Et_2O. The product was then dried, resulting in 9 mg.

4.4.4.3 Synthesis of DND2-2 and DND2-4

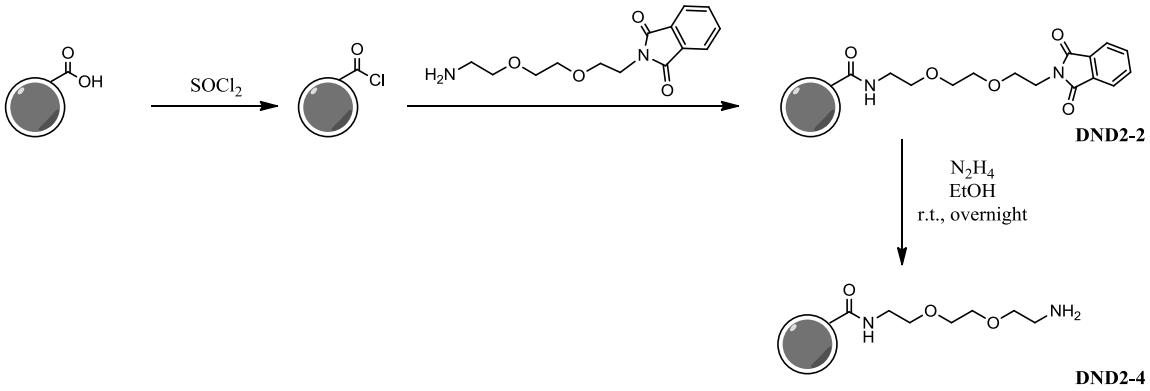

NDs (20 mg) were refluxed with 33 ml of $SOCl_2$ and 0.67 ml of anhydrous N,N-dimethylformamide at 70 °C for 24 h, the yellow-colored liquid was removed under vacuum. The acyl chloride derivative was stirred in the flask with 0.7 g of N-Pht-amino-diethoxy-ethylamine **5** and 1.3 ml of pyridine, using DMF anhydrous as solvent (20 ml). After 48 h the reaction mixture was filtrated and then washed with DMF, water, MeOH, AcOEt and Et_2O. The product was then dried, resulting in 13 mg. The deprotection of the Pht- group was made adding dropwise 0.05 ml of hydrazine monohydrated to a sonicated solution of the obtained compound (7 mg) in 7 ml of EtOH. The mixture was then stirred overnight at r.t.. The nanodiamonds were filtrated and then washed with MeOH, H_2O, water with 1 drop of HCl, H_2O, MeOH and AcOEt. The product was then dried, resulting in 4 mg.

4.4.4.4 Synthesis of DND2-5

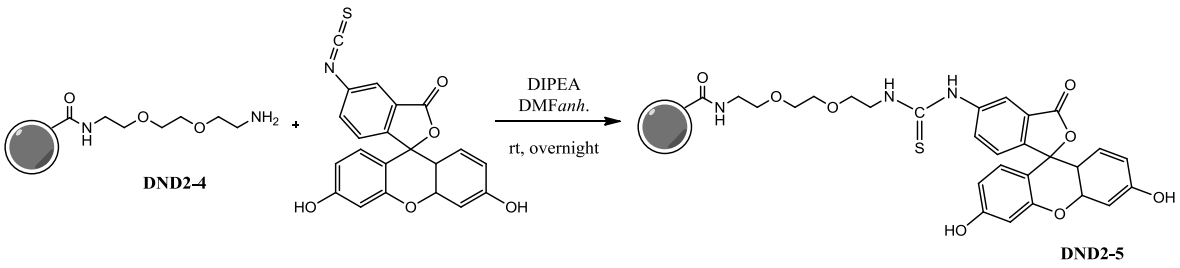

DND2-4 (4 mg) were stirred under Argon atmosphere with FITC(I) (8.5 mg, 0.026 mmol) and DIPEA (11 ml, 0.05 mmol) in 1 ml of anhydrous DMF at rt. After 12h, the reaction mixture was filtrated and NDs were washed with DMF, water, MeOH, AcOEt. The product was then dried, resulting in 4 mg.

4.4.4.5 Synthesis of ANND3

500 mg of detonation nanodiamond **ANND** were placed in a boat and introduced into the quartz tube. The oven was heated to 750 °C, under atmospheric pressure while pure argon was flowing into the oven at a rate of 2 l/min. After maintaining the temperature for 2 h, the oven was switched off and the sample was cooled down and analyzed.

4.4.4.6 Synthesis of ANND4

500 mg of detonation nanodiamond (**ANND**) were placed in a boat and introduced into the quartz tube. The oven was heated to 900 °C, under atmospheric pressure while pure argon was flowing into the oven at a rate of 2 l/min. After maintaining the temperature for 2 h, the oven was switched off and the sample was cooled down and analyzed.

4.4.4.7 Synthesis of DND4-2, DND5-2, DND6-2 and DND7-2

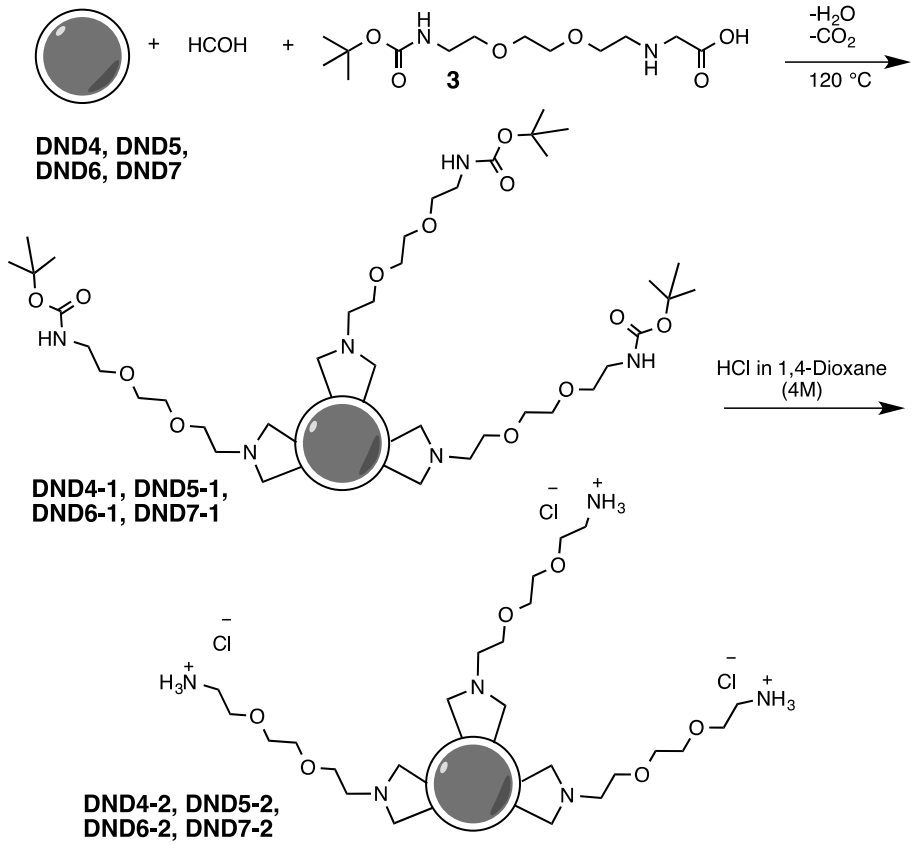

In DMF, 120 °C, 24 h:

A DMF solution (15 ml) of NDs (15 mg), paraformaldehyde (23 mg, 0.8 mmol) and N-Boc-amino-diethoxy-ethylamino-acetic acid **3** (43 mg, 0.14 mmol) was sonicated and the reaction mixture was stirred at 120 °C under reflux. After 2 h same amounts of paraformaldehyde and **3** were added to the solution, the mixture was then sonicated and stirred for 2 h at 120 °C under reflux. This operation was repeated 3 more times. After 24 h the reaction mixture was filtrated and nanodiamonds were washed with DMF, water, MeOH, AcOEt and Et_2O. The product was then dried, resulting in 11 mg. For the deprotection of the Boc- group a sonicated solution of the obtained compound (6 mg) in 6 ml of HCl 4 M in dioxane was stirred

overnight at r.t.. Nanodiamonds were filtrated and then washed with H_2O, DMF, MeOH, AcOEt and Et_2O. The product was then dried, resulting in 5 mg.

In o-DCB, 120 °C, 24 h:
An *o*-DCB solution (10 ml) of NDs (0.010 g), paraformaldehyde (14 mg, 0.47 mmol) and N-Boc-amino-diethoxy-ethylamino-acetic acid **3** (28 mg, 0.08 mmol) was sonicated and the reaction mixture was stirred at 120 °C under reflux. After 2 h same amounts of paraformaldehyde and **3** were added to the solution, the mixture was then sonicated and stirred for 2 h at 120 °C under reflux. This operation was repeated 3 more times. After 24 h the reaction mixture was filtrated and nanodiamonds were washed with DMF, water, MeOH, AcOEt and Et_2O. The product was then dried, resulting in 9 mg. For the deprotection of the Boc- group a sonicated solution of the obtained compound (5 mg) in 5 ml of HCl 4M in dioxane was stirred overnight at r.t.. Nanodiamonds were filtrated and then washed with H_2O, DMF, MeOH, AcOEt and Et_2O. The product was then dried, resulting in 5 mg.

4.4.4.8 Synthesis of DND4-5, DND5-5, DND6-5, DND7-5, DND4-6, DND5-6, DND6-6 and DND7-6

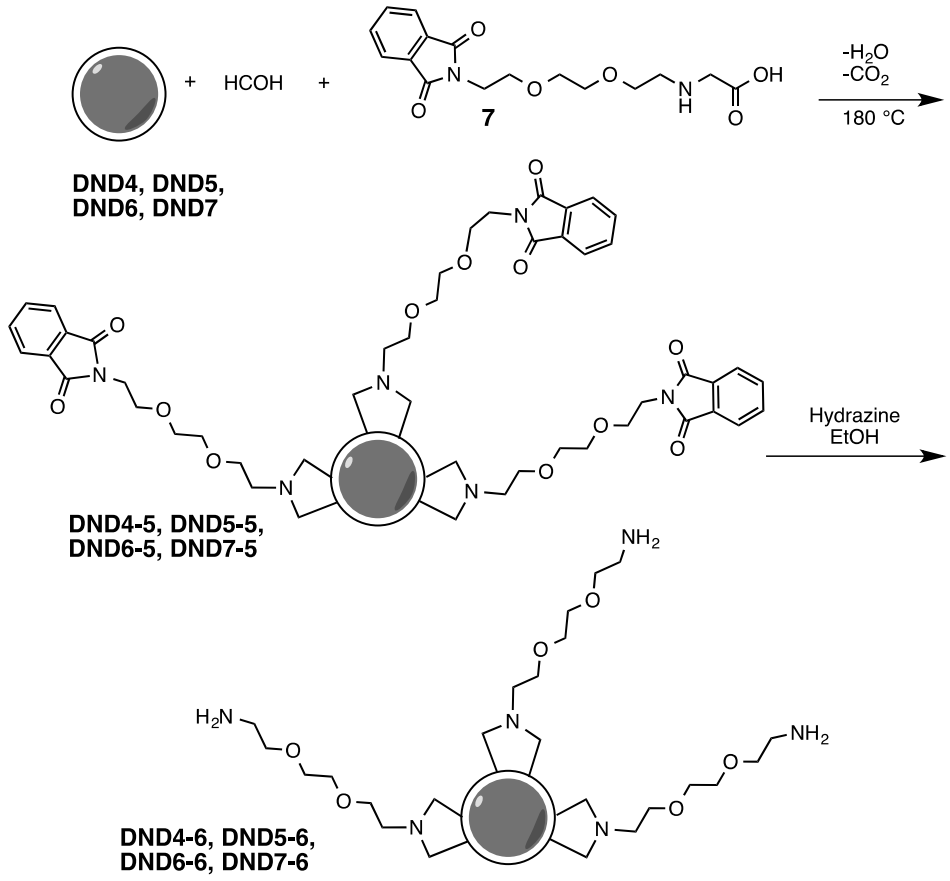

An *o*-DCB solution (15 ml) of NDs (0.015 g), paraformaldehyde (23 mg, 0.77 mmol) and N-Pht-amino-diethoxy-ethylamino-acetic acid **7** (42 mg, 0.12 mmol) was sonicated and the reaction mixture was stirred at 180 °C under reflux. After 2 h same amounts of paraformaldehyde and **7** were added to the solution, the mixture was then sonicated and stirred for 2 h at 180 °C under reflux. This operation was repeated 3 more times. After 24 h

the reaction mixture was filtrated and nanodiamonds were washed with DMF, water, MeOH, AcOEt and Et_2O. The product was then dried, resulting in 16 mg. The deprotection of the Pht-group was made adding dropwise hydrazine monohydrated (0.0357 ml) to a sonicated solution of the obtained compound (5 mg) in 5 ml of EtOH. The mixture was then stirred overnight at r.t.. The nanodiamonds were filtrated and then washed with MeOH, H_2O, water with 1 drop of HCl, H_2O, MeOH and AcOEt. The product was then dried, resulting in 4 mg.

4.4.4.9 Synthesis of DND4-5A

DND4 (12 mg), N-Pht-amino-diethoxy-ethylamino-acetic acid **7** (12 mg, 0.04 mmol), paraformaldehyde (10 mg, 0.3 mmol) were suspended in DCM by sonication in a vial. The solution was transferred into a quartz microwave tube, the solvent was then evaporated using a nitrogen flow. The reaction was performed in a microwave reactor, with 225 W power, using a step-wise heating procedure. After 90 min the reaction mixture was dispersed in DMF, filtrated and nanodiamonds were washed with DMF, water, MeOH, AcOEt and Et_2O. The product was then dried, resulting in 13 mg.

4.4.4.10 Synthesis of DND4-5B

DND4 (12 mg), N-Pht-amino-diethoxy-ethylamino-acetic acid **7** (12 mg, 0.04 mmol), paraformaldehyde (10 mg, 0.3 mmol) were suspended in DCM by sonication in a vial. The solution was transferred into a quartz microwave tube, the solvent was then evaporated using a nitrogen flow. The reaction was performed in a microwave reactor, with 225 W power, using a step-wise heating procedure. After 3h the reaction mixture was dispersed in DMF, filtrated and nanodiamonds were washed with DMF, water, MeOH, AcOEt and Et_2O. The product was then dried, resulting in 12 mg.

4.4.4.11 Synthesis of DND4-5C

DND4 (8 mg), N-Pht-amino-diethoxy-ethylamino-acetic acid **7** (6.8 mg, 0.02 mmol), paraformaldehyde (8 mg, 0.27 mmol) were suspended in *o*-DCB by sonication. The solution was transferred into a quartz microwave tube. The reaction was performed in a microwave reactor, with 50 W power, using a step-wise heating procedure. After 1 h the reaction mixture was filtrated and nanodiamonds were washed with DMF, water, MeOH, AcOEt and Et_2O. The product was then dried, resulting in 9 mg.

4.4.4.12 Synthesis of DND5-7

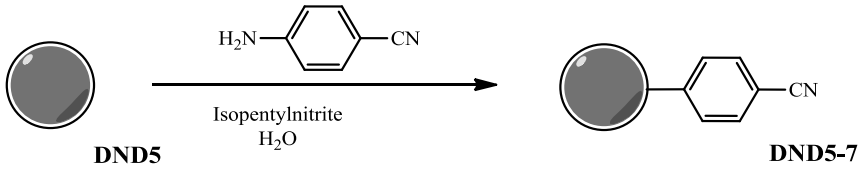

A water solution (5.1 ml) of **DND5** (6 mg) and 4-aminobenzonitrile (49 mg, 0.41 mmol) was sonicated and the isopentyl nitrite (0.099 ml, 96% purity) was added slowly to the reaction flask.

The reaction mixture was stirred at 80 °C overnight. After 16 h the mixture was filtrated and the nanodiamonds were washed with DMF, water, MeOH, AcOEt and Et_2O. The product was then dried, resulting in 5 mg.

4.4.4.13 Synthesis of DND4-7, DND5-8, DND6-7, DND7-7, ANND3-1, ANND4-1, DND4-8, DND5-9, DND6-8, DND7-8, ANND3-2, ANND4-2

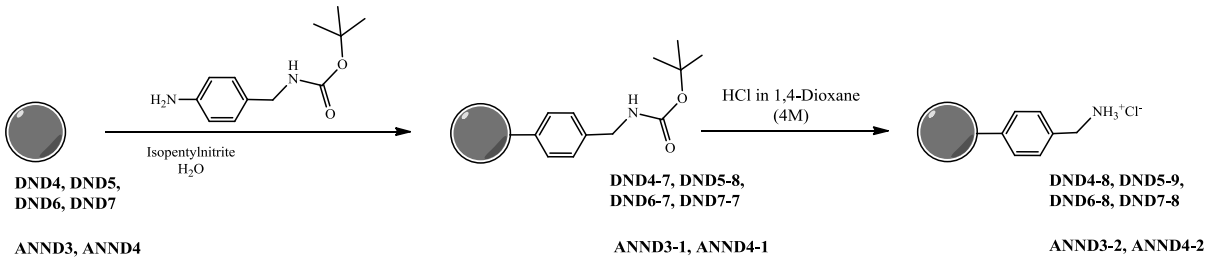

A water solution (8.5 ml) of NDs (0.01 g) and 4-[(N-Boc)aminomethyl]aniline (0.166 g, 0.75 mmol) was sonicated and the isopentyl nitrite (0.166 ml, 96% purity) was added slowly to the reaction flask. The reaction mixture was stirred at 80 °C overnight. After 16 h the mixture was filtrated and the nanodiamonds were washed with DMF, water, MeOH, AcOEt and Et_2O. The product was then dried, resulting in 8 mg. For the deprotection of the Boc- group a sonicated solution of the previous compound (5 mg) in 5 ml of HCl 4 M in dioxane was stirred overnight at r.t.. The nanodiamonds were filtrated and then washed with H_2O, DMF, MeOH, AcOEt and Et_2O. The product was then dried, resulting in 5 mg.

4.4.4.14 Synthesis of DND4-9 and DND4-12

8 mg of **DND4** were sonicated in deionized water (8 ml) together with 4-[(N-Boc)aminomethylaniline] (0.174 g, 0.78 mmol) for 10 min in a 25 ml flask. Isopentyl nitrite (88 µl, 96% purity) was added and a condenser was placed. The mixture was irradiated at 80 °C working at 100 W for 30 minutes. After addition of a new aliquot of isopentyl nitrite (88 µl) the reaction was put at 30 W for 60 minutes. The mixture was filtrated and the nanodiamonds were washed with DMF, water, MeOH, AcOEt and Et_2O. The product was then dried, resulting in 8 mg. For the deprotection of the Boc- group a sonicated solution of previous compound (4 mg) in 4 ml of HCl 4 M in dioxane was stirred overnight at r.t.. The nanodiamonds were filtrated and then washed with H_2O, DMF, MeOH, AcOEt and Et_2O. The product was then dried, resulting in 3 mg.

4.4.4.15 Synthesis of DND4-10 and DND4-13

8 mg of **DND4** were sonicated in deionized water (8 ml) together with 4-[(N-Boc)aminomethylaniline] (0.174 g, 0.78 mmol) for 10 min in a 25 ml flask. Isopentyl nitrite (176 µl, 96% purity) was added. The mixture was irradiated at 80 °C working at 100 W for 35 minutes. The mixture was filtrated and the nanodiamonds were washed with DMF, water, MeOH, AcOEt and Et_2O. The product was then dried, resulting in 8 mg. For the deprotection of the Boc- group a sonicated solution of previous compound (4 mg) in 4 ml of HCl 4 M in

dioxane was stirred overnight at r.t.. The nanodiamonds were filtrated and then washed with H_2O, DMF, MeOH, AcOEt and Et_2O. The product was then dried, resulting in 4 mg.

4.4.4.16 Synthesis of DND4-11 and DND4-14

10 mg of **DND4** were sonicated in deionized water (10 ml) together with 4-[(N-Boc)aminomethylaniline] (0.217 g, 0.98 mmol) for 10 min in a 25 ml flask. Isopentyl nitrite (220 µl, 96% purity) was added. The mixture was irradiated at 110 °C working at 100 W for 15 min. The mixture was filtrated and the nanodiamonds were washed with DMF, water, MeOH, AcOEt and Et_2O. The product was then dried, resulting in 10 mg. For the deprotection of the Boc- group a sonicated solution of obtained compound (5 mg) in 5 ml of HCl 4 M in dioxane was stirred overnight at r.t.. The nanodiamonds were filtrated and then washed with H_2O, DMF, MeOH, AcOEt and Et_2O. The product was then dried, resulting in 5 mg. For the deprotection of the Boc- group a sonicated solution of previous compound (4 mg) in 4 ml of HCl (4 M) in dioxane was stirred overnight at r.t.. The nanodiamonds were filtrated and then washed with H_2O, DMF, MeOH, AcOEt and Et_2O. The product was then dried, resulting in 4 mg.

4.4.4.17 Synthesis of DND4-15

A water solution (2 ml) of **DND4** (10 mg) and 4-aminobenzenesulfonic acid (146 mg, 0.84 mmol) was sonicated and the isopentyl nitrite (0.166 ml, 96% purity) was added slowly to the reaction flask, the reaction mixture was stirred at 80 °C. After 1 h the mixture was filtrated and the nanodiamonds were washed with DMF, water, MeOH, AcOEt and Et_2O. The product was then dried, resulting in 10 mg.

4.4.4.18 Synthesis of DND4-16

5 mg of **DND4** were sonicated in deionized water (5 ml) together with 4-amino-benzenesulfonic acid (0.085 g, 0.49 mmol) for 10 min in a 25 ml flask. Isopentyl nitrite (110 µl, 96% purity) was added. The mixture was irradiated at 110°C working at 100 W for 15 min. The mixture was filtrated and the nanodiamonds were washed with DMF, water, MeOH, AcOEt and Et_2O. The product was then dried, resulting in 5 mg.

4.4.4.19 Synthesis of DND4-19 and DND4-21

A water solution (2 ml) of **DND4** (10 mg), 4-[(N-Boc)aminomethyl]aniline (167 mg, 0.8 mmol) and 4-aminobenzenesulfonic acid (130 mg, 0.8 mmol)was sonicated and the isopentyl nitrite (0.332 ml, 96% purity) was added slowly to the reaction flask. The reaction mixture was stirred at 80 °C for 1 h. The mixture was filtrated and the nanodiamonds were washed with DMF, water, MeOH, AcOEt and Et_2O. The product was then dried, resulting in 10 mg.
For the deprotection of the Boc- group, a sonicated solution of the previous compound (5 mg) in 5 ml of HCl 4 M in dioxane was stirred overnight at r.t.. The nanodiamonds were filtrated and then washed with H_2O, DMF, MeOH, AcOEt and Et_2O. The product was then dried, resulting in 5 mg.

4.4.4.20 Synthesis of DND4-20 and DND4-22

10 mg of **DND4** were sonicated in deionized water (10 ml) together with Boc-protected p-aminomethylaniline (211 mg, 1 mmol, purity 97%) and 4-aminobenzenesulfonic acid (165 mg, 1 mmol) for 10 min in a 25 ml flask. Isopentyl nitrite (440 μl, 96% purity) was added. The mixture was irradiated at 110 °C working at 100 W for 15 min. The mixture was filtrated and the nanodiamonds were washed with DMF, water, MeOH, AcOEt and Et_2O. The product was then dried, resulting in 10 mg. For the deprotection of the Boc- group a sonicated solution of the previous compound (5 mg) in 5 ml of HCl 4 M in dioxane was stirred overnight at r.t.. The nanodiamonds were filtrated and then washed with H_2O, DMF, MeOH, AcOEt and Et_2O. The product was then dried, resulting in 5 mg.

4.4.4.21 Synthesis of DND6-9, DND7-9, DND6-10, DND7-10

7 mg of NDs were dispersed in 70 ml of anhydrous o-DCB and the suspension was degassed for 45 min, then heated at 180 °C. 350 mg (1.34 mmol) of compound **10** were added and the reaction mixture was stirred at 180 °C for 6 hours. The deprotection of the Pht- group was done adding dropwise hydrazine monohydrated (0.0286 ml) to a sonicated solution of previous compound (4 mg) in 4 ml of EtOH. The mixture was then stirred overnight at r.t.. The nanodiamonds were filtrated and then washed with MeOH, H_2O, water with 1 drop of HCl, H_2O, MeOH and AcOEt. The product was then dried, resulting in 4 mg.

4.4.4.22 Synthesis of DND6-11, DND7-11, DND6-12, DND7-12, ANND3-3, ANND3-4, ANND4-3, ANND4-4

7 mg of NDs were dispersed in 70 ml of anhydrous o-DCB and the suspension was degassed for 45 min, then heated at 180 °C. 350 mg (1.34 mmol) of compound **10** were added and the reaction mixture was stirred at 180 °C overnight. The deprotection of the Pht- group was done adding dropwise hydrazine monohydrated (0.0286 ml) to a sonicated solution of previous compound (4 mg) in 4 ml of EtOH. The mixture was then stirred overnight at r.t.. The nanodiamonds were filtrated and then washed with MeOH, H_2O, water with 1 drop of HCl, H_2O, MeOH and AcOEt. The product was then dried, resulting in 3 mg.

4.4.4.23 Synthesis of DND6-13, DND6-14, DND7-13, DND7-14

8 mg of NDs were sonicated in anhydrous o-DCB (2.4 ml) together with 173 mg (0.66 mmol) of **10** for 10 min in a 25 ml flask under argon atmosphere. The mixture was irradiated at 180 °C working at 100 W for 35 min. The mixture was filtrated and the nanodiamonds were washed with DMF, water, MeOH, AcOEt and Et_2O. The product was then dried, resulting in 8 mg. The deprotection of the Pht- group was done adding dropwise hydrazine monohydrated (0.0286 ml) to a sonicated solution of the obtained compound (4 mg) in 4 ml of EtOH. The mixture was then stirred overnight at r.t.. The nanodiamonds were filtrated and then washed with MeOH, H_2O, water with 1 drop of HCl, H_2O, MeOH and AcOEt. The product was then dried, resulting in 4 mg.

4.4.4.24 Synthesis of ANND1-1

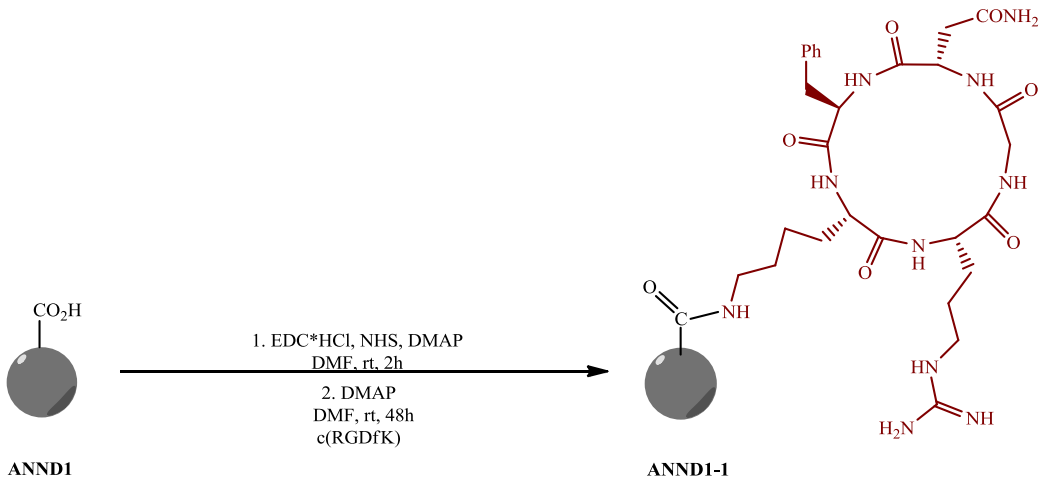

10 mg of **ANND** were sonicated in DMF (12 ml) together with NHS (2.3 mg, 0.02 mmol), EDC*HCl (3.8 mg, 0.02 mmol), DMAP (12.2 mg, 0.1 mmol) for 15 min in a 50 ml flask, then the mixture was stirred at rt for 2h under argon atmosphere. A solution of c(RGDfK) peptide (12 mg, 0.02 mmol) in 8 ml of DMF was added dropwise and the reaction mixture was stirred at working at rt for 48h. NDs were filtered and washed with DMF, water, NMP, MeOH, AcOEt. The product was then dried, resulting in 8 mg.

4.4.4.25 Synthesis of ANND1-2

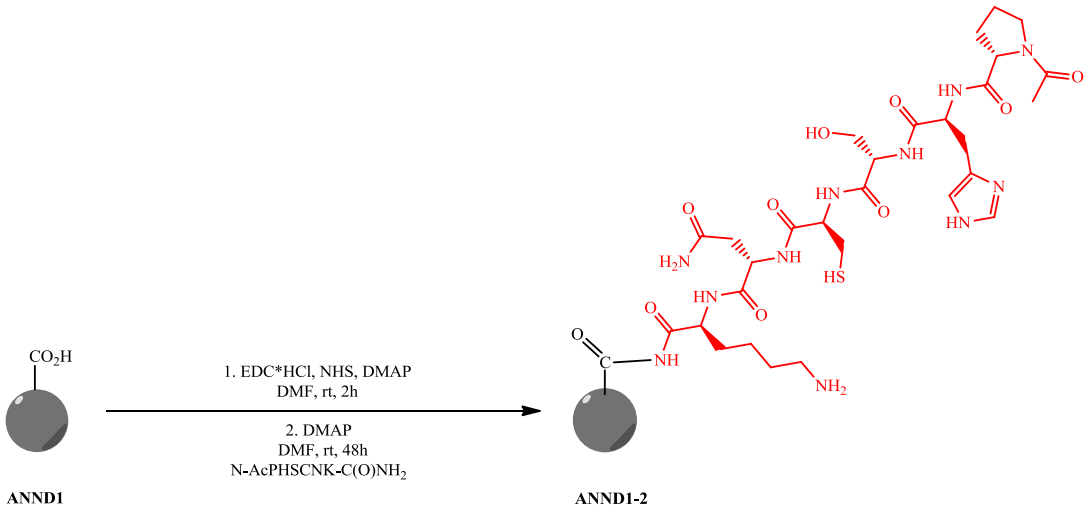

10 mg of **ANND** were sonicated in DMF (12 ml) together with NHS (2.3 mg, 0.02 mmol), EDC*HCl (3.8 mg, 0.02 mmol), DMAP (12.2 mg, 0.1 mmol) for 15 min in a 50 ml flask, then the mixture was stirred at rt for 2h under argon atmosphere. A solution of Ac-PHSCNK-$C(O)NH_2$ peptide (14 mg, 0.02 mmol) in 8 ml of DMF was added dropwise and the reaction mixture was stirred at working at rt for 48h. NDs were filtered and washed with DMF, water, NMP, MeOH, AcOEt. The product was then dried, resulting in 8 mg.

4.4.4.26 Synthesis of ANND1-3, ANND1-4

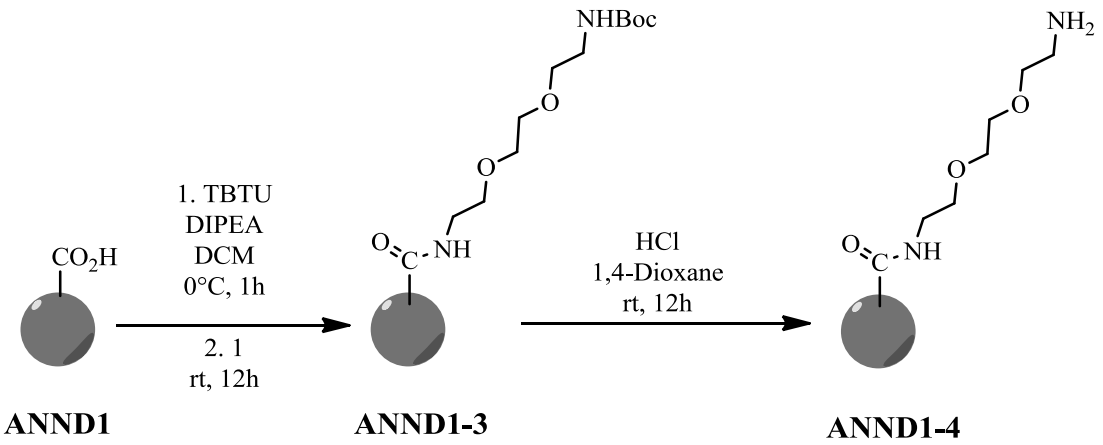

300 mg of **ANND1** were dispersed in 150 ml of dicloromethane in a flask. The system was cooled down to 0 °C and the solution was purged with nitrogen for few minutes. TBTU (780 mg, 2.4 mmol) and DIPEA (3.09 ml, 18 mmol) were dissolved in a separate round bottom flask with 50 ml of dicloromethane and they were transferred into the ice-cold solution of NDs. The reaction was left for 1 h at 0 °C. The compound N-Boc-amino-diethoxy-ethylamine **1** (600 mg, 2.4 mmol) was added into the suspension of NDs and the reaction mixture was stirred at r.t. overnight. After 16 h the reaction mixture was filtrated and then washed with DMF, water, MeOH, AcOEt and Et_2O. The product was then dried, resulting in 296 mg. For the deprotection of the Boc- group, a sonicated solution of the previous compound (250 mg) in 250 ml of HCl 4 M in dioxane was stirred overnight at r.t.. The nanodiamonds were filtrated and then washed with H_2O, DMF, MeOH, AcOEt and Et_2O. The product was then dried, resulting in 250 mg.

4.4.4.27 Synthesis of ANND1-5

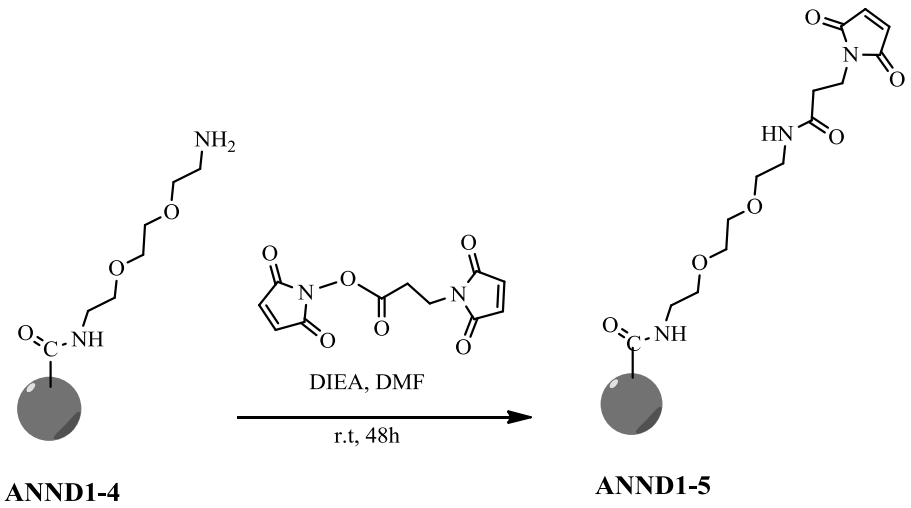

ANND1-4 (40 mg) was suspended in dry DMF (16 ml) and neutralized with dry DIEA (42 µl, 0.24 mmol). After 10 minutes of sonication, a solution of N-succinimidyl-3-

maleimidopropionate (26 mg, 0.1 µmol) in DMF (4 ml) was added. The reaction mixture was sonicated for 20 minutes and then stirred at r.t. under argon for 48h.
The nanodiamonds were filtrated and then washed with DMF, H_2O, MeOH, AcOEt and Et_2O. The product was then dried, resulting in 38 mg.

4.4.4.28 Synthesis of ANND1-6

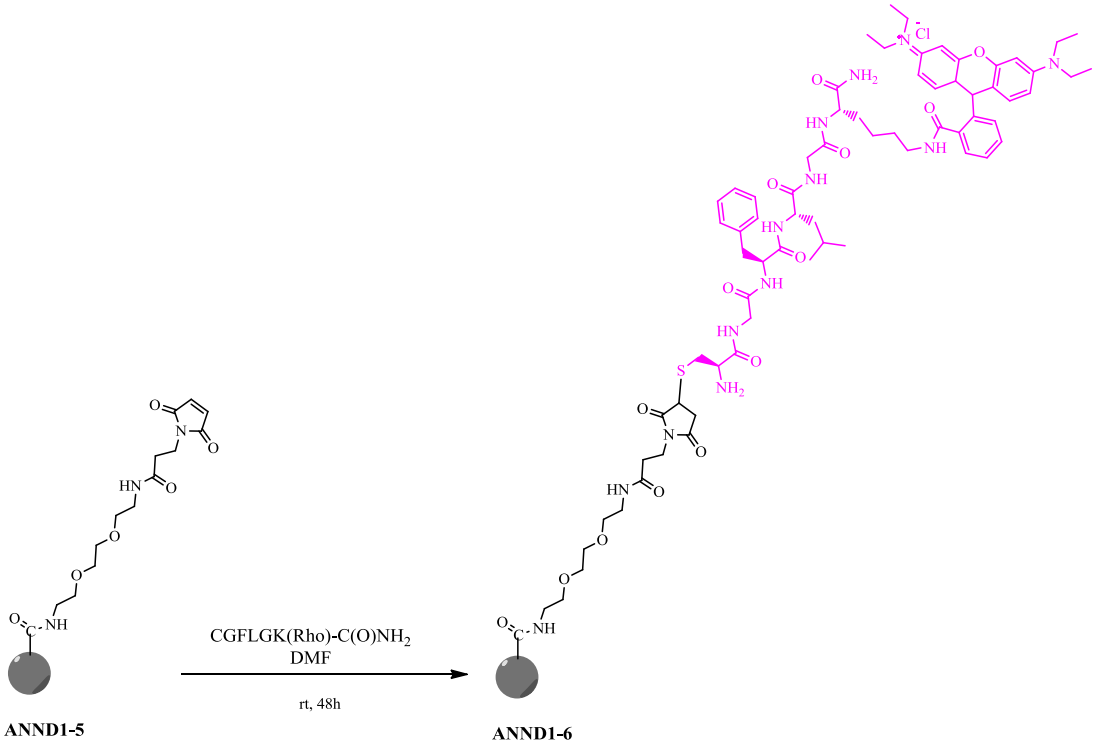

8 mg of **ANND1-5** were dispersed in 8 ml of dry DMF and the suspension was sonicated for 20min under Argon atmosphere. The CGFLGK(Rho)-C(O)NH_2 peptide (3.4 mg, 38 µmol) was added and the reaction was stirred for 48h at rt. NDs were washed with DMF, water, MeOH, AcOEt and Et_2O. The product was then dried, resulting in 7 mg.

4.4.4.29 Synthesis of ANND1-7

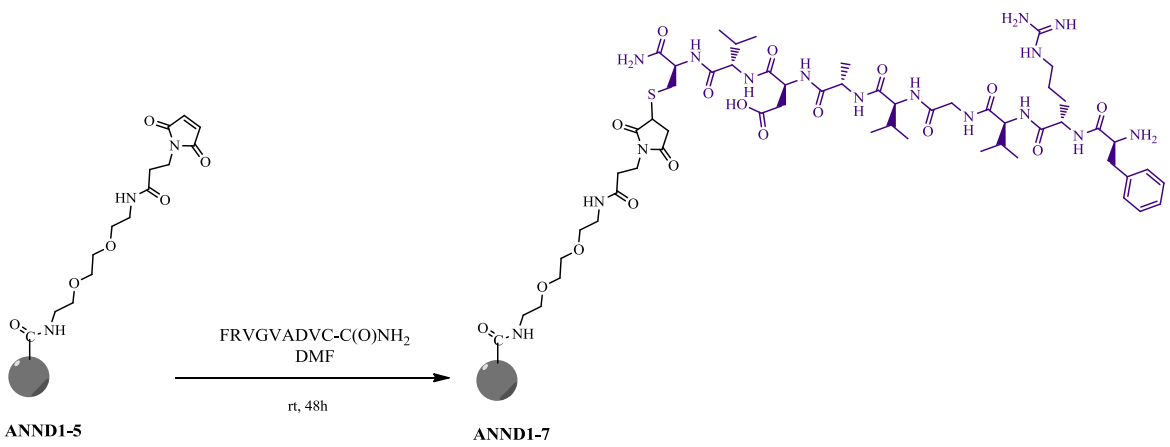

8 mg of **ANND1-5** were dispersed in 8 ml of dry DMF and the suspension was sonicated for 20min under Argon atmosphere. The FRVGVADVC-C(O)NH_2 peptide (3 mg, 3.8 µmol) was added and the reaction was stirred for 48h at rt. NDs were washed with DMF, water, MeOH, AcOEt and Et_2O. The product was then dried, resulting in 7 mg.

4.4.4.30 Synthesis of ANND1-8

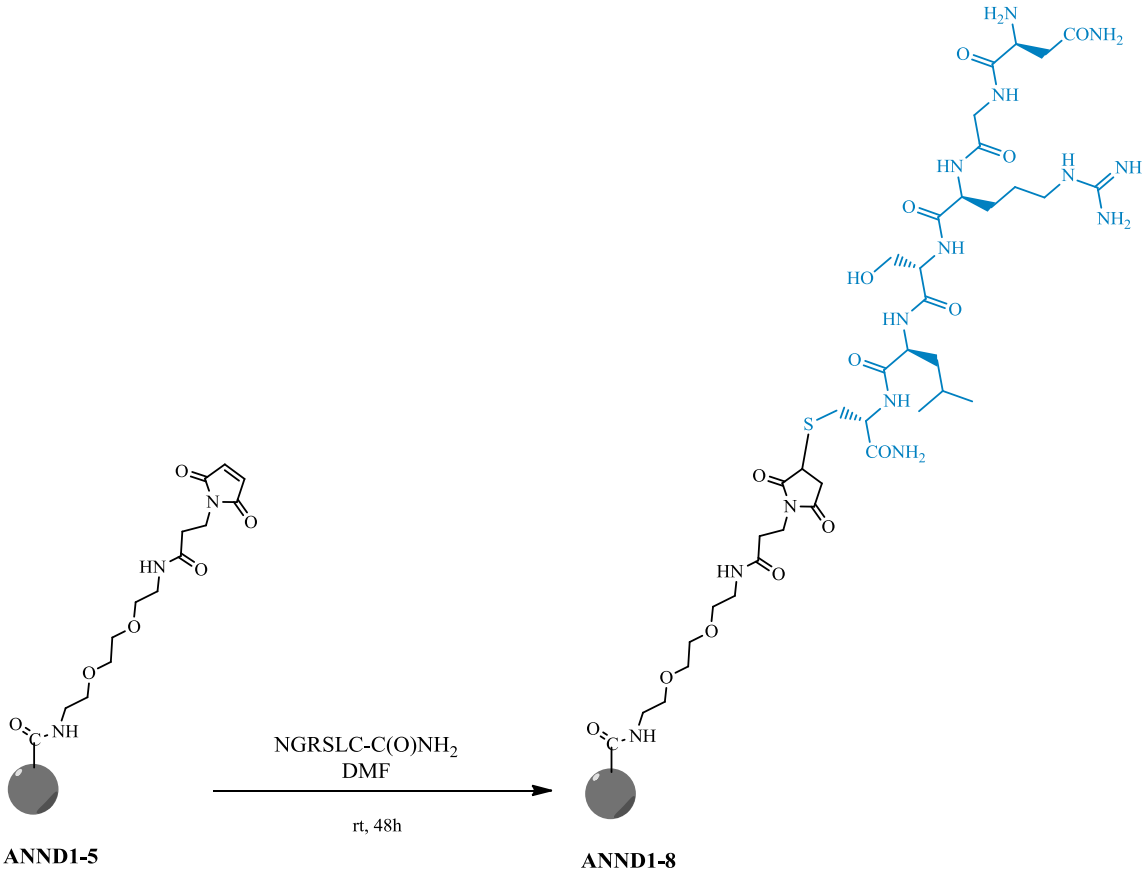

8 mg of **ANND1-5** were dispersed in 8 ml of dry DMF and the suspension was sonicated for 20min under Argon atmosphere. The FRVGVADVC-C(O)NH_2 peptide (3 mg, 3.8 µmol) was added and the reaction was stirred for 48h at rt. NDs were washed with DMF, water, MeOH, AcOEt and Et_2O. The product was then dried, resulting in 7 mg.

4.5 Bibliography

[1] D. L. Gerrard, *Anal. Chem.* **1984**, *56*, 219

[2] a) J. Mayer, L. A. Giannuzzi, T. Kamino, J. Michael, *MRS Bull.* **2007**, *32*, 400; b) D. V. S. Rao, K. Muraleedharan, C. J. Humphreys **2010**, *320*, 1232; c) D. B. Williams, C. B. Carter, *Transmission electron microscopy: A textbook of materials science*, Springer, **2009**

[3] a) J. F. Watts, *Vacuum* **1994**, *45*, 653; b) J. M. Hollander, W. L. Jolly, *Acc. Chem. Res.* **1970**, *3*, 193-200

[4] B. D. Cullity, *Elements of X-ray diffraction*, Addison-Wesley, **1978**

[5] D. M. Moore, R. C. Reynolds, *X-Ray diffraction and the identification and analysis of clay minerals*, Oxford University Press, 1997

[6] R. B. Merrifield, *J. Am. Chem. Soc.* **1963**, *85*, 2149

[7] B. Merrifield, *Angew. Chem., Int. Ed. Engl.* **1985**, *24*, 799

[8] a) C. A. G. N. Montalbetti, V. Falque, *Terahedron* **2005**, *61*, 10827; b) R. B. Merrifield, *Science* **1965**, *150*, 178; c) V. Mäde, S. Els-Heindl, A. G. Beck-Sickinger, *Beilstein J. Org. Chem.* **2014**, *10*, 1197

[9] G. Pastorin, W. Wu, S. Wieckowski, J.-Paul Briand, K. Kostarelos, M. Prato, and A. Bianco, *Chem. Commun.*, 2006, 1182

[10] A. G. Schultz, J. P. Dittami, S. O. Myong, C. –K. Sha, *J. Am. Chem. Soc.* **1983**, *105*, 3273

[11] http://www.americanpharmaceuticalreview.com/

5. Conclusions

The importance of nanoscale diamonds for a variety of high performance technologies has been recently recognized. In fact, several studies suggested that nanodiamonds could find applications in biosensors, composite materials and drug delivery.

In this thesis pristine detonation nanodiamonds were fully characterized by transmission electron microscopy (TEM), thermogravimetric analysis (TGA), X-ray photoelectron spectroscopy (XPS), powder X-ray diffraction (pXRD), Raman, infrared (IR) and UV-visible spectroscopies.

The surface of nanodiamonds was oxidized using a mixture of sulfuric and nitric acids in order to make the surface more homogeneous and to increase the number of carboxylic groups. For this kind of reaction, detonation ultrananocrystalline diamonds were more reactive with respect to commercial ones, based on the TGA values obtained. The oxidation performed on commercial nanodiamonds using sulfonitric mixture or selective oxidation in air has revealed that the first method was the most effective one in terms of degree of functionalization.

The amidation on pristine and oxidized NDs was studied using different coupling reagents and optimizing the experimental conditions. The amine used was the *tert*-butyl (2-(2-(2-aminoethoxy)ethoxy)ethyl)carbamate, so after the Boc- deprotection a further grafting of the NDs was performed with fluorescent dyes. Best results, in terms of reproducibility and degree of functionalization, were obtained using the amine with the Boc- as protecting group and allowing the mixture to react for 48 h. The same reaction performed on pristine and oxidized detonation ultrananocrystalline diamonds has revealed that in the second case better results were obtained, due to an increase of the number of carboxylic groups on the surface.

Reactions typically used for the functionalization of carbon nanotubes were applied on annealed nanodiamonds. The arylation with functionalized aryl diazonium salts, the 1,3-dipolar cycloaddition and the nitrene reactions were applied on annealed NDs studying both classical conditions and microwave irradiation.

For all the reaction performed, the detonation ultrananocrystalline diamond annealed using a hydrogen-plasma treatment in MW-RF-PECVD at 300 °C for 3 h (**DND4**) has given best results. For the arylation with functionalized aryl diazonium salts very good results were obtained for the reaction performed at 80 °C for 1 h using classical conditions. Using the microwave irradiation with a closed system after only 15 min very good results were obtained as well.

For the 1,3-dipolar cycloaddition it was observed that the *o*-DCB was the best solvent used for the reaction performed at 120 °C and an increase of the temperature allowed to have a better functionalization. For the study performed under MW irradiation it was observed that the presence of the solvent (*o*-DCB) helped to reach the desidered temperature, as expected.

The nitrene reaction performed at 180 °C, overnight was the best one in terms of degree of functionalization but similar results were obtained for the reaction performed under MW after only 35 min.

For all the reactions applied on annealed nanodiamonds the use of the microwave system, for the first time reported in this work, permitted to obtain good degree of functionalization in a short time.
A study of the biocompatibility of oxidized and amidated nanodiamonds was performed on peripherical blood mononuclear cells. It was observed the internalization of nanodiamonds and a certain dose-dependent decrease in viability and, at higher concentrations, NDs with free amino groups were found to be more toxic than oxidized NDs.
Nanodiamonds have been researched over the past years for use in various drug delivery systems but minimal work has been done that incorporates targeting capability.
For this reason, oxidized NDs were functionalized with tumor homing and cell-penetrating peptides. Peptide sequences were synthesized using the solid phase peptide synthesis (SPPS) approach and they were fully characterized by reverse-phase high pressure liquid chromatography (RP-HPLC) and high resolution mass spectroscopy. Functionalized nanodiamonds with these peptides will be *in vitro* evaluated, to study the enhanced delivery of chemotherapeutic drugs.

Acknowledgements

First of all I would like to acknowledge my supervisor *Professor Tatiana Da Ros* for the years spent together. She gave me the opportunity to pursue my doctoral studies in an international environment, she believed in me and in these years she guided me throughout my doctoral research.

Many thanks to *Professor Maurizio Prato* because he gave me the possibility to learn always more about chemistry.

Many thanks also to *Professor Davide Bonifazi* for the wonderful opportunity I had in his group in Namur.

Many thanks go to my chicas Agni, Tanja, Giuliana, Ana, Maria and Cristina...thanks for all, for your help, for all the moments...I love you!

I would like to thank all the group in Trieste, you were a second family...dear Arturo, Eleonora, Manuel, Jenny, Federico, Silvia, Tomas, Alexa, Marco, Adrian, Zois, Nuria, Daniel, Caro, Magda.

Many thanks go to all the Bonifazi's group: Dario, Andrea, Rodolfo, Hamid, Riccardo, Antoine, Lou, Rosaria, Davide for their help and my sweet and wonderful friend Valentina!!!

I would like to thank my friends in Rome, expecially Laura, Caterina, Gianluca and Tamara, Emanuela, Gabriele, Marco...the distance was not so big at the end...

Many thanks to Fulvia, Gabriella, Maurizio, Annamaria, Maurizio and Marina!

Many thanks go to my new friends and to all the group of boxe in Trieste...Antonio, Blaso, Igor, Alberto, Nicole and Natasha, you are great!

I would like to thank all my family...my cousins Gisella, Jonny, Salvo, Valeria, Daniele, Sabrina, Serena, Oriana, my uncles and aunts Mariagrazia, Gianni, Uccio, Enza, Tina, Enzo, Giuseppe and my grandmothers Angela and Ciccia...you are my strength.

Thanks to *Ettorino*...my heart!

Valerio, *mum*, and *dad*...words cannot describe how much your presence means to me...you are simply the most important people in my life...I will love you for ever...